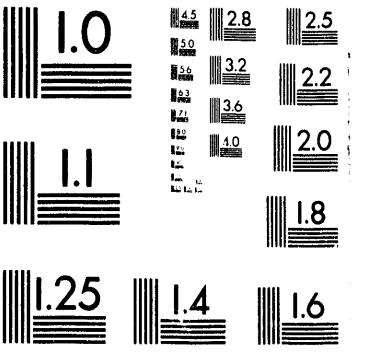
1.0
1.1
1.25
1.4
1.6
1.8
2.0
2.2
2.5
2.8
3.2
3.6
4.0
4.5
5.0
5.6
6.3
7.1

1 of 2

SANDIA REPORT

SAND91-2238 • UC-236
Unlimited Release
Printed March 1994

CIRCE2/DEKGEN2: A Software Package for Facilitated Optical Analysis of 3-D Distributed Solar Energy Concentrators

Theory and User Manual

Vicente J. Romero

Prepared by
Sandia National Laboratories
Albuquerque, New Mexico 87185 and Livermore, California 94550
for the United States Department of Energy
under Contract DE-AC04-94AL85000

Issued by Sandia National Laboratories, operated for the United States Department of Energy by Sandia Corporation.

Available to DOE and DOE contractors from
Office of Scientific and Technical Information
PO Box 62
Oak Ridge, TN 37831

Prices available from (615) 576-8401, FTS 626-8401

Available to the public from
National Technical Information Service
US Department of Commerce
5285 Port Royal Rd
Springfield, VA 22161

NTIS price codes
Printed copy: A07
Microfiche copy: A01

SAND91-2238
Unlimited Release
Printed March 1994

Distribution Category
UC-236

CIRCE2/DEKGEN2: A Software Package for Facilitated Optical Analysis of 3-D Distributed Solar Energy Concentrators

Theory and User Manual

Vicente J. Romero
Thermal and Fluid Engineering Department
Sandia National Laboratories
Albuquerque, New Mexico 87185-0835

Abstract

CIRCE2 is a computer code for modeling the optical performance of three-dimensional dish-type solar energy concentrators. Statistical methods are used to evaluate the directional distribution of reflected rays from any given point on the concentrator. Given concentrator and receiver geometries, sunshape (angular distribution of incident rays from the sun), and concentrator imperfections such as surface roughness and random deviation in slope, the code predicts the flux distribution and total power incident upon the target. Great freedom exists in the variety of concentrator and receiver configurations that can be modeled. Additionally, provisions for shading and receiver aperturing are included. DEKGEN2 is a preprocessor designed to facilitate input of geometry, error distributions, and sun models. This manual describes the optical model, user inputs, code outputs, and operation of the software package. A user tutorial is included in which several collectors are built and analyzed in step-by-step examples.

Acknowledgement

I thank A. C. Ratzel, 1512, from whom I inherited the codes, for his help and advice. Thanks also to R. B. Diver, 6216, who drove the effort and tested the software, and to T. R. Mancini, 6216, whose applications necessitated many of the advanced capabilities that the package now contains. Commendations go to F. Biggs, 9312, and C. N. Vittitoe, 9352, for their diligent documentation of the mathematical models and numerical procedures used in the HELIOS code. Finally, Roy Hogan, 1513, deserves credit for devising the improved scheme that CIRCE2 now contains for integrating periodic flux distributions on axisymmetric receivers.

Preface

In the mid-1980s, A. C. Ratzel and B. D. Boughton, prompted by the need of Sandia solar energy engineers to model point-focus solar collectors, reviewed existing optics simulation codes available to them. These included CAV [1], COPS [2], and HELIOS [3,4,5]. Of these, HELIOS, developed by F. Biggs and C.N. Vittitoe at Sandia National Labs during the 1970s, was best suited for modeling the large variety of reflector and receiver configurations possible for point-focus collector systems. HELIOS, which incorporates much of the solar optics theory developed by George Schrenk [6], is in principle capable of modeling any practical reflector and receiver configuration. However, the computer code was written principally for the purpose of modeling central-receiver collector systems. HELIOS' large size, generality, and predisposition toward central receivers made it cumbersome to use for modelling dish-type collector systems. With the goal of providing users with a tool that is relatively easy to implement and does not require a large investment of time to obtain results, Ratzel and Boughton simplified and specialized HELIOS to be more amenable to analysis of dish-type systems. The resulting analysis package, CIRCE.001 (Convolution of Incident Radiation with Concentrator Errors) [7,8], allowed a user to efficiently build and analyze a variety of point-focus solar concentrators.

The present work has focused on expanding the capabilities of CIRCE.001, optimizing storage and computational efficiency, and increasing user-friendliness. Among the new features offered in CIRCE2 are: an ability to generate and analyze three-dimensional (3-D) internal or external receivers of arbitrary geometry, receiver aperture modeling, the capability to model triangular facets, augmented ability to generate and analyze axisymmetric and nonaxisymmetric facets of arbitrary contour, elimination of rotational constraints on facets, augmented shading capability, more than 20X greater resolution of target flux distributions, an improved integration scheme for calculating total collected power from flux distributions, and more explicit control over convolution of sunshape and concentrator error distributions. Though capabilities have increased, code optimization has increased computational efficiency, and reduced storage requirements by 95%. Computer savings are problem dependent, but significant savings in CPU time are realized for all problems, and reduction of over 300X are observed for some. Thus, CIRCE2 is more PC friendly than ever, and is now coupled to the PC-compatible thermal analysis code AEETES [18].

The user-interface code DEKGEN has been modified to include the new capabilities of CIRCE2 and check user input for correctness where possible. It is now called DEKGEN2. Because of the proliferation of plotting routines, and personal preferences for certain packages over others, the graphics simulation code PLOT accompanying the release of CIRCE.001 has not been carried along with the new software ensemble.

The optical model upon which CIRCE2 is based is documented fully in the HELIOS manuals [3-5]. A concise yet thorough synopsis of the theory can be found in Reference [9]. In this manual, the theory that is essential for competent use of the analysis code is developed for the benefit of the user. Though based on the same paradigm, many differences between CIRCE2 and HELIOS exist in numerical and algorithmic implementation of the theoretical model. The numerical procedures described in this document apply to CIRCE2, and supercede those described in the HELIOS documentation where overlap exists.

Caution

The CIRCE2 family of codes discussed in this report is still under development. Numerous test cases have been run against HELIOS and qualitative and quantitative comparison with measured data from several receivers have been made to verify the code. However, solution techniques are approximate and there may still be "bugs" in the simulation. The author should be informed if any problems are uncovered while using the codes so that future releases will reflect all possible upgrades. Users should contact the author periodically to learn if any "bugs" in the code have been discovered/corrected. The author may be contacted by phone at (505) 844-5890, by E-mail at vjromer.eng-sci.sandia.gov, by fax at (505) 844-8251, or correspondence at Vicente J. Romero, Sandia National Laboratories, Box 5800, Albuquerque, NM 87185-0835. The Sandia personnel locator service at (505) 844-5678 has updated information in case these destinations change.

Table of Contents

List of Figures

List of Tables

List of Important Notes and Warnings

1 INTRODUCTION

If you need to get started quickly, or find it extremely painful to wade through such things as solar optics theory and numerical methods, you may want to proceed immediately to Chapter 8, the user tutorial, after reading this section. There you will find four examples that, in a step-by-step manner, take the user through the rigors of running CIRCE2 and DEKGEN2. The examples introduce the user to many of the capabilities of the software package. Explanatory comments and interpretation of significant results are provided, and where supplementary information is required, the user is directed to key sections of the manual. Once all four examples are read and understood, sufficient familiarity with the software and the underlying theory will have been achieved to enable the reader to use the analysis package.

CIRCE2 and DEKGEN2 are design and analysis tools for the study and optimization of dish-type solar collectors. With inputs of concentrator and receiver geometry, sunshape (angular distribution of incident rays from the sun), and concentrator imperfections such as non-unity reflectivity, surface roughness, and random deviation in slope, CIRCE2 uses statistical optics to predict flux-density distribution and total incident power on the target. After the above information is supplied, the normal mode of operation is as follows: the user discretizes the concentrator into a number of smaller subareas called subfacets; a grid of points on the target surface is established; the contribution of each subfacet to the normally incident flux at each target point is evaluated; and the resulting discrete flux distribution at the target points is numerically integrated over the target surface to determine total incident power.

In developing the codes, two comprehensive goals were set at the start. First, the code should be user-friendly and versatile —enabling rapid and easy construction and analysis of collector systems of common geometries, though general enough to investigate more complex or unconventional designs. Accordingly, a user-interface code, DEKGEN2, has been written to help build collector system data decks, and great freedom exists in CIRCE2 for the types of reflectors, sun models, and targets that can be analyzed. Concentrators can be comprised of one facet, such as a continuous-surface parabolic dish, or several facets (up to 350) that can be aligned automatically by DEKGEN2. Facets can have circular, rectangular, or equilateral triangular projected shape. They may have spherical, parabolic, or flat contour, or may have a custom profile generated by revolution of a user-specified curve. Alternatively, the user has the freedom to supply a subroutine that describes a facet's contour —whatever it might be. Shading and blocking by the target and support structures or other objects can be accounted for. Completely arbitrary 3-D target geometries may be accomodated. In addition, "standard" planar targets of rectangular or circular shape, and internal or external 3-D receivers of spherical, cylindrical, or conical (upright or inverted) shape are supported. These targets are not limited to "complete" shapes, i.e., just the frustrum of a cone may be analyzed, or only a small angular section of the frustrum as opposed to the full axisymmetric region. Moreover, axisymmetric **"hybrid"** receivers can be constructed from the above component shapes. Thus, CIRCE2 is particularly well suited for treating axisymmetric "cavity" type receivers, which are the kind most commonly used in dish/receiver applications. Additionally, the receiver aperture is automatically taken into account for axisymmetric

receivers and can be separately defined for other targets. To investigate the effects of instantaneous tracking errors, the freedom to specify sun position relative to the concentrator has been included.

Second, the code should have the capability to run on mainframe and personal computer systems and be adaptable to the computing environment. Accordingly, CIRCE2 has many options that can be used to economize on CPU time (at slight sacrifices in accuracy) for PC analyses. For more powerful systems, the full capability of the HELIOS code is at hand. Moreover, CIRCE2 enjoys intrinsic accuracy advantages over HELIOS for analyzing dish-type concentrators –featuring 20X greater target-flux resolution, more accurate integration of flux distributions on the target surface, and several deep-dish correction factors, while having vastly lower storage requirements and a restructured computational algorithm that results in large computational savings.

This manual describes the mathematical model, user inputs, code outputs, and run environment for the CIRCE2 and DEKGEN2 codes. It is important that the user be aware of the theory and numerical procedures upon which CIRCE2 is based before using it in a simulation. This will help in deciding how to model a given collector and sun condition (what geometric quantities affect results most and therefore are most important to capture accurately?, how does sunshape figure into the calculation?, what is the effect of a single convolution vs. multiple convolutions? etc.), and in interpreting results. Chapter 2 outlines the important concepts in a statistical treatment of real reflecting surfaces in the presence of a sun that is treated as a disk- (not point-) source. Chapter 3 introduces the preprocessor code DEKGEN2, its structure, mode of operation, and interface with CIRCE2. The file system associated with the codes is also described. Chapters 4 through 7 describe the parameters that DEKGEN2 prompts for when building a data deck, and provide the background information necessary for competently choosing parameter values and analysis options. Chapter 4 summarizes the sun models and concentrator-error distributions, and their manipulation in a statistical treatment of real reflecting surfaces. The parameters that control the numerical implementation of the statistical algorithm are explained, and guidelines are given for appropriate use of these parameters under various circumstances. Chapter 5 is devoted to target geometry and mesh generation, output of target flux distributions, and numerical integration schemes for calculating total incident power. Chapters 6 and 7 are concerned with geometric modeling of individual reflectors and of the aggregate concentrator. Finally, Chapter 8 is a tutorial for familiarizing the user with the CIRCE2/DEKGEN2 system. Four varied examples are used to illustrate important capabilities of the software package and to provide guidance for competent usage.

2 OVERVIEW OF THEORY

It is important for the user of CIRCE2 to know the underlying physical principles and mathematical approximations upon which the code is based. Without going into too much detail, it is the purpose of this section to inform the user of the optical theory in the CIRCE2 model of solar collector systems. In this and following chapters, the numerical treatment necessary for computer implementation of the theoretical model is outlined where necessary to equip the user with information to make competent modeling decisions and interpret analysis results correctly. Further details are thoroughly documented in the references cited in the discussions below. A concise synopsis of the theory is presented in Reference [9].

2.1 Solar Optics for Perfect Reflectors

Fundamental to solar optics is the existence of the sun as an energy source of finite dimension. Looking up at the sun, it appears to be a disk of small but non-zero radius. Since the sun is not a point source but a disk, it irradiates a point on a reflector surface as a cone of energy rays instead of as a single ray, as Figure 2.1 illustrates. Rays originating from one diametric line across the solar disk are shown. As the variation in vector magnitudes along this line indicates, the intensity of energy incident from each point across the solar disk may vary. The angular distribution of energy with respect to the "**central ray**" (ray from the center of the solar disk) is called the "**sunshape**". A perfect (ideal) reflector has a smooth surface and no absorption of incident radiation. Thus, all energy in a given wavelength band incident upon the surface is specularly reflected (angle of incidence = angle of reflection). For a perfect flat reflector, this means that the reflected cone is a mirror image of the incident cone. So, treating the sun as a disk source implies foregoing the classical techniques of ray tracing for the more applicable cone methods, and requires using an angular distribution function to describe solar-flux intensity over the disk surface.

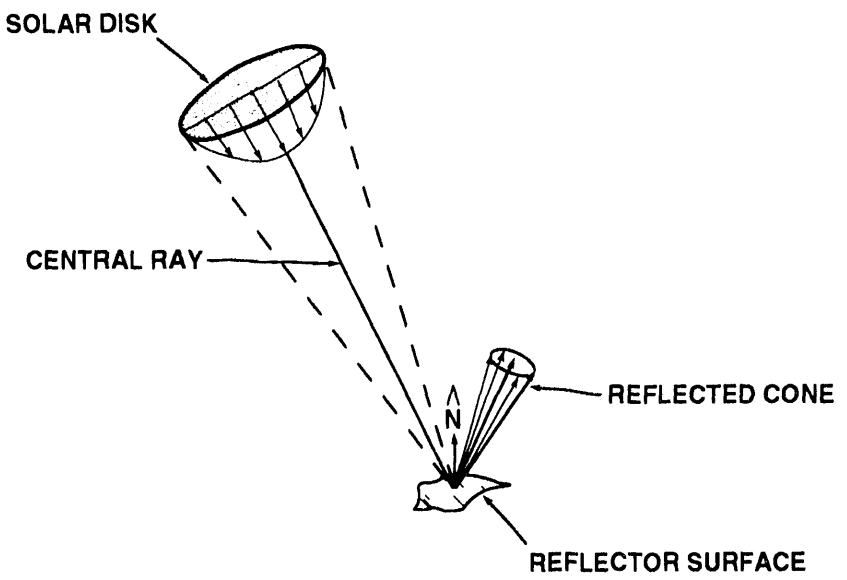

Figure 2.1 Solar Disk and Reflected Cone.

Consider the insolation at two adjacent points A_1 and B_1 on the flat reflector depicted in Figure 2.2. By the definition of solar optics [6], the incident sunshape and incoming direction of the central ray with respect to the absolute X-Y-Z reference frame are identical at the two points (and in general at all points on the reflector). The central rays reflected from points A_1 and B_1 on the reflector strike the flat target at points A_2 and B_2, respectively. Since the reflector is flat, the reflected central rays are parallel. If the surface had some curvature to it, the central rays, and thus the points of intersection on the target, would diverge or converge depending upon the magnitude and direction of the curvature.

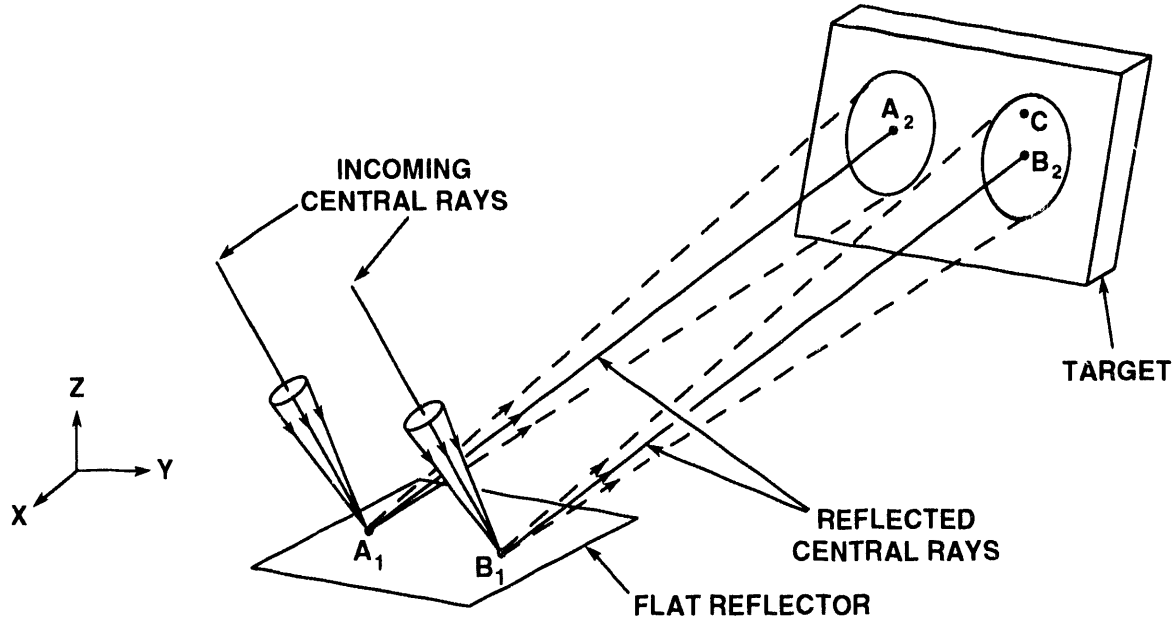

Figure 2.2 Sun-Reflector-Target Sequence.

The reflected cones of light from points A_1 and B_1 illuminate the outlined areas on the target about points A_2 and B_2 as shown. The flux at target point C is desired. Reflector point A_1 will have no contribution. Point B_1 will, however. A flux vector of a certain magnitude strikes point C from B_1. The component of this vector in the direction normal to the target at C constitutes the contribution from reflector point B_1 to the incident flux at target point C. Summing the contribution from every point on the reflector surface gives the total flux incident at C due to the reflector.

2.2 Statistical Optics for Real Reflecting Surfaces

In CIRCE2, the effect of non-ideal reflectors is taken into account by statistical means. An attempt is made here to inform the user what this entails, while avoiding the substantial mathematical details of the process.

A real (imperfect) reflector deviates from a perfect reflector in many respects. First, all of the energy striking the surface does not leave because of surface absorption. This is handled by allowing the user to specify a specular solar-band reflectance. Additionally, in the CIRCE2 simulation, reflecting surfaces are assumed to conform to certain ideal geometries, such as flat, paraboloidal, etc. Real reflectors cannot be made to conform to these shapes exactly without introducing great expense. The overall profile of reflectors in use will generally deviate from the ideal shapes. For example, waviness may exist on the reflector surface. Deviation from the ideal slope is called a **"slope error"**. The better the quality control in manufacturing the reflector, the smaller the slope errors will be. Slope errors will cause the surface normal to deviate from that of an ideal surface. A distribution function can be used to assign a probability to the direction taken by the actual surface normal. A perfect (specular) reflector is microscopically smooth, which dictates that the surface normal at any point is unambiguously associated with the geometry of the surface. A real reflector, however, has surface roughness that creates ambiguity in the actual direction of the surface normal and makes the reflection diffuse. A separate distribution function can be associated with these errors as was done for the slope errors. The smoother the surface, the smaller the standard deviation of this error distribution.

Up to five such distributions, for slope errors, specularity errors, facet misalignment, etc. can be specified. The errors, all assumed to be random, are described by either 1-D circular-normal or 2-D elliptic-normal error distributions. The combined effect of the concentator errors is obtained by convolving these distribution functions, as discussed in Section 4.4. The result is an effective distribution of normal directions about the "**ideal normal**" of the surface, $\hat{N}_0$. This distribution is assumed to be invariant over the entire surface of the concentrator. Since the distribution represents a multitude of surface-normal directions as Figure 2.3 illustrates, it is sometimes referred to as the "**concentrator error cone**".

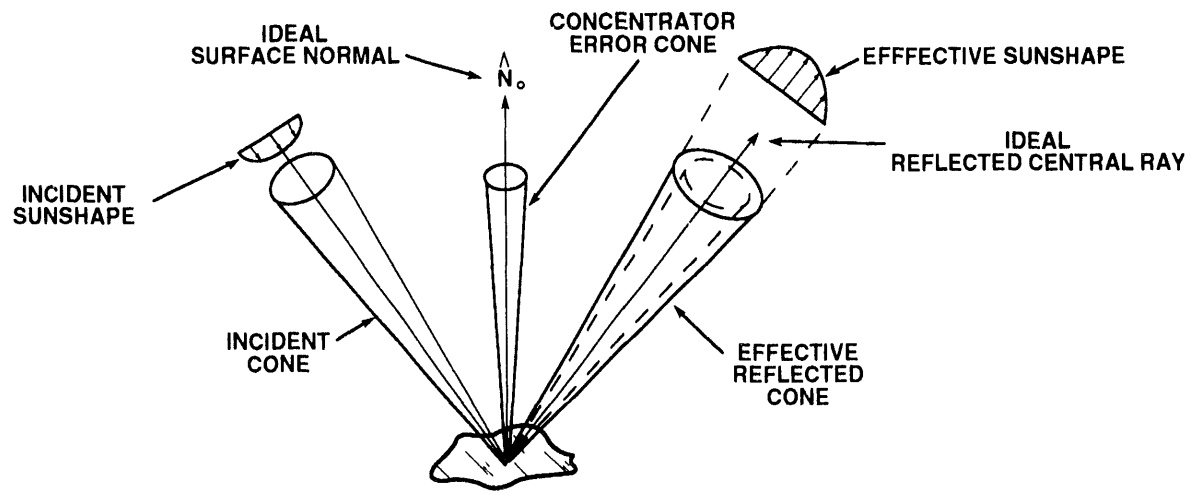

Figure 2.3 Important Distributions in the CIRCE2 Statistical Model of Real Reflecting Surfaces.

The last step in the process of modeling real reflecting surfaces is to convolve the sunshape with the concentrator error-cone. A cone of light is reflected from any point on the concentrator due to the sun being a disk-source (c. f. Figure 2.1). The reflected cone is centered about the central reflected ray and may vary in intensity with angular direction from the central ray. Now, the direction of the reflected central ray depends upon the incident central ray and the surface normal direction. However, since there is a multitude of possible normal directions (*i.e.* the error cone), the reflected cone may exit in any of a number of directions. As conceptually illustrated in Figure 2.3, the distribution of energy is dependent upon both the incident angular distribution of incoming rays (sunshape) and the concentrator error-cone probability distribution. These two distributions are combined in a convolution integral ("convolved") to obtain the directional probability distribution of energy leaving the surface. This effective reflected distribution is referred to as the "**effective sunshape**" distribution, *ESUN*. Chapter 4 addresses the calculation of the effective sunshape. The chapter includes the information the user needs to know to model the sun, define concentrator errors, and control the convolution process.

2.3 Application to Solar Collector Systems

Some additional considerations must be taken into account when modeling collector systems. Figure 2.4 shows a generic solar collector system. An analysis requires definition of the three aspects of the collector system: concentrator geometry, target geometry, and the sun model. An absolute X-Y-Z coordinate system is used as the reference frame for setting up the problem. It is also referred to as the global or **"collector coordinate system"**. Concentrator geometry is described in terms of this system. A local 1-2-3 **"target coordinate system"** is used to generate the target. The target coordinate system is translated (not rotated) from the collector coordinate system. Its origin is located in the collector coordinate system at the point (X=Xo,Y=Yo,Z=Zo). The sun position is specified by definition of a vector, $\vec{V}_S$, pointing toward it from the origin of the collector coordinate system. The negative of this vector gives the direction of the incoming central ray.

On its way from the sun to the concentrator, and then to the receiver, a ray may be stopped in several ways. The receiver, or supporting structures, may block rays as they descend toward the concentrator, shading portions of it. In turn, such structures may block some of the energy reflected from the concentrator toward the target. It is also possible that facets may shade/block portions of themselves and/or other facets. These effects can be accounted for with a shading/blocking factor B_j (see Equation 2.3) that corresponds to the fraction of shaded surface of each facet, which also includes the fraction of the surface whose reflected rays are being blocked. The aperture of a receiver may block some rays reflected from the concentrator, and should also be taken into account when modeling a collector system.

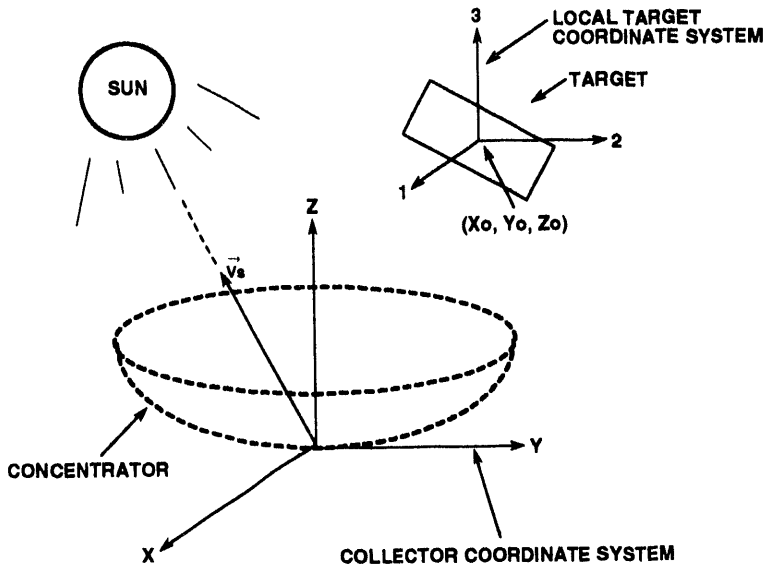

Figure 2.4 Generic Collector System.

For purposes of numerical computation, the concentrator is usually subdivided into relatively small reflecting surfaces called "**subfacets**". Figure 2.5 shows in schematic a subfacet and target section. Both are flat for convenience in this example. The incident central ray, ideal normal $\hat{N}_o$, and ideal reflected central ray are shown.

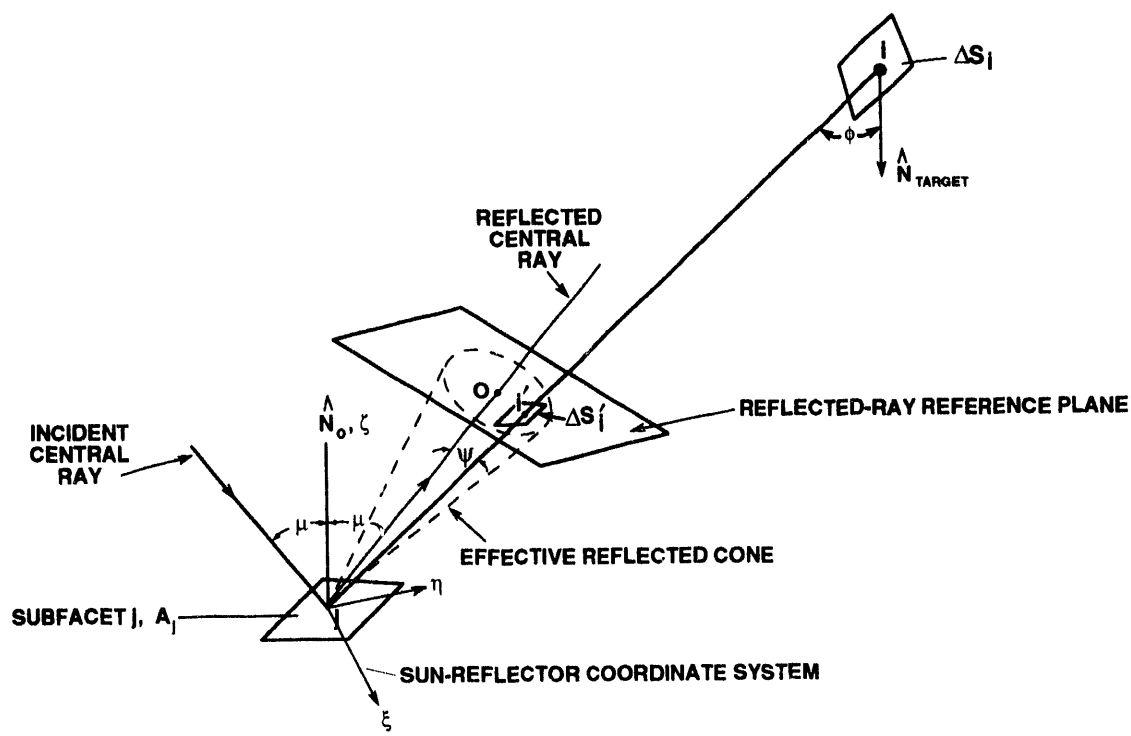

Figure 2.5 Schematic Used in Derivation of Flux Incident at Target Point i from Reflecting Surface j.

The plane containing these vectors defines the ζ-η plane of the **"sun-reflector coordinate system"**. The angular distribution of energy contained within the effective reflected error-cone is projected upon a computationally convenient plane, as suggested in [6], called the "**reflected-ray reference plane**". This plane is normal to the reflected central ray and at unit distance from point j on the subfacet. The differential area dS on the target is contained within a solid angle $d\omega$ given by:

$$d\omega = dS\cos\phi/d^2 \tag{2.1}$$

where d is the distance between point i on the target surface and point j on the reflector surface, and $dS\cos\phi$ is the projection of dS normal to the line between points i and j. This solid angle intercepts the area dS' on the reflected-ray reference plane. With respect to the reference plane, $d\omega$ is defined by:

$$d\omega = \frac{dS'\cos\psi}{(\sec\psi)^2} \tag{2.2}$$

where $dS'\cos\psi$ is the projection of dS' normal to the line between points j and i', and the distance between these points is $\sec\psi$, recalling that the plane is at unit distance (along the reflected central ray) from j. Since they share the same solid angle, the total power intercepted by dS and dS' is the same.

At this point, an approximation is made to enable numerical solution of the problem we are formulating. The energy reflected from all points on the subfacet surface is assumed to originate from the point j. The total power (P) reflected from subfacet j is given by the solar insolation, I, multipied by $A_j\cos\mu\,(1-B_j)$ which is the unshaded and unblocked intercepted reflector area where B_j is the fraction of the subfacet that is shaded/blocked and μ is the angle of incidence/reflection as shown in Figure 2.5, multiplied by the facet's specular reflectance for sunlight, κ. Thus,

$$P = I\kappa A_j\cos\mu\,(1-B_j) \tag{2.3}$$

In section 6.3 we address the determination of the important subfacet quantites A_j, $\hat{N}_o$, and source-point location.

The distribution of energy within the reflected cone is given by the effective sunshape probability distribution $ESUN(u,v)$, where u and v are orthogonal coordinates in the reflected-ray plane. The origin of the coordinate system is at the point O where the reflected central ray intersects the plane. $ESUN$ is a normalized distribution such that its integration over the illuminated area of the plane yields a value of unity. Thus, the probability that power passes through the plane at any point i' is given by $ESUN(u_{i'},v_{i'})$. The power intercepted by dS' is then approximated by multiplying the total power reflected from the subfacet element by $ESUN(u_{i'},v_{i'})dS'$, which is the fraction of power passing through dS'. Expressing dS' in terms of dS by equating (2.1) and (2.2), the power intercepted by dS' can be written:

$$P_{dS'} = \frac{P \times ESUN(u_{i'}, v_{i'})\, dS \cos\phi}{d^2 \cos^3\psi} \tag{2.4}$$

The flux density, F_{ij}, at target point i due to subfacet j is given by:

$$F_{ij} = P_{dS}/dS = P_{dS'}/dS = I\kappa \frac{[\,(1 - B_j)\cos\mu\cos\phi\, A_j ESUN(u_i', v_i')\,]}{d^2 \cos^3\psi} \tag{2.5}$$

where the fraction term is a function of the locations i and j.

The total flux at target point i is obtained by summing the contributions from each of the j subfacets on the concentrator:

$$F_i = \sum_j F_{ij}\ ;\ j = 1, NUM_{subfacets} \tag{2.6}$$

2.4 Determination of Total Power Intercepted by Target

To determine total power collected, the incident flux at a regular pattern of grid points on the target surface is numerically integrated. Here, "regular" means: at intervals on the target surface described by equi-incremental stations of the curvilinear coordinates that describe the surface. For example, consider a spherical target section, which is completely described by variations of the coordinates Θ and φ on the surface defined by the equation ρ=constant. The total angular extents $\Delta\Theta$ and $\Delta\varphi$ are divided into equal increments $\delta\Theta$ and $\delta\varphi$, such that $\Delta\Theta = n\delta\Theta$ and $\Delta\varphi = m\delta\varphi$ where n is the number of divisions in the Θ-direction and m is the number of divisions in the ϕ-direction. An orthogonal net of lines if formed on the surface with $\delta\Theta$ and $\delta\varphi$ spacing. The grid of points located by the intersections of the mesh lines represents a "regular" discretization of this two-coordinate surface.

Quadrature is performed over a flat, rectangular domain in the surface coordinates. For example, in the spherical case, the surface integral becomes:

$$\iint_R F(\Theta, \varphi)\, \rho^2 \sin\varphi\, d\Theta d\varphi = \iint_R \tilde{F}(\Theta, \varphi)\, d\Theta d\varphi \tag{2.7}$$

where $F(\Theta, \varphi)$ is the flux distribution on the target. Orthogonal coordinates Θ and φ can be visualized to preside over a flat domain upon which the Jacobian-weighted scalar function $\tilde{F}$ is defined. The grid of points becomes rectangular and equi-spaced in this domain, and the value of $\tilde{F}$ is known at each of the points. The specific numerical techniques employed to evaluate this double integral are summarized in Section 5.2.2.

3 DATA-FILE GENERATION AND OUTPUT OF RESULTS

3.1 DEKGEN2: A Preprocessor and Data-Deck Generator

Sections 4-7 of this manual provide the necessary information to build and analyze solar concentrators. DEKGEN2 is an interactive preprocessor that guides the user through the building process and creates the data file necessary to run the analysis. DEKGEN2 provides on the computer screen a description of the current parameter whose value needs to be input, along with an associated keyword in capital letters. DEKGEN2 keywords are the same as those in this manual. Once the user gains an understanding of each of the parameters that CIRCE2 uses, the manual rarely has to be consulted because of the detailed prompts in DEKGEN2. However, referring to the manual for more complete information is expedited by Appendix G. It lists keywords, grouped by category (see below), in alphabetical order. Beside each keyword is a short description, statement of dimensional units in which the value should be input, and page number in the manual where it is described further. Keywords are written in all capital letters, hopefully making them easy to spot on a page.

Input data is organized into four categories:

- Sun and Concentrator-Error parameters
- Target/Receiver parameters
- Facet/Reflector parameters
- Concentrator parameters

A user-input title precedes each data group.

DEKGEN2 can be used to create a new data file or can be used to modify an existing one. When the latter option is specified, DEKGEN2 asks for the old file's name and displays its parameters for the first data group. The user is then prompted as to whether any of the values need to be altered. If one parameter is to be altered, then all parameters from the data group must be redefined (input). After completing the first data group, DEKGEN2 advances through the other data groups similarly. For certain information lists that can be quite lengthy, such as tabular sunshape data and facet data for a concentrator with a large number of facets, DEKGEN2 can read-in pre-existing files. The files can be generated outside of DEKGEN2, saving the user laborious interactive input of data. All data files are read in free-format.

WARNING

Use of DEKGEN2 is strongly encouraged even for the experienced user because of operations such as unit conversions and creation of unit vectors that the user may not be aware of. Also, one entry in a data deck may affect quantities in other places in the file. For these reasons, changing entries by editing the data file may lead to unexplained errors and should be avoided. Much work has gone into making DEKGEN2 user-friendly, fast, and painless to use. Internal logic is used where possible to simplify and shorten the data input process. Checks are made in many places to ensure that information input is consistent with previous information and/or within the acceptable ranges of the parameters.

3.2 Coupling between DEKGEN2 and CIRCE2

Upon completion of a DEKGEN2 session, the code will create an output file named "**input**" for CIRCE2's use, whether it was generated from scratch or modified from a pre-existing file. Appendix D contains a sample **input** file. If the receiver modeled is a hybrid target (see Section 5.4.6) the file "**hybrid**" containing the geometry of the receiver will also be output for CIRCE2's use. Example problem 4 in Chapter 8 contains a sample **hybrid** file. If a user-defined custom target is to be analyzed, DEKGEN2 outputs the file "**usertarg**" for CIRCE2's use. Example 1 of Chapter 8 illustrates the file-coupling between CIRCE2 and DEKGEN2 in an in-depth manner.

3.3 CIRCE2 Results Files

In the course of an analysis, CIRCE2 reads the relevant input files and outputs the files: "**output**," "**flux**," and "**messages**." The contents of these files are presented in the Chapter 8 examples, with commentary as appropriate. Briefly:

The **output** file echos input data, lists convolved sunshape information, locations and normals (referred to the collector coordinate system) of target grid points, computed flux at each target point, total integrated power incident upon the target, the number of subfacets reflecting rays to each target point ("hit map"), system efficiencies, and the maximum target-point flux calculated ("peak flux").

The **flux** file contains a concise subset of information from **output**. The matrix forms of the flux distribution and hit map are given along with the results summary table. The results summary table is located at the bottom of both the **output** and **flux** files. Appendix E contains a sample **flux** file.

The **messages** file contains messages pertaining to "unusual" occurances during the analysis and should be checked at the completion of each run.

3.4 Coupling between CIRCE2 and AEETES

The AEETES computer program [18] predicts the thermal performance of axisymmetric cavity-type solar receivers such as the Sandia reflux pool-boiler and heat-pipe receivers. CIRCE2 can create, at the user's request, a data file of the flux-density profile on the receiver surface that may be read directly into the preprocessor for the AEETES program. The file, "**circ2aee**", can only be generated if the receiver is modeled as a "hybrid" receiver (Section 5.4.6).

4 CALCULATION OF THE EFFECTIVE SUNSHAPE DISTRIBUTION, *ESUN*

The existence of the sun as a disk source, coupled with imperfections of real reflecting surfaces yields to statistical treatment as explained in Sections 2.1 and 2.2. In this section, the parameters used in defining sunshape and concentrator-error distributions are discussed. The convolution process for combining the two distributions to yield the reflected sun image (effective sunshape distribution *ESUN* in Equation (2.5)) is also described, along with the parameters that control the process. Guidance is also given for choosing the most appropriate combination of convolution parameters to match a given set of circumstances.

4.1 Sun Position

The first consideration in modeling the sun is the definition of its location relative to the concentrator. Definition of the vector $\hat{V}_s$ in Figure 2.4 determines the sun position. The sun vector is defined in DEKGEN2 by the components SV(i), i=1-3, referred to the global X-Y-Z coordinate system. $\hat{V}_s$ does not have to be a unit vector. Freedom in specification of the sun position allows investigation of instantaneous tracking errors, facet or collector astigmatism effects, etc.

4.2 Sunshape Distribution

The sunshape is the angular intensity distribution of incoming rays about the sun's central ray. Assuming a perfect surface, the reflected sunshape is the same as the incident sunshape. With this in mind, it is convenient to describe the incident sunshape with the ideal reflected sunshape depicted in Figure 4.1. The reflected cone illuminates a circular area on the reflected-ray reference plane, whose orientation is normal to the reflected central ray as explained in Section 2.3. Since the plane is by definition (see Section 2.3) a unit distance from point of incidence/reflection, ρ of Figure 4.1 is given by (1) ($tan\ \gamma$) = $tan\ \gamma$. If the sunshape is an azimuthally symmetric distribution, which is the customary assumption, it can be described by one coordinate —the angle γ, or equivalently through the small-angle approximation, the measure ρ. It is more convenient to use ρ in integrating the distribution over the illuminated area. Figure 4.2 gives some example sunshape distributions, $S(\rho)$, where ρ has units of milliradians (mrad) because of its equivalency to γ at these small angles (though is really not an angle). The quantity $S(\rho)\ 2\pi\rho d\rho$ gives the amount of solar energy incident from a differential ring on the illuminated spot of Figure 4.1. Integrating over the area of the spot gives the total energy reflected from one point on the reflector surface, which is equal to the solar insolation I (for our temporarily assumed-perfect reflector).

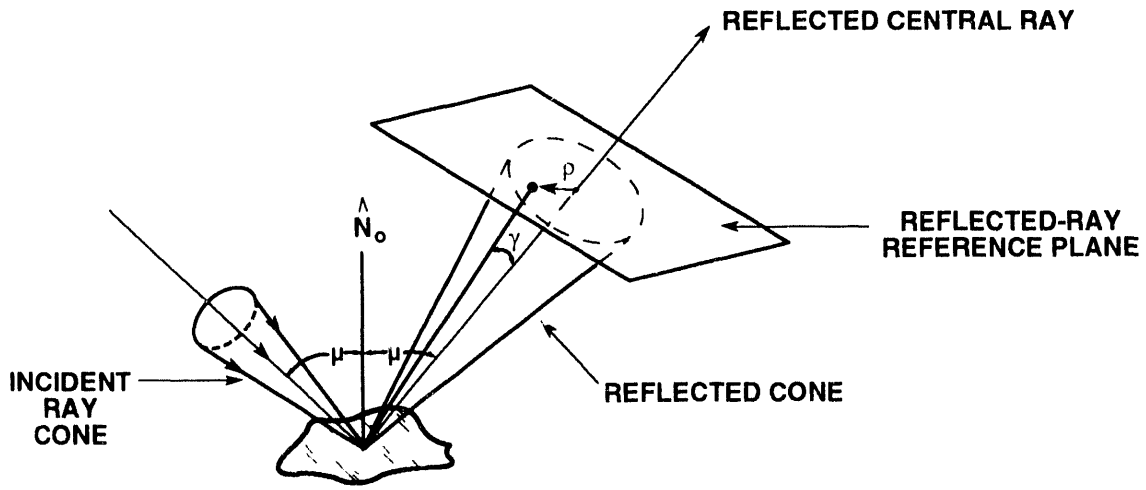

Figure 4.1 Incident and Reflected Ray-Cones for a Perfect (error-free) Surface

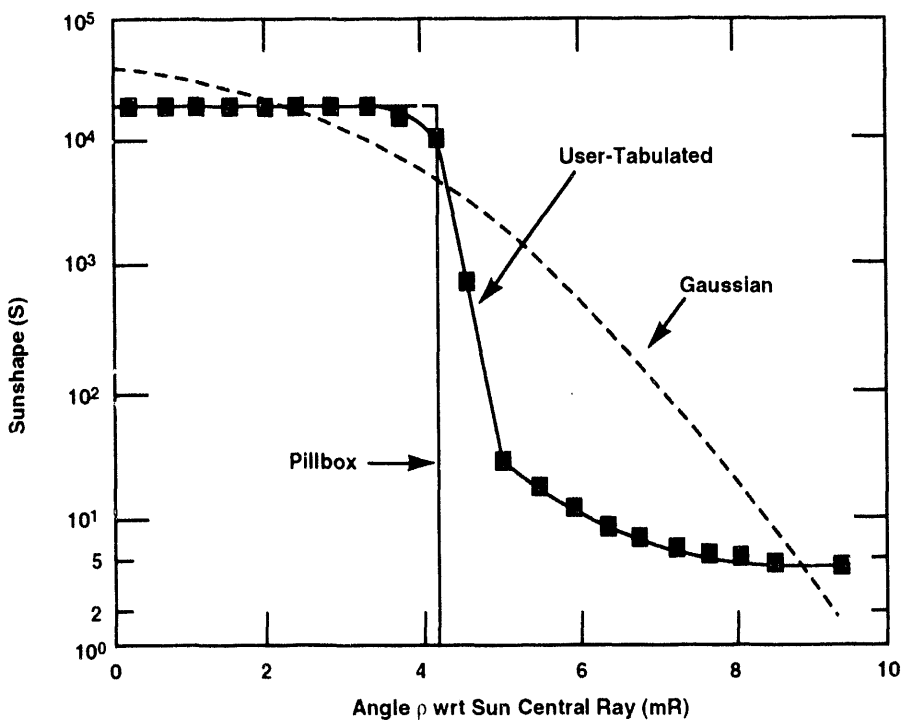

Figure 4.2 Typical Sunshape Distributions Used in CIRCE2.

CIRCE2 allows separation of the total insolation I ($Watts/m^2$) from the shape of the insolation distribution. Thus, the distribution $S(\rho)$ input for the sunshape can have any units or be unitless. In CIRCE2, the value of the sunshape at a given value of ρ is given by Equation (4.1), where $\bar{S}(\rho)$ is the "**normalized**" distribution function given by Equation (4.2) such that Equation (4.3) holds. Here ρ_{edge} is the angle formed by the solar central-ray and the outer limit of the illuminated region beyond which intensity falls to zero. Note that, because Equation 4.3 applies, the integral of $\tilde{S}(\rho)$ in Equation 4.4 is equal to I, as required.

$$\tilde{S}(\rho) = I \times \bar{S}(\rho) \tag{4.1}$$

$$\bar{S}(\rho) = \frac{S(\rho)}{\int_0^{\rho_{edge}} S(\rho)\, 2\pi\rho d\rho} \tag{4.2}$$

$$\int_0^{\rho_{edge}} \bar{S}(\rho)\, 2\pi\rho d\rho = 1.0 \tag{4.3}$$

$$\int_0^{\rho_{edge}} \tilde{S}(\rho)\, 2\pi\rho d\rho = I \tag{4.4}$$

Sun modeling is a subject unto itself. A good synopsis of sun modeling and discussion of the large sensitivity of collected power to sunshape variation for the Solar Central Receiver Test Facility at Sandia, Albuquerque is presented in [3, chapter 6]. References [10] though [14] may be consulted for further information on sunshapes.

In CIRCE2, three modeling options for the sunshape distribution are available, as defined by the choice of the parameter JSUN.

JSUN = 1 - User-tabulated distribution
2 - Gaussian distribution
3 - Uniform, or "pillbox," distribution

The distributions in Figure 4.2 are representative examples of these options. (Note the semi-log scale.)

When JSUN=1, the user must provide a table of SVAL vs. RHO (*i.e.* $S(\rho)$ vs. ρ) data. The number of points in the table is controlled by the variable NTABL (≤ 50). The first point in the table must be at $\rho = 0$, *i.e.* RHO(1)=0, with subsequent tabular entries at increasing distance ρ from the solar central-ray. As previously mentioned, the units of $S(\rho)$ do not matter as long ρ is measured in milliradians. With the tabular option, sunshape is assumed to vary linearly between data points. The radius of the last data point is taken to be ρ_{edge}, beyond which intensity is zero. If desired, a file containing the tabular data may be read into DEKGEN2 in preference to entering the data interactively. A sample file is presented in Example 1 of Chapter 8 (pp. 76).

The option JSUN=2 generates a Gaussian sunshape of specified dispersion DIPSUN. A normalized **Gaussian (1-D circular-normal) distribution** is given by

$$S(\rho) = \frac{1}{2\pi\sigma^2} exp\left[-\frac{\rho^2}{2\sigma^2}\right] \tag{4.5}$$

where σ is called the "**dispersion**", or "**root-mean-square-width**" (**rmsw**) of the distribution. In many cases it is advantageous to approximate circumferentially-symmetric distributions with circular-normal (Gaussian) distributions. This is done with JSUN=1 and JSUN=3 sunshapes when analytic convolution of the projected error-cone and sunshape distributions is requested (see Section 4.6.2). The basis for "equivalency" between tabular or pillbox sunshapes and their Gaussian approximations is equivalency of their rms radii. (All of the sunshapes plotted in Figure 4.2 have equal rms radii.) The "**root-mean-square-radius**" (**rmsr**) of a normalized circumferentially-symmetric distribution $S(\rho)$ of finite radius ρ_{edge} (beyond which the distribution is zero-valued) is defined as

$$rmsr_{1-D} = \left[\int_0^{\rho_{edge}} \rho^2 S(\rho) 2\pi\rho d\rho\right]^{1/2} \tag{4.6}$$

The rms width, or dispersion, of an azimuthally symmetric distribution is related to its the rms radius by

$$rmsr = \sqrt{2}\sigma \tag{4.7}$$

When analytic convolution is used, the equivalent rms width of tabular and pillbox sunshapes is reported in the **output** file.

The option JSUN=3 allows specification of a pillbox sun of radius RHOEDGE (ρ_{edge}). The normalized sunshape is described by

$$S(\rho) = \frac{1}{\pi(\rho_{edge})^2} \tag{4.8}$$

Equation 4.6 simplifies in the case of a pillbox sun to

$$rmsr = \frac{\rho_{edge}}{\sqrt{2}} \tag{4.9}$$

4.3 Concentrator Error Distributions

Concentrator imperfections such as slope errors, surface roughness, random facet misalignments, etc., have impact on the actual normal at the concentrator surface. These imperfections give rise to error distributions, which assign a probability to the chances that the actual surface normal will take a given direction. Concentrator imperfections can usually be modeled with 2-D elliptic-normal error distributions.

A (normalized) **elliptic-normal distribution** having rms widths or "**standard deviations**" σ_r and σ_s along the major (r) and minor (s) axes, respectively, is described by:

$$E_{2D}(r,s) = \frac{1}{2\pi\sigma_r\sigma_s} exp\left[-0.5\left[\frac{r^2}{\sigma_r^2} + \frac{s^2}{\sigma_s^2}\right]\right] \tag{4.10}$$

It is convenient to represent such a distribution by the contour obtained by setting the argument of the exponential term in Equation (4.10) equal to -1/2. The principal axis intercepts of such a contour are equal to the standard deviations of the distribution, as shown in Figure 4.3. In the figure, a reflector section is shown with its associated "**sun-reflector coordinate system**". Such a system has its origin at a representative center point of the reflecting section. The ideal normal there defines the direction of the ζ-axis. The ξ–η plane is perpendicular to the ζ-axis. A central ray from the sun that strikes at the origin reflects in a direction whose projection onto the ξ–η plane defines the direction of the η-axis. The ξ-axis completes the rectalinear right-handed (ξ, η, ζ) coordinate system. When the ζ-axis lines up with the sun vector, no solar projection of the ζ-axis exists. The ambiguity is resolved by: lining up the ξ- and η- axes with the absolute X- and Y- axes for the case where the ζ-axis is vertical (lines up with the global Z-axis); otherwise, the ξ-direction is defined by the crossing the horizontal projection of the ζ-axis onto the ζ-axis. Note that the orientation of the sun-reflector coordinate system with respect to the absolute collector reference frame changes from point-to-point on the concentrator (see Example 4, Chapter 8).

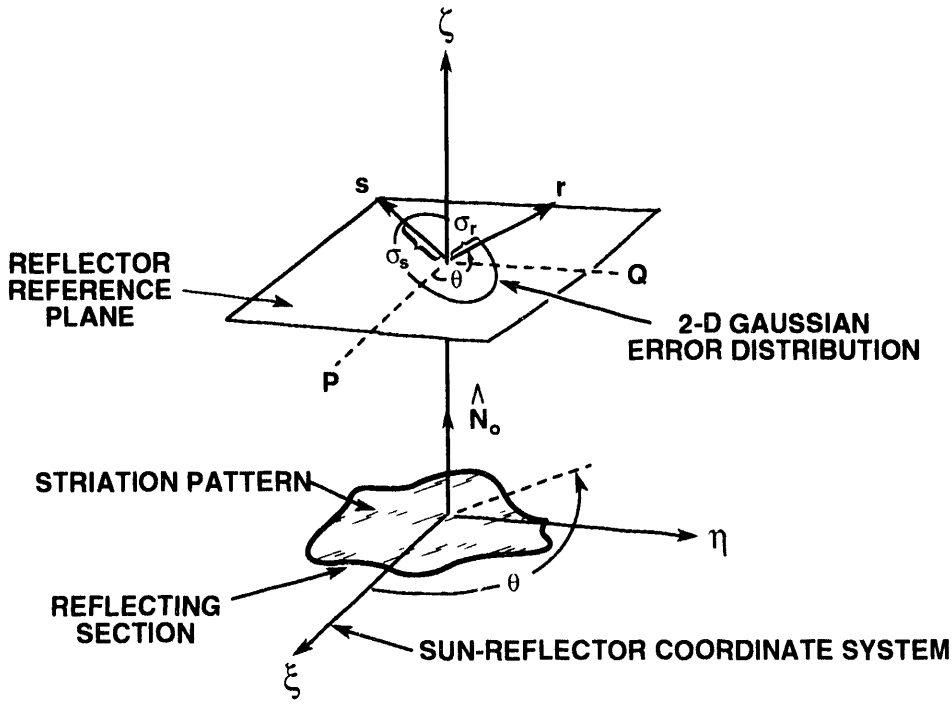

Figure 4.3 Concentrator Error Distribution on the Reflector Reference Plane.

In the figure, random surface roughness exists on the reflector, along with a slight striation pattern in the θ direction. This will tend to make the surface-normal less predictable in the direction perpendicular to the striations (*s* direction) than in the parallel (*r*) direction. A "**reflector reference plane**" at normal incidence to the ideal normal and at unit distance from the origin of the ξ–η–ζ system is also shown. The ellipse on the plane represents the 2-D elliptic normal error distribution arising from these surface imperfections. For this case, the parameter σ_r (SIGR) that describes standard deviation in the *r* direction would be smaller than σ_s (SIGS) which describes standard deviation in the *s* direction. The counter-clockwise rotation angle, Θ (TH), of the *r*-axis from the ξ-axis of the sun-reflector coordinate system is input in degrees.

For the other error types, corresponding error distributions are input in a like manner. Up to 5 concentrator error types are allowable. The quantity is controlled by the parameter NER. If errors are truly random without a predisposition in any direction), it is appropriate to model them with 1-D circular-normal distributions. These distributions, special cases of the elliptic-normal distribution, are used for most error types. Circular-symmetric Gaussian distributions result when the input quantities SIGR and SIGS are equal. In this case, Equation (4.10) reduces to:

$$E_{1D}(\tilde{r}) = \frac{1}{2\pi\sigma^2} exp\left[-\frac{\tilde{r}^2}{2\sigma^2}\right] \qquad (4.11)$$

where $\tilde{r} = [r^2 + s^2]^{1/2}$, and σ_r and σ_s are equal to the dispersion σ. In this case, the rotation angle θ is immaterial, and a dummy value is input for TH.

4.4 Calculating the Concentrator Error-Cone Distribution *E(P,Q)*

If two independent error distributions exist such that each direction of the first distribution is subject to the directional probability described by the second one, the resultant effective distribution can be obtained by mathematical convolution. Let both distributions be functions of the planar coordinates P and Q. One is described by $E_1(P,Q)$ and the other by $E_2(P,Q)$. The distributions combine to create a new distribution $E_{1,2}(P,Q)$. The value of the new distribution at some point ($P=P_o, Q=Q_o$) is described by the convolution integral

$$E_{1,2}(P_o, Q_o) = \int_{-\infty}^{\infty}\int_{-\infty}^{\infty} E_1(P_o - P, Q_o - Q)\, E_2(P, Q)\, dP\, dQ \tag{4.12}$$

The process of combining two elliptic-normal distributions by convolution integral is done analytically, as described in [3, Section 5.3]. If more than two error distributions are input, the third is convolved with the convolved product of the first two, etc., until all concentrator errors are accounted for. The result is the "**concentrator error-cone**" distribution, *E(P,Q)*.

The result of convolving many elliptic-normal distributions, even though their principal axes may not coincide (i.e., TH is not the same for all), is also an elliptic-normal distribution. In the event that all individual error distributions are 1-D circular-normal, the resulting error cone is a 1-D circular-normal distribution (Eq. 4.10) whose dispersion σ_t is related to the dispersions of the K_t individual errors by

$$\sigma_t = \sqrt{\sum_{k=1}^{K_t} \sigma_k^2} \tag{4.13}$$

4.5 Mapping the Error Cone into a Distribution *M(U,V)* of Directions for Ray Reflection

The error cone represents the probability function governing the likelihood that the actual surface-normal will assume a given direction. Naturally, this implies a distribution of possible directions for the reflected ray. We seek to obtain the latter distribution from the former one.

With reference to Figure 4.4, consider the solar central-ray incident on an element of reflector surface. The direction of incidence is given by the vector $\hat{A}$. The vector $\hat{B}_o$ indicates the direction of reflection that corresponds to the ideal surface normal $\hat{N}_o$. The **P-Q reflector-reference plane** is normal to $\hat{N}_o$, its P and Q axes aligned along the ξ and η sun-reflector axes. The **U-V reflected-ray plane** is normal to the central reflected-ray, its U axis being aligned with the ξ axis and its V-axis being orthogonal to U and $\hat{B}_o$. By definition, both planes are at unit distance from the point of incidence (though they are not depicted as such in the figure). Consider a perturbation of the surface-normal to the direction $\hat{N}$, while holding the direction of incidence $\hat{A}$ fixed. Where will the reflected ray pierce the U-V plane? For small angles between $\hat{N}$ and $\hat{N}_o$, the (U,V) coordinates where this occurs are related to the (P,Q) coordinates where the extension of $\hat{N}$ pierces the P-Q plane by the formulas

$$U = 2P\cos\mu \tag{4.14}$$

$$V = 2Q \tag{4.15}$$

These relations are used to transform the concentrator error-cone distribution $E(P,Q)$ in the reflector reference plane to a distribution of directions that a reflected ray may be expected to take. The latter distribution is termed the "**mapped (projected) error cone distribution**", $M(U,V)$, and is described in terms of (U,V) coordinates in the reflected-ray reference plane. The details of the mapping are given in [9] and [3, section 5.4]. It turns out that, whether the error cone is elliptic-normal or circular-normal, the mapped error-cone on the reflected-ray plane is elliptic-normal, having a form represented by Equation (4.10), [except for the combination of normal incidence, $\mu=0$, and a circular-normal error cone $E(P,Q)$, in which case the mapped error-cone defaults to a 1-D circular-normal distribution in the form of Equation (4.11)].

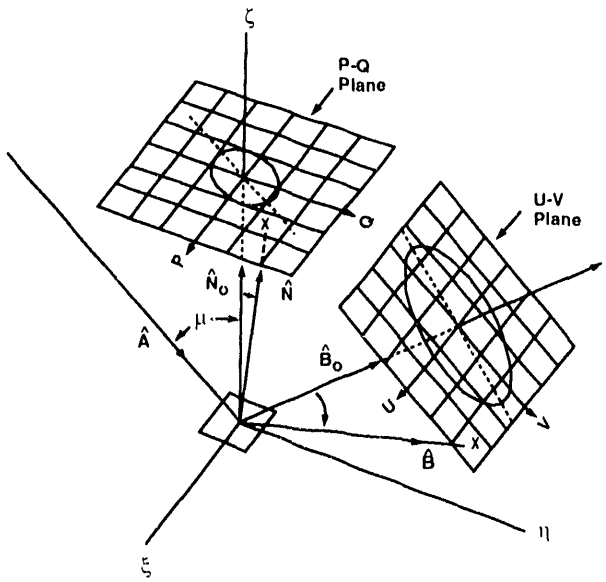

Figure 4.4 Mapping the Error Cone from the Reflector (P-Q) Reference Plane to the Reflected-Ray (U-V) Reference Plane.

4.6 Convolution of the Sunshape with the Mapped Error-Cone

The approximation is made that all rays within the incident solar cone may be expected to reflect in a spread of directions given by the mapped error-cone. This is not strictly true because the mapped error-cone is derived based upon the *nominal* incidence angle μ between $\hat{A}$ and $\hat{N}_o$, though the incidence angle actually varies over the cone of rays. However, the approximation is a good one since the small solid angle occupied by the solar cone guaranties that only small deviations about the nominal incidence angle exist within the cone. If the above approximation is taken as exact, a convolution of the mapped error-cone and sunshape distributions results in the **effective sunshape distribution** (*ESUN (U,V)* of Equation (2.5)) describing the reflected solar image.

The mapped error-cone distribution on the reflected-ray plane is ordinarily 2-D elliptic-normal, whereas the sunshape distribution on this plane (Figure 4.1) is always 1-D circular-symmetric, though usually not circular-normal because in most cases a Gaussian distribution is not a realistic sun model. Thus, in general, an elliptic-normal distribution is convolved with a circular-symmetric (non circular-normal) distribution to obtain a 2-D effective sunshape. Strictly, this operation must be done by approximate numerical techniques, and can be quite expensive. However, several options exist to approximate the effective sunshape to various levels of accuracy with corresponding reductions in computational effort. As explained in Section 4.6.3, the reflected solar image changes from point-to-point on the concentrator, and, strictly, should be recalculated at each subfacet. In most cases, however, this is unnecessary and could get prohibitively expensive. The next three sections explain the options for controlling the convolution process. Since imprudent use of these options can result in needless and excessive computer run-time and/or large inaccuracies in the predicted flux distribution, a fourth section provides recommendations for appropriate use of the convolution parameters.

4.6.1 IDIM: 1-D vs. 2-D Effective Sunshape

IDIM controls the dimensionality of the mapped error-cone and, thus, the effective sunshape.

IDIM = 1- 1-D approximatin to 2-D mapped error-cone
2 - 2-D mapped error-cone

IDIM=2 preserves the 2-D elliptic-normal character of the mapped error-cone that, when convolved with the circularly-symmetric sunshape, results in a 2-D effective sunshape. IDIM=1 causes the mapped error-cone to be approximated with a 1-D circular-normal distribution of equivalent root-mean-square radius, where *rmsr* for a normalized 2-D distribution *M(U,V)* is given by

$$rmsr_{2-D} = \sqrt{\int_{-\infty}^{\infty}\int_{-\infty}^{\infty} (U^2+V^2)\,M(U,V)\,dU\,dV} \qquad (4.16)$$

Equating (4.7) and (4.16) provides a relation for the dispersion of the 1-D Gaussian approximation to the 2-D mapped error-cone. The mapped error-cone distribution then takes the form of Equation (4.5) or (4.11), and convolution with the sunshape results in a 1-D (usually non-Gaussian) distribution. The operations represented by evaluating Equation (4.16) and substituting into (4.7) result in a simple algabraic formula [3, section 5.4.3] relating the dispersion σ to the standard deviations along the principal axes of the error cone $E(P,Q)$. Evaluating this formula is less involved than obtaining the standard deviations and principal directions of $M(U,V)$ by the mapping process of Section 4.5, and therein lies the computational advantage of choosing IDIM=1. The tradeoff is that the reflected solar image loses its 2-D character. The relative merits of choosing IDIM=1 or IDIM=2 are discussed in Section 4.6.4.

4.6.2 IANLYT: Numerical vs. Analytic Convolution

The IANLYT parameter dictates whether numerical or analytic procedures are used to convolve the sunshape and mapped error-cone distributions.

IANLYT = 1 - analytic convolution
0 - numerical convolution

At the expense of some accuracy, much computational effort can be saved by convolving the sunshape and mapped error-cone distributions analytically, as opposed to numerically. This can be accomplished if the 1-D (non-Gaussian) sunshape is converted into an "equivalent" 1-D circular-normal (Gaussian) sunshape of comparable rms radius. When the IANLYT=1 option is chosen, the equations of Section 4.1 are used to construct a Gaussian approximation to the input sunshape. (When a Gaussian sunshape (JSUN=2) is input, IANLYT automatically defaults to 1.) Convolution with the mapped error-cone, whether treated as 1-D or 2-D, can then be performed analytically (see Section 4.4).

For IANLYT=0, the tabular or pillbox sunshape input is numerically convolved with the mapped error-cone (or its 1-D approximation if IDIM=1 has been selected). Fast-Fourier Transforms are used for numerical convolution.

Figure 4.2 shows a tabular, a pillbox, and a Gaussian sunshape whose rms radii are equal. The semi-log scale somewhat disguises the physical differences between the tabular sunshape and its Gaussian approximation, which are quite significant. Even so, the two distributions will perform much the same in a convolution, provided the mapped error-cone has rms widths or standard deviations (see Equation 4.10) along its principal axes that are "large" relative to the rms width, or dispersion, of the sunshape distribution. Then, analytical convolution (IANLYT=1) can be used in preference to the more expensive numerical convolution with very little loss in accuracy. In contrast, when the rms widths of the mapped error-cone are "small" relative to the rmsw of the sunshape, analytic convolution is extremely innacurate, and numerical convolution (IANLYT=0) should be used instead. One might begin to be concerned about the accuracy of analytic convolution when the ratio of mapped error-cone rms width-to-sunshape rms width approaches 2, and should probably run an accuracy check against a numerically

convolved result when this factor drops below 1.5. Certainly, when the ratio falls below one, numerical convolution should always be used. CIRCE2 puts a warning in the **messages** file to alert users when the ratio is less-than or equal-to one. The rms widths of the sunshape and error-cone distributions are printed in the **output** file. If the IANLYT=1 option is chosen, the user should check this file for the rms values of the two distributions to determine whether the requirements for using this option have been met.

With regard to the accuracy of numerical convolution, the technique employed is robust provided the grid density is adequate to accurately resolve both the sunshape and mapped error-cone distributions. When the sunshape distribution varies abrubtly (the elliptic-normal mapped error-cone distribution is guaranteed to be smooth) or when the width scales of the two distributions are widely disparate, the numerical approach may be inaccurate. The present grid in CIRCE2 is probably sufficient to maintain acceptable accuracy over a range from 0.1 to 10 in the ratio of the mapped error-cone rmsw -to- the sunshape rmsw.

4.6.3 NEWCONV: Controlling the Number of Convolutions Performed

The angle of incidence μ between the nominal surface-normal $\hat{N}_o$ and the incoming central sun-ray changes from point-to-point on the concentrator. Correspondingly, the relative positioning of the reflector- and reflected-ray reference planes (whose orientations differ by the angle μ, Figure 4.4) also changes from point-to-point. This affects the mapping of the error-cone distribution, through Equation 4.14, and ultimately the effective sunshape distribution *ESUN(U,V)*. Ideally, a new convolution should be performed at every subfacet of the concentrator to most accurately capture the variation in the reflected solar image over the concentrator surface. However, since the calculation is relatively expensive (especially for the more accurate (2-D and numerical) convolution options), this may not be feasible or even advisable on cost/benefit basis. (This issue is explored in the next section.) Accordingly, the options also exist to reconvolve at just the center of each facet, or at only one location on the concentrator. The "degree" of convolution over the concentrator surface, *i.e.* the number and placement of locations at which a new effective sunshape is calculated, is controlled by the parameter NEWCONV:

NEWCONV = 1 - convolve only once at:
INCPICK = 1 - specified angle of indence (INCANGL)
2 - center/vertex of first facet listed in data file
2 - convolve at center/vertex of each facet
3 - convolve at center of each subfacet

NEWCONV=1, the "minimal" convolution option, directs CIRCE2 to calculate the effective sunshape at only one point on the concentrator, and to use this *ESUN* distribution when evaluating Equation 2.5 for each subfacet/target-point combination. Under this option, one of two accompanying options is selected via the INCPICK parameter.

For INCPICK=1 the user inputs the incident angle INCANGL (μ) through which the error cone is mapped before convolution with the sunshape to determine the *ESUN* distribution. To first order, the optimum value of INCANGL is $\bar{\mu}$, the average angle of incidence of sun rays striking the concentrator:

$$\bar{\mu} = \frac{1}{A}\int_S \mu dS = \frac{1}{A}\int_S acos\,(\hat{N}_0 \bullet \hat{V}_s)\,dS \tag{4.17}$$

where S represents the concentrator surface, A the concentrator surface-area, $\hat{N}_o$ the nominal surface-normal, $\hat{V}_s$ the unit vector pointing toward the sun, and *acos*( ) the inverse-cosine function. Unfortunately, the integral does not appear to succumb to analytic integration even for standard spherical and parabolic geometries. The user might opt for numerical integration (especially for faceted concentrators), or might simply estimate a value for $\bar{\mu}$. For axisymmetric geometries, a practical and effective approximation to $\bar{\mu}$ may be found in the manner outlined in Appendix B. There, an approximate $\bar{\mu}$ is derived for the common case of a parabolic dish of rim-radius R and focus f that is on-axis with the sun. The result is

$$\bar{\mu}\,(R,f) \approx acos\,(\hat{N}_{avg} \bullet \hat{z}) = acos\,(\,[1 + [R/(3f)]^2]^{-1/2}\,) \tag{4.18}$$

As explained in Appendix B, the use of this simple equation can increase the accuracy of the NEWCONV=1 option by over an order of magnitude.

The other choice available for the parameter INCPICK is INCPICK=2. With this selection, the convolution is performed at the center/vertex of a continuous-surface dish concentrator or at the center of the first facet listed in the data file for a faceted concentrator. For the latter, it is advisable that the first facet input be one whose normal-direction at the facet vertex makes a representative angle, *i.e.* $\bar{\mu}$, with the incident solar central-ray. A facet located about 2/3 of the way out from the vertex of the concentrator is probably appropriate.

Since the NEWCONV=1 option is much faster than the other NEWCONV choices, by careful selection of INCANGL for INCPICK=1, or of which facet to list first if INCPICK=2, execution time can be cut dramatically without a corresponding loss in accuracy.

NEWCONV=2, the "intermediate" convolution option, directs CIRCE2 to perform a new convolution at the center/vertex of each facet of a multiple-facet concentrator.

NEWCONV=3, the "full" convolution option, directs the program to calculate anew the reflected solar image at the center of each subfacet of the concentrator.

4.6.4 Appropriate Choice of Convolution Options

Along with concentrator subdivision, the convolution options outlined in the three sections above can affect accuracy and execution-time dramatically. One must subdivide the concentrator (into subfacets) and select convolution options in an integrated fashion, as improper choice of the convolution options can impair improvements in accuracy that finer concentrator subdivision should produce. Moreover, since the cost of concentrator subdivision is tightly coupled to the convolution options, it is important not to invoke parameter combinations that provide only marginal increases in accuracy at relatively large cost, thereby spuriously constraining the degree to which the concentrator can be economically subdivided. Respecting the tradeoff between accuracy and computational cost, this section provides guidance for optimal use of the convolution options. A detailed quantitative study of the effect of convolution options on predictions and execution times is presented in Appendix B. Based on this and other convolution studies, the following strategy is suggested:

I For a faceted concentrator with less than 15-20 facets, the parameter combination IDIM=2/IANLYT=0/NEWCONV=2 should be used. This will result in essentially the same accuracy as the (most accurate) IDIM=2/IANLYT=0/NEWCONV=3 combination, but at a much reduced cost.

II For a faceted concentrator with more than about 20 facets or for continuous-surface concentrators, the following are more appropriate options:

i) If the user either: a) has a fast computer or a lot of time and/or only wants to run one simulation and be done with it, or b) does not have a good estimate of μ and/or knows absolutely nothing about the relative rms widths of the mapped error-cone and sunshape distributions, then the combination IDIM=1/IANLYT=0/NEWCONV=3 should be used. This combination of parameters requires minimal user involvement and typically matches the accuracy of full 2-D numerical convolution to within 1% in 1/40 the CPU time. Though optimally fast for the degree of robustness exhibited, this parameter combination is relatively inefficient compared to the parameter sets below, which apply under more narrow sets of conditions and require more involvement of the user.

ii)With a little more user involvement, more accurate and efficient parameter combinations than the above may be invoked. Before proceeding, if nothing is known about the relative widths of the sunshape and mapped error-cone distributions, then a quick, inexpensive run with the settings IDIM=1/IANLYT=1/NEWCONV=1 should be performed. The resulting **output** file should be examined for the widths of these distributions. This information directs the user to one of two approaches:

*a)*If, according to the criteria of section 4.6.2, a relatively *narrow* error cone exists, then the combination IDIM=2/IANLYT=0/NEWCONV=1 gives accuracy to within 0.1% of full 2-D numerical convolution in 1/300 the CPU time. Moreover, if a good approximation to μ is supplied via the INCPICK=1/INCANGL parameters, accuracy to within 0.01% results at

no additional cost. The same effect can be obtained with the INCPICK=2 option by listing, as the first facet in the data file, a facet that is about 2/3 of the way out from the vertex of the concentrator.

b) If, according to the criteria of section 4.6.2, a relatively *wide* error cone exists, then one of two approaches is taken:

1) If a good approximation to $\bar{\mu}$ is available or if a certain facet is known to have at its center/vertex a normal that makes with the solar central ray an angle representative of $\bar{\mu}$, then two distinct options exist:

A) For scoping or parametric studies where speed is relatively more important than accuracy, the recommended parameter combinations are, as the case may be, IDIM=1/IANLYT=1/NEWCONV=1/ INCPICK=1/ INCANGL $\approx \bar{\mu}$ or IDIM=1/IANLYT=1/NEWCONV=1/INCPICK=2/appropriate facet listed first. These parameter sets typically match the accuracy of full 2-D numerical convolution within 1% in 1/1800 the execution time.

B) For final results where accuracy is the dominant concern, the recommended parameter combinations are, as the case may be, IDIM=2/IANLYT=0/NEWCONV=1/INCPICK=1/ INCANGL $\approx \bar{\mu}$ or IDIM=2/IANLYT=0/NEWCONV=1/INCPICK=2/appropriate facet listed first. These parameter sets typically match the accuracy of full 2-D numerical convolution within 0.2% in less than 1/270 the execution time.

2) If a good approximation to $\bar{\mu}$ is *not* available and, for faceted concentrators, it is also not known which facet is most "representative", then two distinct options exist:

A) For scoping or parametric studies where speed is relatively more important than accuracy, the appropriate choice is IDIM=1/IANLYT=1/NEWCONV=3. This parameter set typically matches the accuracy of full 2-D numerical convolution within 1.3% in about 1/880 the execution time.

B) For final results where accuracy is the dominant concern, the recommended parameter set is IDIM=1/IANLYT=0/NEWCONV=3. This parameter set typically matches the accuracy of full 2-D numerical convolution within about 0.9% in 1/36 the execution time.

It should be emphasized that in trying to keep within a given CPU budget, going to less expensive convolution options than those suggested here in order to get an even finer division of the concentrator surface will probably be counter-productive. Fortunately, in many cases the recommended parameter sets are among the least costly.

5 TARGET/RECEIVER MODELING

This chapter explains the process of generating target geometry and imposing a grid of points on the target surface. It is also convenient here to discuss output of analysis results, which includes flux distribution and "hit" map over the target surface, total collected power, and optical disk efficiency. The integration schemes used in determining total power are also addressed.

5.1 Target Geometries, Coordinate Systems, and Mesh Generation

CIRCE2 can be used to determine the flux distribution on targets of custom shape (see Section 5.3). Beyond this, the flux distribution can be integrated to determine total collected power for targets of certain characteristic geometries. This section and the next pertain to these characteristic geometries. In particular, surfaces of spherical, cylindrical, and conical (upright or inverted) contour can be modeled, as well as planar targets of circular or rectangular aspect. Such targets are not limited to complete shapes, i.e., just the frustrum of a cone may be analyzed, or only a small angular section of the frustrum as opposed to the full axisymmetric region. Additionally, axisymmetric "hybrid" receivers can be constructed from multiple axisymmetric component shapes. Certain target shapes that cannot be properly handled are outlined in Section 5.5.

Targets are generated by a local **target coordinate system** whose basis is the translated but unrotated reference frame (1-2-3) shown in Figure 2.4. The target is moved relative to the concentrator by specifying the global coordinates (Xo,Yo,Zo) of the target-system origin. The origin is also referred to as the "center of generation" of the target. The target coordinate system may be cylindrical, spherical, conical, polar, or rectangular, depending upon the characteristic shape of the target. The target, which is a 2-D Riemannian surface, can be described by two curvilinear coordinates that lie in the target surface. This will be referred to as the **K-L parametric coordinate system**. The origin of the K-L system is at the parametric center of the target, referred to as the "center" of the target. All linear dimensions used in defining targets must be in meters and angular measures are in degrees.

A grid of points must be imposed over the target surface in order to determine the flux distribution. A mesh of up to 2601 points (51 in the K direction by 51 in the L direction) can be generated for each target entity. For curvilinear targets, K is in the azimuthal direction, and L is in the orthogonal direction. The grid is regular and rectangular in K-L parametric space (in the sense of section 2.4) but is not necessarily so in physical space. Examples will be presented later. For hybrid receivers, each component target can have a 51x51 grid of points. The number of grid points in each direction must be odd. Section 5.2.2 discusses the specific quadrature techniques used in CIRCE2 to evaluate total collected power once the flux distribution has been established.

> IMPORTANT: Integrated power has sometimes been found to be extremely inaccurate when the flux distribution is only slightly underresolved by the mesh. When using a sparse target mesh for scoping studies, a representative result should be verified against a run with a 51x51 mesh to check if unanticipated loss of accuracy with the sparse mesh has occurred.

5.2 Output of Analysis Results

As explained in Section 3.3, CIRCE2 creates several output files. This section concerns the most important information output: flux distribution and total collected power. Sample output information of the type described below is presented and explained further in the examples of Chapter 8, particularly Examples 2 and 3.

5.2.1 Convention for Output Distributions

CIRCE2 outputs two important distributions. The target flux distribution consists of the normally-incident flux at each of the grid points on the target. The "**hit map**" distribution indicates the number of subfacets reflecting energy to each target point. Flux distributions and hit maps are output in both list and matrix forms. In matrix form, rows and columns are associated with the two target-generation coordinates characteristic of the particular target shape (e.g. angular coordinates θ and ϕ for a spherical surface). A counting index, starting at the left-top entry in the matrix and ending at the right-bottom entry (using the regular left-to-right and top-to-bottom reading convention) is associated with each element of the matrix. This same numbering system is used to number grid points on the target surface, as examples below will demonstrate. In list form, information such as target-point index, flux, number of hits, and global X-Y-Z coordinates, are printed for each of the grid points. (Example 3 of Chapter 8 presents flux and hit map distributions resulting from a CIRCE2 run.)

5.2.2 Calculation of Total Collected Power

The flux distribution on the target surface is numerically integrated to determine the total collected power. In order to perform the quadrature, the target geometry is transformed to K-L parameter space as explained in the subsections of 5.4 for supported geometries. The integral transformation is explained by way of example in Section 2.4. The generalization of Equation 2.7 is:

$$\int_S F(K,L)\,dS = \int\int_S \tilde{F}(K,L)\,dK dL \tag{5.1}$$

where $\tilde{F}(K,L)$ is the Jacobian-weighted flux distribution over the transformed domain.

The transformed domain in K-L coordinates becomes a planar rectangle where the target mesh forms a regular rectangular grid of points. The integrand is known at each of these grid points, so integration is a matter of choosing an interpolation scheme to accomplish the quadrature. Two different algorithms are employed in CIRCE2, depending upon the target geometry:

For all target types, CIRCE2 uses a variant of the 9-point integration schemes ([3], Section 7.1) implemented in the HELIOS code. Appendix C summarizes the HELIOS schemes and derives the new 9-point method (here termed "Hogan's method")

that CIRCE2 uses. Essentially, Hogan's method uses the trapezoidal rule to integrate along the K-coordinate and Simpson's rule to integrate along L. It has been found (Appendix C) that Hogan's method gives results that are far less dependent upon limits of integration for axisymmetric targets and, by implication, it appears to be more accurate for other geometries than the HELIOS methods. For all targets, the Jacobian is either constant or varies only as a function of L. Additionally, the conventions adopted in CIRCE2 are generally expected to result in flux distributions that will exhibit greater variation along L than along the K, or azimuthal, direction. The combined effect of these two factors is that the integrand of Equation 5.1 is expected to vary much more rapidly in L than in K. Appropriately, Hogan's method affords greater resolution in the L-direction.

For flat-target quadrature, a slightly more accurate but much more expensive Legendre-Gauss/Newton-Cotes algorithm is used in addition to Hogan's 9-point scheme. It employs the Sandia SLATEC library routine QAGS (adaptive Legendre-Gauss technique) to integrate in the K-direction, and the more robust Newton-Cotes adaptive algorithm QNC79 to integrate the relatively rapidly varying function in the L-direction. Although the results from both methods are reported, whenever flat targets are analyzed the answer from the Legendre-Gauss/Newton-Cotes algorithm is used in subsequent calculations and is the value reported in the results summary tables.

5.2.3 "Optical Disk Efficiency" Table for Flat Circular Targets

For flat circular targets, a table labelled "Optical Efficiency for Aperture Disk" is created. It posts cumulative integrated power versus radius for "aperture disks" of increasing size that are concentric with the physical target. Collection efficiencies versus radius are reported based upon two denominators: total power incident on the target and total power incident on the unshaded concentrator. These efficiencies are relevant in making decisions involving tradeoffs between aperture size, which affects the competing effects of flux spillage and receiver losses, and receiver size, which affects concentrator shading but also has other driving factors. (Example 2 of Chapter 8 presents the optical efficiency table resulting from a CIRCE2 run.)

5.3 User-specified Custom Targets, ITARSH=2

In CIRCE2, the capability exists to determine the incident flux at any given point(s) in space, or the distribution of flux on a target whose geometry does not conform to the supported shapes described in Section 5.4. This capability is invoked by selecting ITARSH=2 during the DEKGEN2 session and either interactively specifying the spatial coordinates (XTA, YTA, ZTA) at each point and direction cosines VMTx, VMTy, and VMTz of the normal-vector, or by naming a file to be read-in that contains this data. The parameter NTART specifies the number of target grid-points to be input (NTART≤2601). The price of maintaining freedom in target geometry and grid-point placement is that the resulting flux distributions are not integrated by CIRCE2. However, standard Finite Element technology [15] may be employed to integrate over arbitrary target geometries

where the flux has been determined at irregularly placed points. In the special case where grid placement satisfies the conditions stipulated in Section 2.4, e.g. grids generated with boundary-fitted coordinates [16], the more convenient method of integration explained in Appendix C may be used.

5.4 Standard Target Shapes

The following are the choices for the target geometries that CIRCE2 supports. All but choice #2 involve "standard" geometries over which an integration for total incident power is performed. Choice #2 is addressed in Section 5.3, all other choices are described in individual subsections below.

ITARSH =
- 0 - Flat rectangular target
- 1 - Spherical target section
- 2 - Custom target, user-supplied subroutine
- 3 - Cylindrical target section
- 4 - Conical target section
- 6 - Flat circular sector
- -N - Hybrid receiver made up of N components

5.4.1 Flat Rectangular Target: ITARSH=0

Figure 5.1a shows a rectangular target in X-Y-Z space. Rectangular targets are restricted to having horizontal top and bottom edges (*i.e.* to be parallel to the planes defined by the 1-2 and X-Y axes). Since the target is flat, its center and center of generation coincide, and the parametric K-L coordinate system, whose origin is at (Xo,Yo,Zo), is used to generate the target. The K-L system defines the plane of the target. Orientation is established by the rotation angle α (ALPHA) and tilt angle β (BETA) of the (+)L-axis as shown. The tilt angle BETA is the acute angle that the axis (and target) makes with the horizontal 1-2 plane. The angle must be non-negative (giving the L-axis an upward component for nonzero BETA). The target is rotated by rotating the L-axis about the 3-axis of the local target system. The rotation angle ALPHA is counted positive from the 1- toward the 2- axis.

Figure 5.1b (opposite Figure 5.1a) shows a typical rectangular target with its associated parametric coordinates. The *irradiated* side of the target (side facing the concentrator) is viewed *at normal incidence* (target lies in the plane of the page). This is the convention used for flux output for planar targets. For rectangular targets, the (+) K-axis is to the right and the (+) L-axis is up, resembling a conventional x-y right-handed coordinate system. The parameter KEXT defines length in the K direction, while LEXT defines length in the L direction. In generating the target grid, from 3 to 51 (must be an odd number) equally spaced points may be specified along the K direction (KPTS) and from 3 to 51 (must be an odd number) points in the L direction (LPTS). In the example, KPTS=3 and LPTS=5, yielding a regular rectangular grid of NTART=KPTSxLPTS=15 points. Note the grid point indexing scheme. Upon output, grid points are identified by

their (K,L) generation coordinates and the indexing scheme. The labeling system for the output flux distribution also makes use of this convention.

It is also possible to model a rectangular target which has a rectangular or circular hole in it. Such a case might arise in calculating spillage on a rectangular or circular aperture plate. The process is described in the next section.

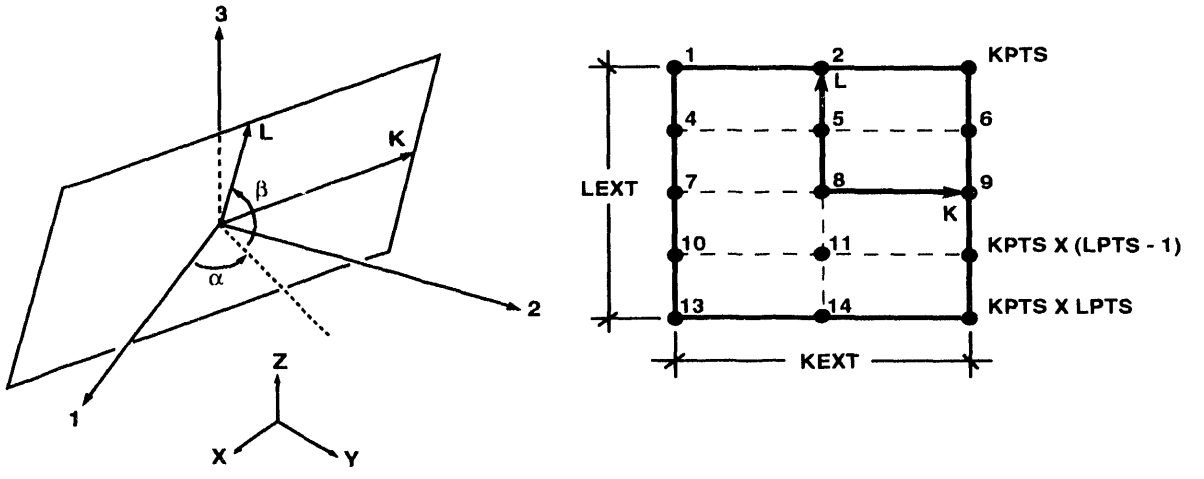

Figure 5.1 (a) Rectangular Target Orientation. (b) Flux Grid for Rectangular Target.

5.4.2 Flat Circular Target Sector: ITARSH=6

A flat circular target can be defined with a cylindrical coordinate system, as is done when it is part of a hybrid receiver (Section 5.4.6) or with a polar coordinate system (ITARSH=6). As explained here, the ITARSH=6 option allows the target to be tilted, whereas the other option does not. To orient the flat target, a *virtual* K-L coordinate frame that lies in the plane of the target, as shown in Figure 5-2, is used. The K-L system, thus the target, is oriented by the same process described in Section 5.4.1 above. Thus, the rotation angle α (ALPHA) and tilt angle β (BETA) controlling the orientation of the K-L system are as depicted in Figure 5.1a. The target generation system becomes a polar (R, θ) system in which θ is measured positive from the (+)K-axis to the (+)L-axis.

A target mesh of RPTS (from 3 to 51, odd) equally spaced radial points by TPTS (from 1 to 51, odd) equi-angular points may be generated. The outside radius of the target (RMAX) and total angular span (THETAMAX) must also be input. [Whenever the user specifies a full circular target (THETAMAX=2π), an Optical Disk Efficiency table is generated (see Section 5.2.3)]. Figure 5.2 diagrams a THETAMAX=90 degree circular target section. Node numbering corresponds to RPTS=5 and TPTS=3. Grid points are identified by their (R, θ) generation coordinates in the output flux table. For the purposes of numerical integration, L of Section 5.2.2 becomes R, and K becomes θ.

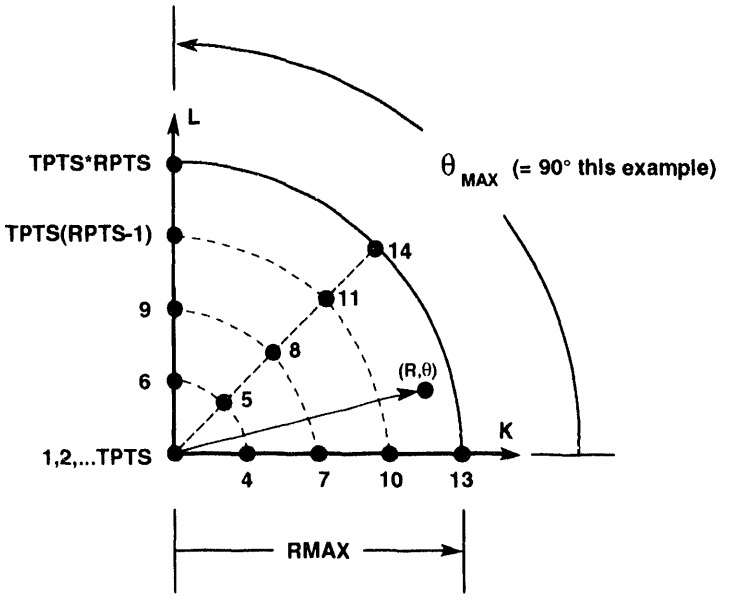

Figure 5.2 Geometry and Flux Grid for a Circular Target Section.

IMPORTANT:
Circular targets generated with ITARSH=6 are different from those generated for use as a component of a hybrid receiver (Section 5.4.6). For ITARSH=6, θ is measured relative to the virtual K-L system, which can have any number of orientations relative to the 1-2-3 target system, as specified by the user. When a circular target is part of a hybrid receiver, the geometry and node numbering may be obtained as a special case of a conical receiver (Section 5.4.5) with zero height and zero top radius. In particular, the target is constrained to be perpendicular to the 3-axis, and θ is counted positive when proceeding from the 1- toward the 2- axis. This is *opposite* the direction of positive θ when an untilted circular target is created with ITARSH=6. Likewise, the azimuthal indexing of target grid points is opposite for the two cases. This can be a possible point of confusion unless the user is forewarned. In either case, the global (X,Y,Z) coordinates output for grid points alleviates any ambiguity.

For flux distributions with azimuthal symmetry, it is only necessary to obtain variation in flux along a target radial line. Such a flux distribution would be expected to exist, for example, on an uncanted circular target whose center is pierced by the axis of a one-piece axisymmetric dish that is on-axis with the sun. This is a common configuration. In this case, the user can reduce execution time significantly by assigning TPTS=1 (THETAMAX=2π is obligatory in this case).

In some cases, it may be desirable to model flat targets with circular or rectangular holes in them. Such a case might arise, for example, in finding the spillage on the annular aperture plate shown in Figure 5.3. To find the flux distribution, the ring would be first modeled as a circular target. To find the total power incident on the ring,

a second run would be made with the target diameter equal to the inside diameter of the aperture plate. Total integrated power from the second run would then be subtracted from results of the first run to determine the spillage.

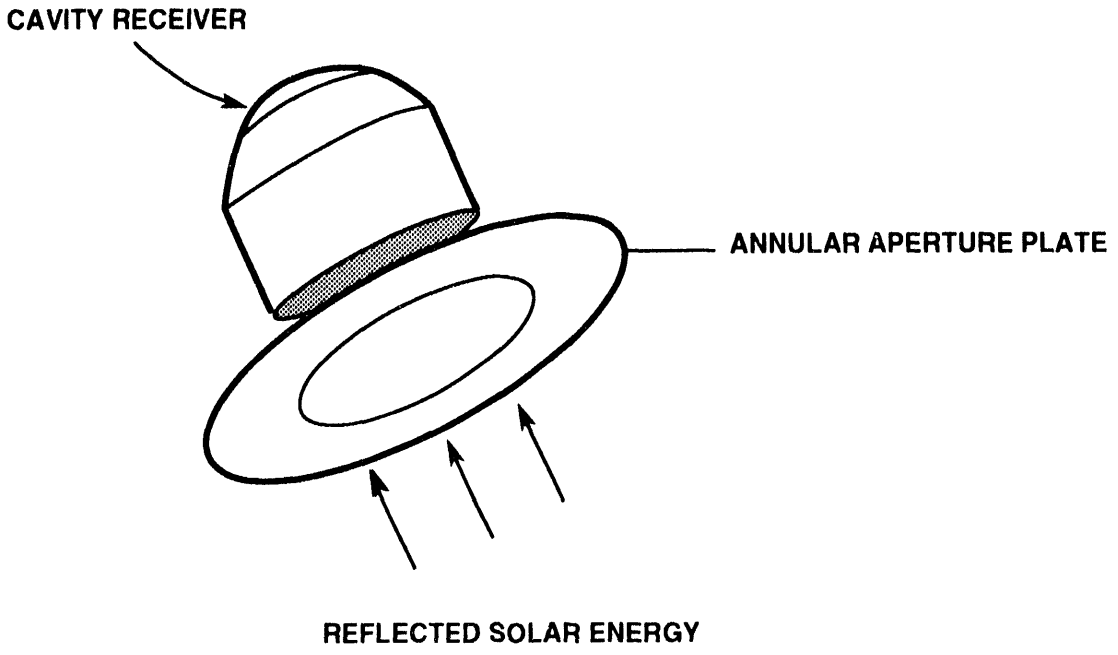

Figure 5.3 Spillage on Annular Aperture Plate.

5.4.3 Spherical Target Section: ITARSH=1

To generate spherical target sections, a spherical coordinate system is used. Figure 5.4 demonstrates the use of this system to generate a section of a spherical surface. Note that any portion of a spherical surface, such as the one shown, can be analyzed. The target center point (origin of the K-L parametric coordinate system) is first established by specifying radius of curvature RCURV (ρ) and angular coordinates THETAC (θ_c) and PHIC (φ_c) of the target center. (Note that with the definition of target center used here, PHIC for a concave-down hemisphere would be $\pi/4$.) The parametric coordinate K corresponds to the direction of increasing θ and the L coordinate lies in the direction of increasing φ.

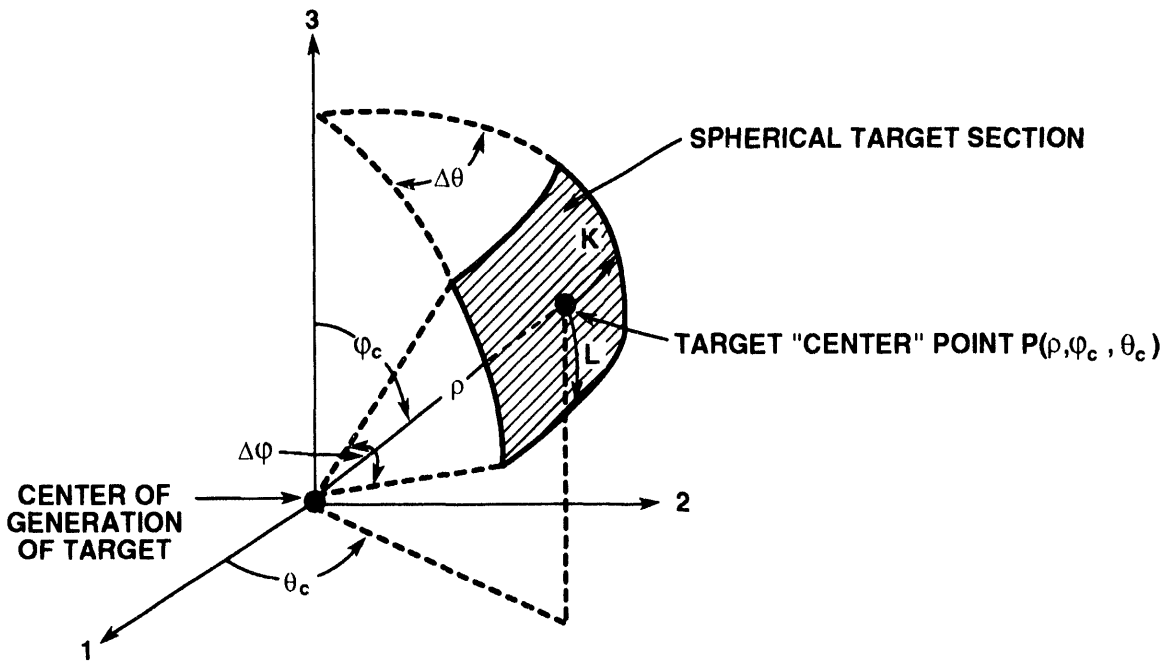

Figure 5.4 Spherical Target Generation Parameters.

The dimensions of the target, $\Delta\theta$ and $\Delta\varphi$, are given by KEXT and LEXT, respectively. Figure 5.5 depicts the node numbering scheme for a spherical target section. In the example, KPTS=5 and LPTS=7. KPTS must be an odd integer from 3 to 51 and LPTS an odd integer from 3 to 51. Grid points are identified by their (θ, φ) generation coordinates in the output flux table.

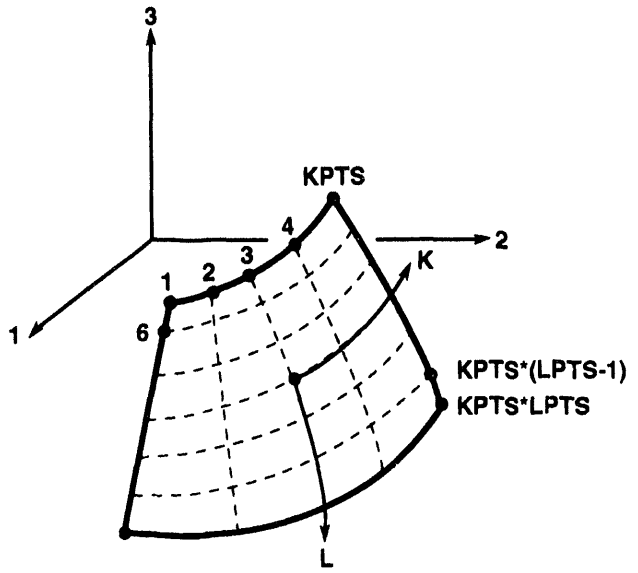

Figure 5.5 Flux Grid for Spherical Target Section.

5.4.4 Cylindrical Target Section: ITARSH=3

For cylindrical target sections, a cylindrical coordinate system like that shown in Figure 5.6 is used. The target center-point location is established by defining the appropriate radius RADIUS (r) and angle THETAC (θ_c). The target center is restricted to be in the 1-2 plane (z=0). The parametric coordinate K corresponds to the direction of increasing theta, and the L coordinate runs *opposite* the direction of increasing z.

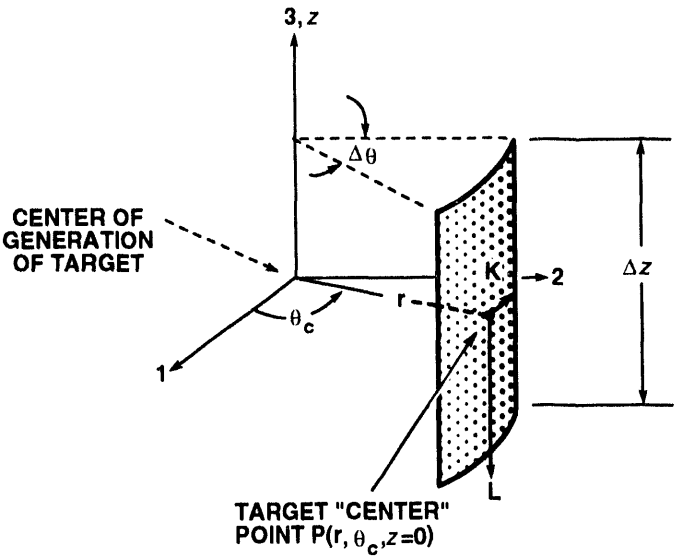

Figure 5.6 Cylindrical Target Generation Parameters.

The dimensions of the target, $\Delta\theta$ and Δz, are given by KEXT and LEXT, respectively. Figure 5.7 illustrates the node numbering scheme for the target section. In the example, KPTS=5 and LPTS=9. KPTS must be an odd integer from 3 to 51 and LPTS an odd integer from 3 to 51. Grid points are identified by their (θ, z) generation coordinates in the output flux table.

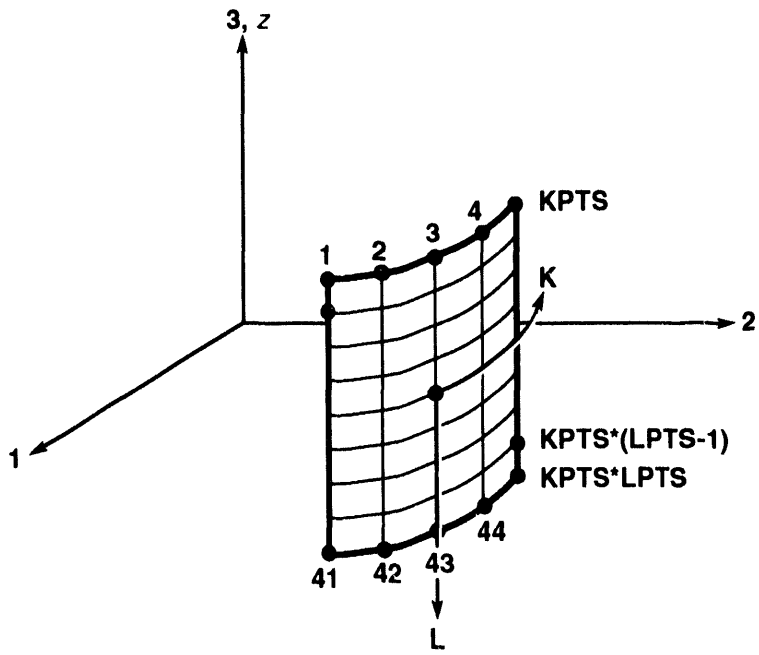

Figure 5.7 Flux Grid for Cylindrical Target Section.

5.4.5 Conical Target Section: ITARSH=4

Conical target sections are generated with a cylindrical coordinate system as shown in Figure 5.8. The parametric coordinate K corresponds to the direction of increasing θ, and the L coordinate lies in the surface of the cone as shown. Target generation can be accomplished with the two coordinates (θ, z), since the r-coordinate can be written as a function of z, using the fact that the surface is part of a right circular cone. The target parametric center is restricted to be in the 1-2 plane (z=0). Because the z coordinate does not lie in the surface of the cone, it must be related to the surface coordinate L by specification of the bottom and top radii of the section, RBOT and RTOP. With this formulation, it is only necessary to define the angle THETAC (θ_c) to the parametric center of the target. In DEKGEN2, the value input for LEXT is the height, Δz, of the section, though this is not really the target extent in the parametric direction L. KEXT is the angular extent, $\Delta\theta$, of the section.

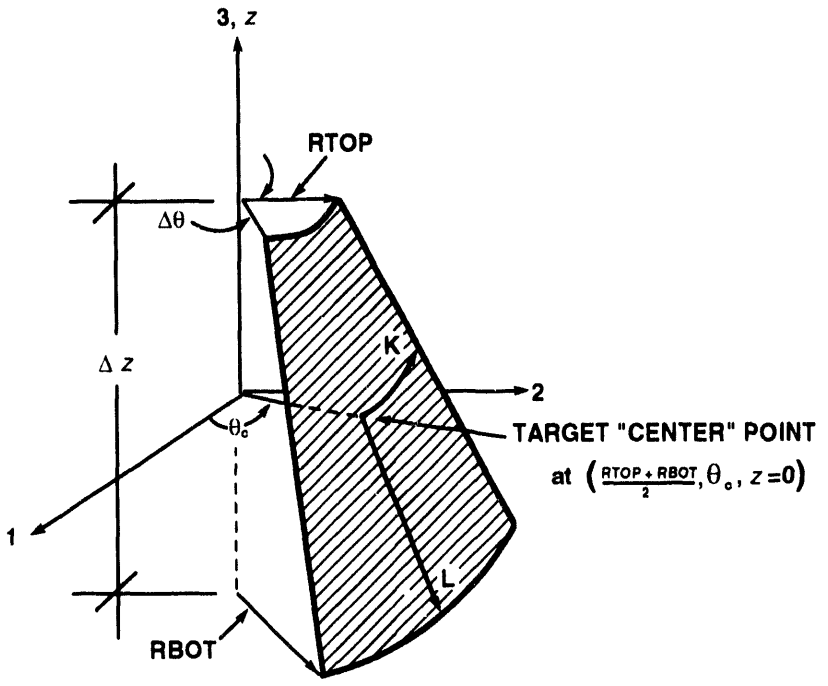

Figure 5.8 Conical Target Generation Parameters.

KPTS divides the cone in the θ direction and LPTS divides it in the *L* direction. A mesh with KPTS=3 and LPTS=5 is pictured in Figure 5.9. KPTS must be an odd integer from 3 to 51 and LPTS an odd integer from 3 to 51. Grid points are identified by their (θ, *z*) coordinates in the output flux table.

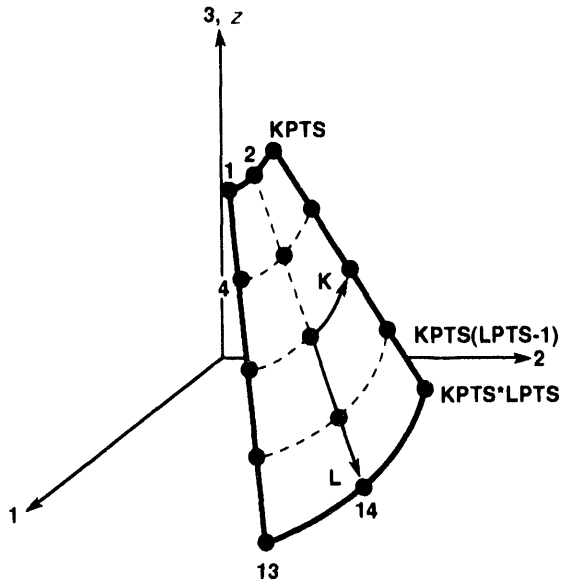

Figure 5.9 Flux Grid for Conical Target Section.

5.4.6 Hybrid Receivers: ITARSH=-N

Axisymmetric cavity-type receivers are an integral part of modern point-focus collector systems. The capability to easily build and analyze internal and external receivers of widely varying geometry is included in the present analysis package. Additionally, for hybrid receivers, CIRCE2 can output a data file for input to the cavity-receiver thermal analysis code AEETES [18]. Thus, a fairly seamless capability to model these types of collector systems has been established.

The user should be aware that there are limitations to properly posed geometries, as the *WARNING* in the next section explains in greater detail. DEKGEN2 interactively guides the user through the construction steps necessary to build geometrically correct targets that do not violate the restrictions. If a hybrid receiver is built without using DEKGEN2, deliberate care must be taken to meet these considerations. A good understanding of the target-generation coordinate systems of the individual component types is needed in order to construct targets that do not have overlapping sections or leave gaps in the receiver walls. In short, it is best to use DEKGEN2 to build and reposition these more complex receivers.

Hybrid targets may be constructed from axisymmetric ($\Delta\theta = 2\pi$) cylindrical, conical, spherical, and flat-circular component shapes. DEKGEN2 is alerted that the receiver will be a hybrid target when the choice for the parameter ITARSH is input as a negative integer, $-N$, where N is the number of component shapes that the receiver will be constructed from. The receiver is generated from the bottom up, with the local target coordinate system having its origin at the center of the receiver aperture. (The aperture is the opening at the bottom of the receiver.) Just as for the other target types described above, the local target coordinate system remains unrotated relative to the collector frame, but can be moved about by specification of the collector-system coordinates (Xo,Yo,Zo) of its origin. Points on the target mesh are defined in global (X,Y,Z) coordinates, and the fluxes are reported in terms of a local (r,θ,z) cylindrical system in the output flux table.

> Note that results for spherical and flat-circular targets generated with the hybrid target option are output in terms of cylindrical coordinates rather than in the natural coordinates used in the ITARSH=1 and ITARSH=6 options. This can be a possible point of confusion unless the user is forewarned.

For each component, from 3 to 51 points are allowable in the azimuthal (K) direction and from 3 to 51 points in the L direction. Even though only physically axisymmetric receivers ($\Delta\theta = 2\pi$) can be analyzed, they can be *modeled* with sections of lesser angular extent in order to save computational time if flux distributions are expected to be cyclically symmetric (see Example 4 of Chapter 8 for an illustration of this case). For such analyses, collected power reported by the program will be proportional to the receiver area modeled. If only 1/4 of the receiver is modeled for a quarter-symmetric problem, the collected power output by CIRCE2 should be multiplied by four to obtain total power collected by the physical (axisymmetric) receiver. Thus, a receiver angular extent (KEXT) of less than 360 degrees is allowable for such cases, but the whole concentrator must still be modeled.

As with other target types (including custom (ITARSH=2) targets), the user may use DEKGEN2 to reposition (translate) hybrid receivers, perhaps to investigate effects of receiver axial positioning with respect to the focal plane of a parabolic dish. After the new (Xo,Yo,Zo) coordinates of the target-system origin are specified, DEKGEN2 automatically reconstructs the target in the new location (and defines the new coordinates of the associated aperture for hybrid receivers). Example 4 of Chapter 8 explains the steps involved in the creation of a four-component hybrid receiver.

5.5 Internal/External Receivers and Aperture Considerations

Curved surfaces may be designated as either internal or external receivers, depending upon the parameter INORM:

INORM = 0 - flat target
1 - internal receiver, energy is to be collected on the concave side
2 - external receiver, energy is to be collected on the convex side

Any rays hitting the side of the target not designated as the receiving side will be discounted. For flat targets, INORM is internally set to zero and the side of the target facing the concentrator is assumed to be the receiving side.

Allied to the choice of INORM is the parameter IAPT, which designates whether an aperture exists, and the type of aperture (circular or square) if it does exist.

IAPT = 0 - no aperture exists for the collector system
1 - rectangular aperture
2 - circular aperture
3 - internally generated circular aperture for axisymmetric receivers

If an aperture is specified, only reflected raysthat go through the aperture are allowed to strike the target if it is an internal receiver (INORM=1) or a flat target. If the target is an external receiver (INORM=2), only rays not passing through the aperture are allowed to strike the target surface. Figure 5.10 depicts reflected rays passing through an aperture. The aperture is defined by specifying the elements of the matrix AC(i,j) of the collector-system (X,Y,Z) coordinates for the ith corner point (i=1,4). As the figure suggests, the points are input in the order encountered when the aperture boundary is traversed in a clockwise manner as viewed by a ray entering the aperture. The aperture may be tilted with respect to the concentrator and does not have to be centered about the collector Z-axis. If it is tilted, the edges defined by the corners 1,2 and 3,4 must remain horizontal. That is, the Z coordinate of corners 1 and 2 must be the same, and the Z coordinate of points 3 and 4 must be the same. The four points must all lie in the same plane, and opposite edges of the rectangle must be equal in length. Appendix F outlines an algorithm by which the coordinates of the corner points can be calculated. Example 3 of Chapter 8 provides an occasion for such a calculation.

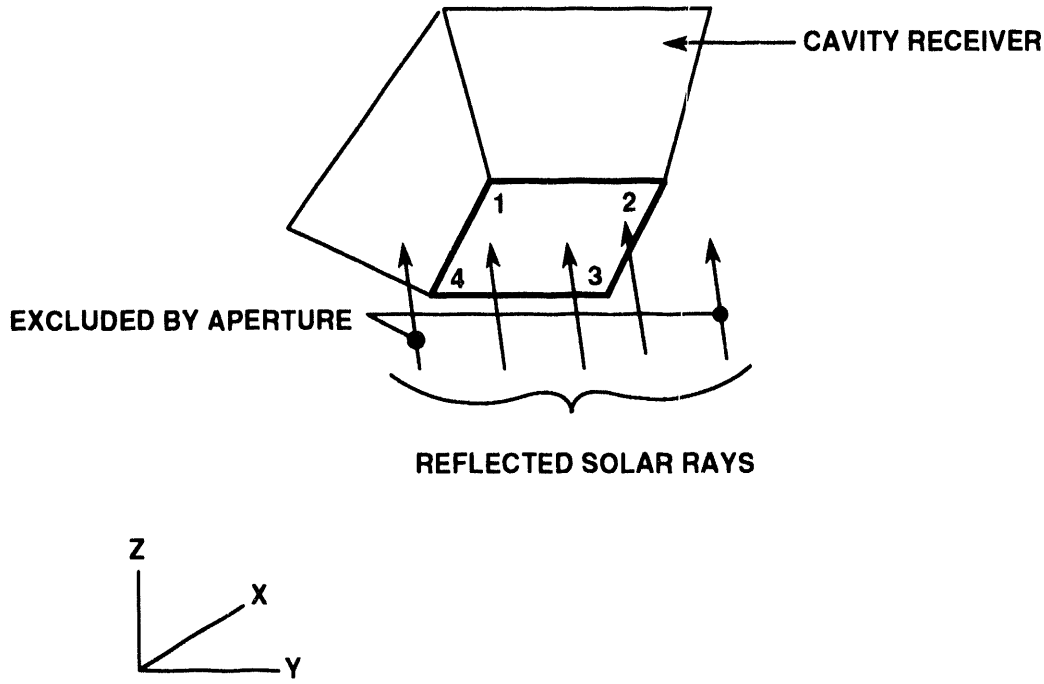

Figure 5.10 Geometry Convention for a Rectangular Aperture.

IAPT=2 indicates a circular aperture. A square can be inscribed within a circle such that its vertices lie on the circle. Conversely, if the four corners of a square are specified, the corresponding circle is also defined. Locating and orienting a circular aperture, then, is just a special case of the process used to define a rectangular aperture. The four points must lie in the same plane and all edge lengths must be equal. Even though they are defined similarly, the circular and rectangular apertures are treated differently in CIRCE2.

IAPT=3 should be chosen when analyzing full axisymmetric ($\Delta\theta = 2\pi$) receivers such as a cylinder, cone, hemisphere, or a hybrid combination of these shapes. All axisymmetric receivers have apertures defined by the target geometry. For example, the bottom opening of an internal cylindrical receiver is itself an aperture; only rays entering through the bottom can impinge upon the receiver surface. The choice IAPT=3 directs DEKGEN2 to generate the coordinates of the points that define the aperture. The resulting aperture is geometrically consistent with the target geometry, including hybrid receivers.

WARNING:

In general, when analyzing physical concave (internal) receivers that are not fully axisymmetric, such as the one shown in Figure 5.11, an aperture should not be defined because it will cut off rays that should be allowed to strike the internal surface. For example, ray 1 in the figure should be able to strike the target at point P1 even though it does not go through the aperture. However, not defining an aperture also has a drawback in that rays that should be cut off by the aperture will be allowed to strike the surface. If no aperture is defined, the program will allow ray 2 to strike the target at P2, even though this is not physically possible. Whether or not this is a problem depends on the target section being analyzed and the position (location and orientation) of the target relative to the concentrator. For some geometries the problem does exist, but the user should be aware of this fact when modeling concave targets that are not axisymmetric. When dealing with external receivers, problems of this nature do not exist.

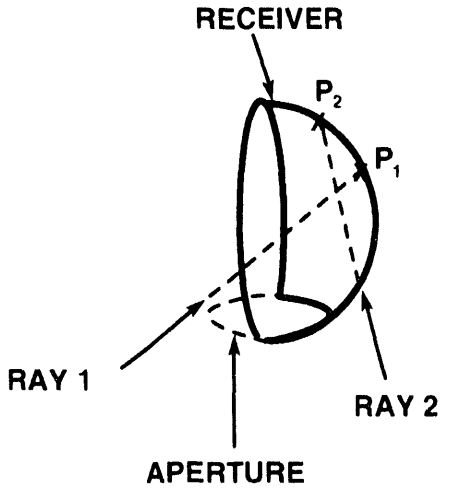

Figure 5.11 Conflict Arising from Modeling an Incomplete Axisymmetric Internal Receiver.

When modeling hybrid receivers, care should be taken to avoid geometries that exhibit multiple apertures. Such a case is illustrated in Figure 5.12. This hybrid cavity receiver is a combination of two inverted cone frustrums (components 1 and 2), a cylinder (component 3), and a flat circular disk (component 4). Aperture 1 is established automatically by DEKGEN2 when IAPT=3 is chosen. However, the second aperture at the junction of components 1 and 2 would not be accounted for, allowing the ray shown to strike component 3 as well as component 1, an instance of double-counting. Figure 5.13 shows

in cross section another cavity receiver that cannot be currently treated by CIRCE2. The back wall intercepts the ray; it should not be allowed to strike the side wall also, but does so with the present algorithm. CIRCE2 counts or ignores rays based upon which side of the target is the receiving side and whether it did (did not) pass through the aperture for an internal (external) receiver. The program does not determine whether a ray has already struck another part of the receiver when it counts or discounts rays. Using this knowledge, the user must carefully examine the receiver he wants to analyze and determine whether it is valid for this analysis code.

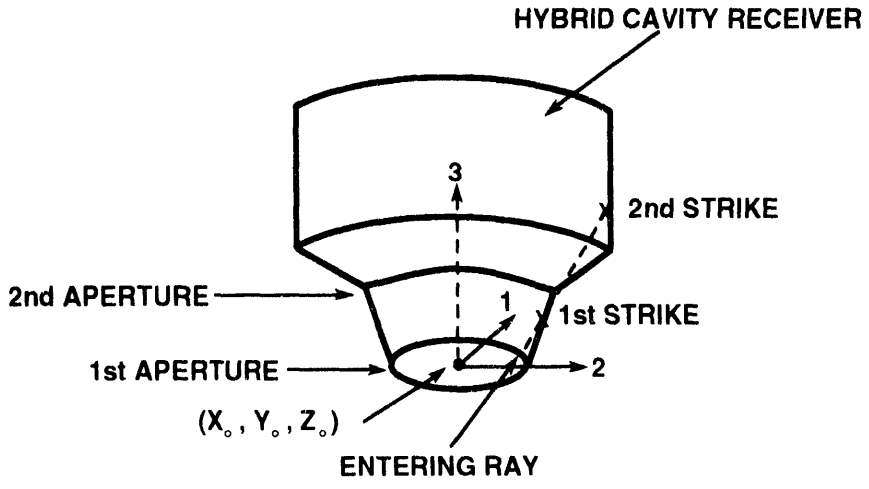

Figure 5.12 Hybrid Cavity Receiver with Multiple Apertures (not allowed).

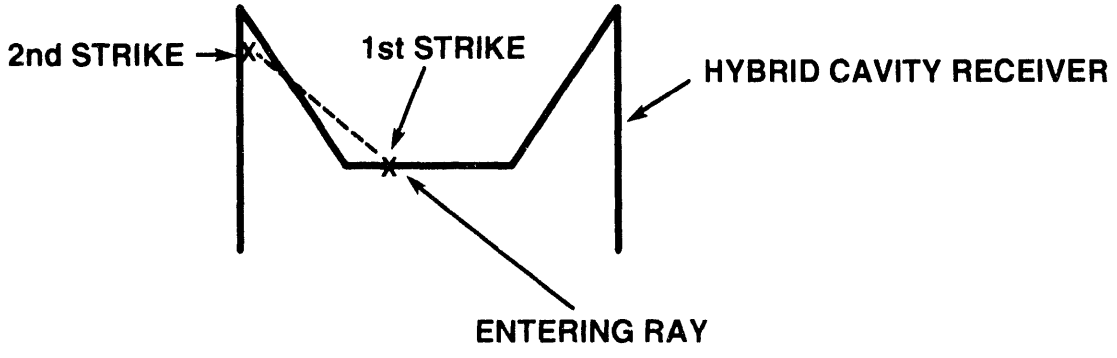

Figure 5.13 Cross-Sectional View of an Unallowable Hybrid Cavity Receiver.

6 REFLECTOR/FACET MODELING

A concentrator may comprise one or several reflectors. A continuous-surface reflector is called a "**facet**." CIRCE2 can analyze solar concentrators whose reflector(s) can be approximated with the facet shapes described below, or a combination of those shapes. If one is creative, almost any concentrator can be modeled with the available facet shapes. Of extreme importance is the subdivision of the facet into "subfacets," or reflector elements, each of which is treated in the manner described in Section 2.3.

6.1 Facet Projected Shape

Facet geometry is described by projected shape and contour. Figure 6.1 helps visualize the meanings of these terms. The facet shown has its vertex at the origin of the x–y–z "**facet coordinate system**" and its axis is along the z-direction. The facet has a spherical contour. Its projection onto the x–y plane is called its "**projected shape**." The centroid of the projected shape coincides with the origin of the facet coordinate system. In the example the projected shape is triangular. Projected shape is controlled by the parameter KORD. The following options are available.

KORD = 1 - circular
2 - rectangular
3 - equilateral triangular

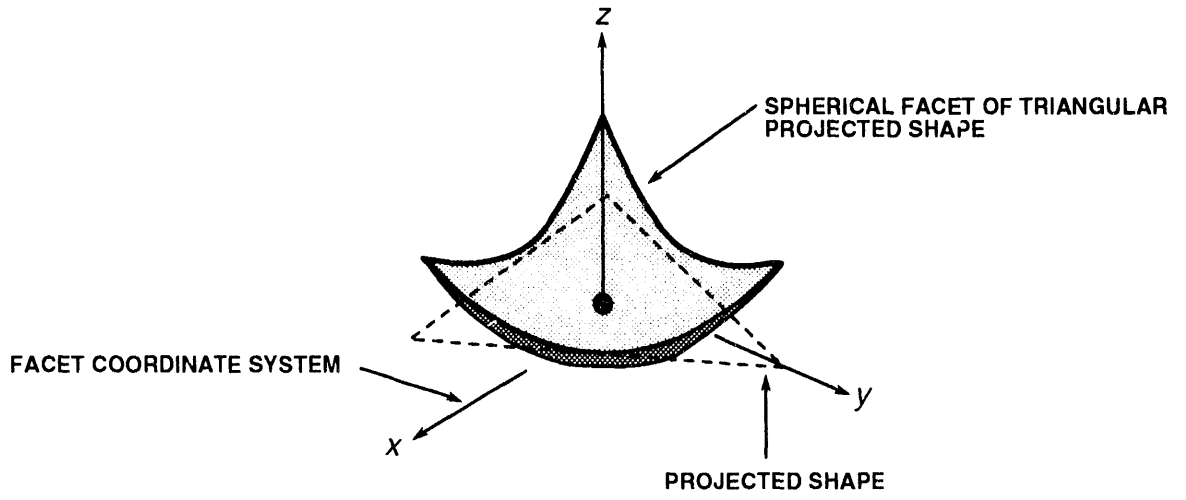

Figure 6.1 Facet Contour, Projected Shape, and Coordinate System.

The size of the projected shape is specified by one or two characteristic lengths input in meters. Facets of circular projected shape require only specification of projected radius (FLENG). Triangular facets require that the length of a side (FLENG) be specified. Rectangular facets require specification of length (ELENX) and width (ELENY) (ELENX ≥ ELENY). This is described in more detail below.

6.2 Facet Subdivision

Before describing the options available for facet contour, it is necessary to address division of a facet into **subfacets**. As stated in Section 2.3, this process is necessary for numerical integration over the facet surface. If the facet is very small relative to the total reflective area of the concentrator, it may not be necessary to divide it into subfacets. However, in the great majority of cases, subdivision is justified and necessary. The smaller the subfacets, the closer the mathematical approximations of Section 2.3 match solar optics theory (see subtitled articles of Section 6.3). The finer the surface division, however, the more costly the analysis is in terms of time and computer expense. Clearly, the user should divide the concentrator as finely as economically reasonable. Convolution options greatly alter the effect that the degree of facet subdivision has on computer requirements. This dependence was discussed in Section 4.6.4. This information will likely impact how the user chooses to subdivide the concentrator surface.

Division of a facet is dependent upon division of its projected shape. Circular projected shapes (radius = FLENG) are divided in the following way. A division parameter, NSUBF (≤100), is specified which divides the circular projection into NSUBF pieces: a circle of radius R_0 where

$$R_0=\text{FLENG}/(2\text{xNSUBF}) \tag{6.00}$$

and NSUBF-1 circular rings of width Δr where

$$\Delta r= (\text{FLENG-R0})/(\text{NSUBF-1}). \tag{6.0}$$

Each ring is then automatically subdivided into M equally sized angular sectors such that arc length on the outside of the sector is no greater than the ring width, where

$$M = INT(2\pi b/\Delta r) + 1 \tag{6.1}$$

$$\text{and } \Delta\theta = 2\pi/M\ , \tag{6.2}$$

where b is the outer radius of the k^{th} ring and $\Delta\theta$ is the angular extent of the sector. As an example, Figure 6.2 depicts the subdivision of a circular projected shape into "**projected subfacets**" for the case NSUBF=4. The division map is not necessarily accurate; it is only illustrative. The facet itself is divided into subfacets by projecting this division map up onto the facet surface. A subfacet and its associated projected subfacet are shaded in the figure. In general, execution time is proportional to the total number of subfacets analyzed, which is a product of the number of facets on the concentrator by the number of subfacets per facet (all facets are constrained to be divided similarly). The

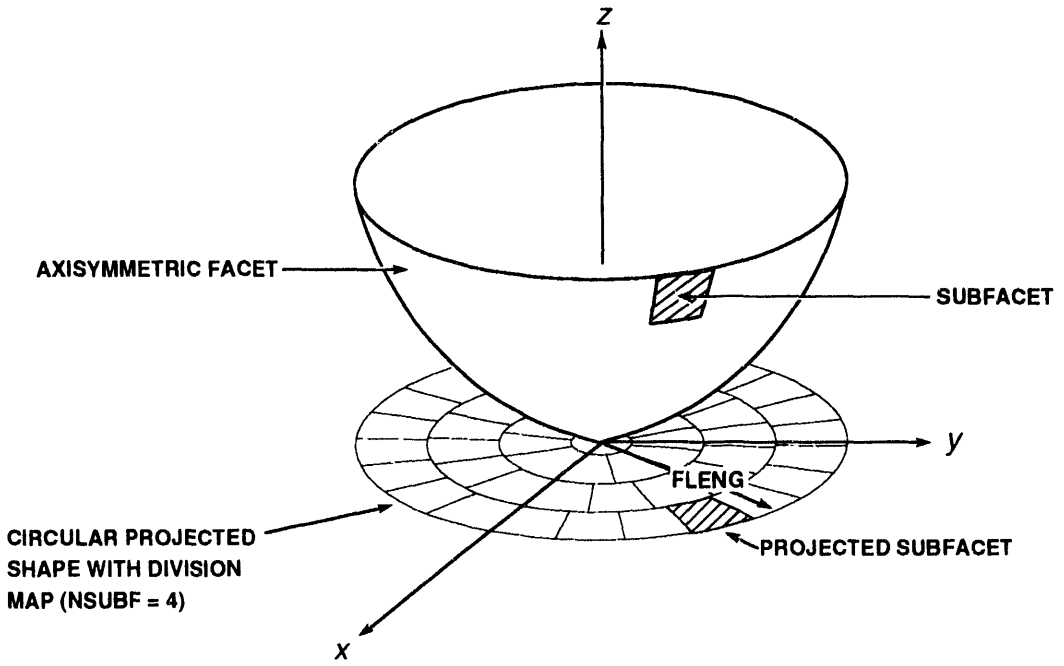

Figure 6.2 Facet of Circular Projected-Shape and Division into Subfacets.

number of radial divisions (NSUBF) must be less than or equal to 100, but the number of subfacets increases dramatically as NSUBF goes up. Table 1 gives the number of subfacets per facet as a function of NSUBF (for a 14-meter diameter projected shape, *i.e.* FLENG = 7 m.) The total number of subfacets increases rapidly as the division parameter NSUBF increases, and the rate of rise increases for larger facets. The user must be aware that execution time is a strong function of the parameter NSUBF.

Table 1. Number of Subfacets vs. Division Parameter NSUBF for Circular Projected Shapes (FLENG = 7 meters)

Division Parameter NSUBF	Number Subfacets N_F
3	25
6	124
10	372
15	873
25	2500

A rectangular projected shape is shown in Figure 6.3. Observe that the facet coordinate system x-axis lies along the major length (ELENX), while the y-axis lies along the minor length (ELENY). The length of the projected shape (in the x-direction) is divided into NX equal sections, and the width (y-direction) is divided into NY equal sections. This produces (NX) x (NY) subfacets. This particular figure has NX = 4 and NY = 2.

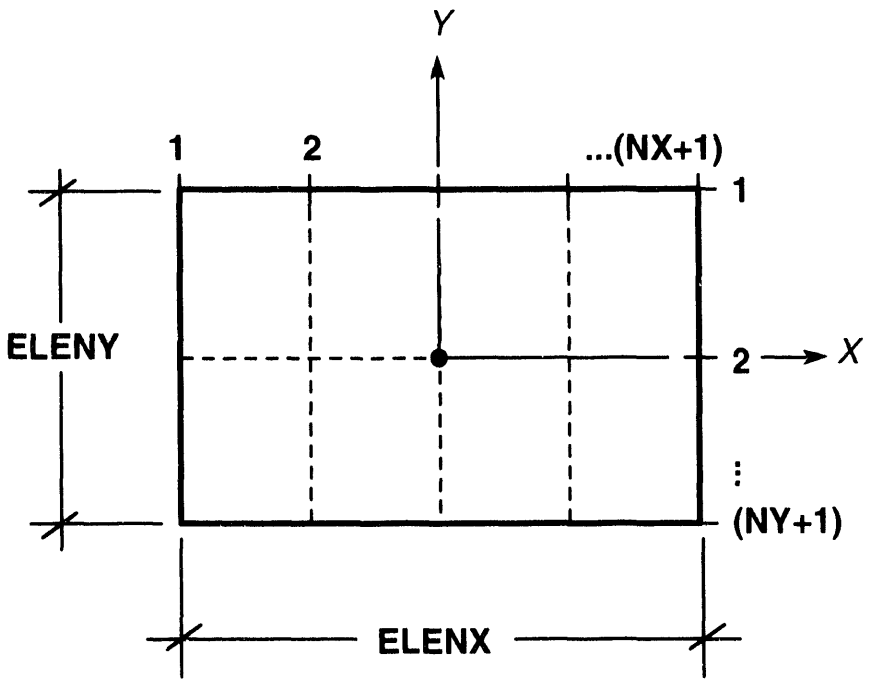

Figure 6.3 Rectangular Projected Shape and Associated Division Map.

Triangular projected shapes are divided according to specification of the parameter NSUBF. Each edge of the equilateral triangle is sectioned into NSUBF equal lengths, and division is continued inward in a manner that produces (NSUBF)x(NSUBF) equilateral triangles. Figure 6.4 illustrates the case NSUBF=3. Note that the triangle is oriented such that one edge lies parallel to the x-axis of the facet coordinate system.

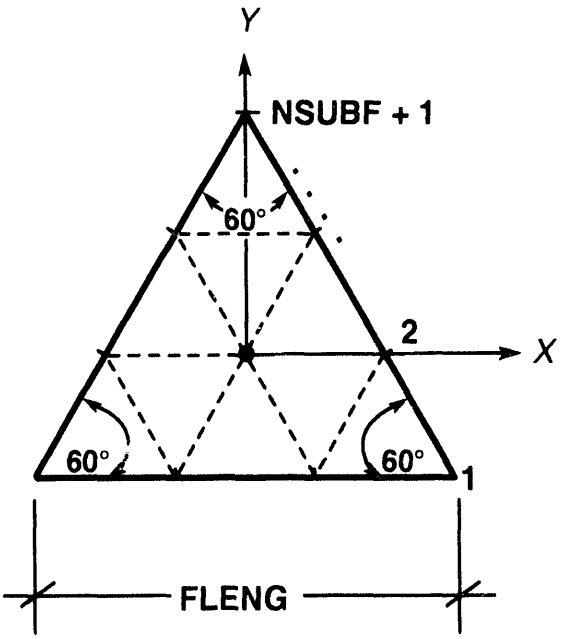

Figure 6.4 Triangular Projected Shape and Associated Division Map.

6.3 Facet Contour

The facet in Figure 6.1 has a characteristic contour that is produced by rotation about the z-axis of a circular arc. Facets of rectangular and circular projected-shape may have contours similarly produced. More arbitrary facet contours (not describable by rotating a curve about an axis) may be prescribed with a user-supplied FORTRAN subroutine. The parameter IOPT controls the contour options:

IOPT = 1 - parabolic arc, rotated
2 - flat segment, rotated
3 - circular are, rotated
4 - polynomial curve, rotated
5 - curve by table of radius vs. z-displacement, rotated
6 - curve by table of radius vs. z-displacement, rotated, with user-supplied subfacet normals (only for use on facets of circular projected shape)
7 - dish contour by user-supplied FORTRAN subroutine

For IOPT=1, the focal length (FOC) for the parabola is required. For IOPT=3, the radius (FOC) of the circular arc must be input. For reflectors that can be modeled as effective parabolic dishes, DEKGEN2 uses Equation 6.3 to compute the effective focal length, f, given the effective dish radius r_{dish} (DISHRAD), and rim angle[1] η (RIMANG). This is useful for defining Z_0 of the target coordinate system.

$$f = 0.5 r_{dish} \left(cot\eta + \left| cot^2\eta + 1 \right|^{-0.5} \right) \tag{6.3}$$

Contour modeling options IOPT=4, 5, and 6 allow evaluation of innovative concentrators, such as stretched-membrane reflectors, which have custom shapes described with an analytically or experimentally obtained table of radius vs. z-displacement.

Effective use of the IOPT parameter demands a good understanding of the important subfacet quantities involved in Eq. (2.5). These are: the direction of the ideal normal $\hat{N}_o$; the location of a representative point j from which all reflected energy is assumed to originate; and the area A_j of the subfacet element. A few comments on each of these quantities are in order:

Source-Point Location

All energy reflected from the jth subfacet to the ith target point is treated as though it comes from point j in Figure 2.5. It is not always clear what location would be most appropriate for point j, though the subfacet centroid seems reasonable. Calculation of the centroid for arbitrary curved surfaces is difficult. Fortunately, calculation of the exact centroid is unnecessary since a good approximation to it is easy to obtain and the location of the source point j is less critical to results than other subfacet quantities.

Direction of Ideal Normal

An accurate direction for the subfacet normal is vitally important because it determines the placement of the reflected flux on the target surface. Small deviations in the normal affect the target flux distribution much more than small deviations in the position of the source-point j. To obtain the ideal normal $\hat{N}_o$, it is necessary to determine a surface-normal representative of the entire subfacet surface. As described in Appendix B, this can be obtained by an area-weighted average of the normal-vector over the surface. However, such a calculation is difficult and expensive. Further complications are introduced for axisymmetric facets whose shape is described by a table of radius vs. height data and not an analytic function. Thus, approxmate methods must be used in CIRCE2, but efforts are made to make the approximations as accurate as reasonably possible.

[1] The rim angle is the angle formed between the rays from the focal point to the dish vertex and to the edge of the parabolic dish. Alternatively, parabolic dishes are often defined by f/d ratios, where d=2 x r_{dish}. For these cases $\tan\eta = \frac{8f/d}{(4f/d)^2-1}$.

Subfacet Area

The total energy reflected from subfacet j to a target point i is obtained by calculating the flux from the source point j to the target point, and then multiplying by the projection of the subfacet area A_j in the direction of the target point. Subfacet area A_j is determined in a round-about manner. By way of illustration, in Figure 6.2 the projection of the curved subfacet onto the x-y plane yields the shaded sector shown. In CIRCE2, a reverse procedure is used to obtain subfacet area. Given the shaded sector in the x-y plane, determine the corresponding subfacet, or more exactly, the area quantity A_j, if the geometry of the facet surface is specified. To first order, this can be done by choosing a representative geometric unit normal $\hat{N}_g$ for the subfacet, determining its direction cosine with the facet coordinate system z-axis, and dividing the area of the projected circular sector by this quantity. (The geometric normal $\hat{N}_g$ is not necessarily the same as the ideal normal $\hat{N}_o$. For reasons that will become apparent later, separation of the geometric and ideal normals can be advantageous.) Physically, this procedure has the effect of modeling the subfacet as a flat element normal to $\hat{N}_g$.

For flat (planar) facets, calculation of the above three quantities is straightforward —the facet and projected shape are one and the same. IOPT=2 is the option used for flat facets, whose subfacets are also flat. Source-point locations are taken to be at the subfacet centroids, and the geometric and most probable normals are given by the facet normal. The area A_j is equal to the jth subarea of the discretized projected shape.

For curved facets, the difficulty of calculating the subfacet quantities requires that approximations be used. The errors between the approximations and exact quantities increase with increasing surface curvature and decreasing degree of discretization of the facet. Surface curvature is fixed by the concentrator geometry, but the discretization of the surface is adjustable, presenting opportunity to affect accuracy of the calculation.

For parabolic (IOPT=1) or spherical (IOPT=3) facet contours, the following approach is taken to determine subfacet quantities. The approach is explained with reference to Figure 6.2, but is analogous for facets of triangular and rectangular projected shapes. First, the centroid of the shaded sector is calculated. The projection of this point up onto the facet is taken to be the "**subfacet centroid**." This is treated as the source-point for all energy reflected from the subfacet. The analytic surface-normal at this point is taken to be the ideal normal. The analytic surface-normal is also used as the geometric normal from which subfacet area A_j is calculated.

IOPT=4 allows modeling of facet contour by revolution about the z-axis of a polynomial curve of order NTERMS (≤10). (Facets of rectangular and triangular projected shape are permitted here.) Subfacet normals and source-point locations can be obtained using a polynomial as the analytic function (as the equations of a parabola and a circle are used for IOPT=1 and 3, respectively). Usually, the polynomial coefficients A_k (ASUB (k)) are obtained from a regression analysis of measured radius vs. z-displacement data. The form of the concentrator profile is given by:

$$z(r) = \sum_{k=1}^{K} A_k r^k, \; 1 \le K \le 10 \tag{6.4}$$

It is assumed that the z-displacement is a function of the radial position as measured from the facet center. Note that there is no constant term in the polynomial, constraining the vertex of the modeled facet to coincide with the origin of the x–y–z facet system. The option for parabolic surfaces (IOPT=1) is a special case of the polynomial option with the only non-zero coefficient being *ASUB(2) = 1/(4 f)*, where f is the focal length of the parabola. The circular arc that produces a spherical facet cannot be exactly described with a polynomial. To quantify the level of approximation involved in the various curve-fitting options (IOPT=4,5), the following investigation is undertaken.

The z-displacements vs. radial location for a 14-m diameter spherical dish with an f/d of unity (see Example 3, Chapter 8) are listed in Table 2. The 15 data points are fit with a least-squares proceedure assuming second and fourth order polynomial fits to the data. The resulting equations, in which the constant terms have been discarded so that z=0 at r =0 as required, are:

$$z_2(r) = -1.83299\,(10^{-3})\,r + 1.83601\,(10^{-2})\,r^2 \tag{6.5}$$

$$z_4(r) = -2.12534\,(10^{-5})\,r + 1.78794\,(10^{-2})\,r^2 - 7.45046\,(10^{-6})\,r^3 + 6.55119\,(10^{-6})\,r^4 \tag{6.6}$$

Table 2. Radius vs. Axial Displacement for a 14m Diameter Spherical Dish (f/d=1)

Point	r(m)	$z(r)$ (m)
1	0.0	0.00000000
2	0.5	0.0044646398
3	1.0	0.017862840
4	1.5	0.040207438
5	2.0	0.071519911
6	2.5	0.11183047
7	3.0	0.16117819
8	3.5	0.21961123
9	4.0	0.28718707
10	4.5	0.36397278
11	5.0	0.45004538
12	5.5	0.54549122
13	6.0	0.65041137
14	6.5	0.76491237
15	7.0	0.88911659

Assuming a division parameter of NSUBF=10 for the continuous-surface spherical dish, the radial locations of subfacet "centroids" are listed in Table 3. Centroidal radii r are calculated with the following equation.

$$r = [4(a^2 + ab + b^2)\sin(\Delta\theta/2)]/[3(a+b)\Delta\theta] \quad (6.7)$$

where a and b are the inner and outer bounding radii and $\Delta\theta$ the angular span of the circular sectors on the x-y plane. These quantities can be calculated from Equations (6.1) thru (6.4). Heights (z-displacements) at the radii of Table 3 are obtained by various means. The exact heights, calculated with the equation of a circle (IOPT=3), are compared to those obtained from the IOPT=4 option with 2nd- and 4th- order regression polynomial fits, Equations (6.5) and (6.6), respectively.

The fourth-order fit obviously performs better than the second-order fit, which does not have the necessary degrees of freedom to closely follow the spherical shape. However, this trend cannot be generalized. Since polynomials of higher order tend to exhibit "wiggliness," using polynomials of increasingly higher order might yield successively poorer height and slope quantities. Thus, shapes being analyzed with the polynomial option should be amenable to description with a fairly low-order polynomial.

Table 3. Comparison of IOPT=3, IOPT=4 Options for Spherical Facet Contour

Point	Radial Position of subfacet centroids (m)	Height (m) Analytic (IOPT=3)	Height (m) IOPT=4, O(2)	Δ%	Height (m) IOPT=4, O(4)	Δ%
1	0.00000	0.0000000	0.0000000	0.0	0.0000000	0.0
2	0.76987	0.0105858	0.0094709	-10.5	0.0105797	0.05
3	1.47998	0.0391407	0.0375021	-4.2	0.0391370	0.00
4	2.21040	0.0873833	0.0856534	-2.0	0.0873852	0.00
5	2.94584	0.1553936	0.1539288	-0.9	0.1553969	0.00
6	3.68243	0.2432041	0.2422184	-0.4	0.2432043	0.00
7	4.41987	0.3510437	0.3505676	-0.1	0.3510413	0.00
8	5.15776	0.4791451	0.4759702	-0.0	0.4791417	0.00
9	5.89606	0.6278152	0.62745435	-0.1	0.6278160	0.00
10	6.63439	0.797334	0.7959614	-0.2	0.7973381	0.00
			$\sqrt{\frac{\Sigma(\Delta\%)^2}{10}} = 3.6\%$		$\sqrt{\frac{\Sigma(\Delta\%)^2}{10}} = 0.02\%$	

The IOPT=5 and 6 options (IOPT=6 is restricted to facets of circular projected shape) are available for modeling reflector contour by interpolating tabular data (INTERP=0 for linear interpolation and INTERP=1 for cubic interpolation). The table of radius vs. z-displacement (height) data may be generated by analytic or experimental means. The table may be read-in from a file or entered interactively during the DEKGEN2 session. A sample file is presented in Example 3 of Chapter 8 (pp. 85). The maximum number of points allowable is 99. The data can be in uneven radial increments, but radius must increase for successive table entries. The first point must be at the facet vertex (r=z=0) and the last point must be at the outer radius (r=FLENG).

Suppose that 8 non-equally-spaced data points are obtained from direct measurement of a stretched-membrane facet and plotted in Figure 6.5. Employing IOPT=5 and NSUBF=4 for a circular facet, the heights at the subfacet boundaries are obtained by either linear (INTERP=0) or cubic (INTERP=1) interpolation of the data. In this example, linear interpolation is used and the interpolated heights at the subfacet boundaries are marked with "X"s.

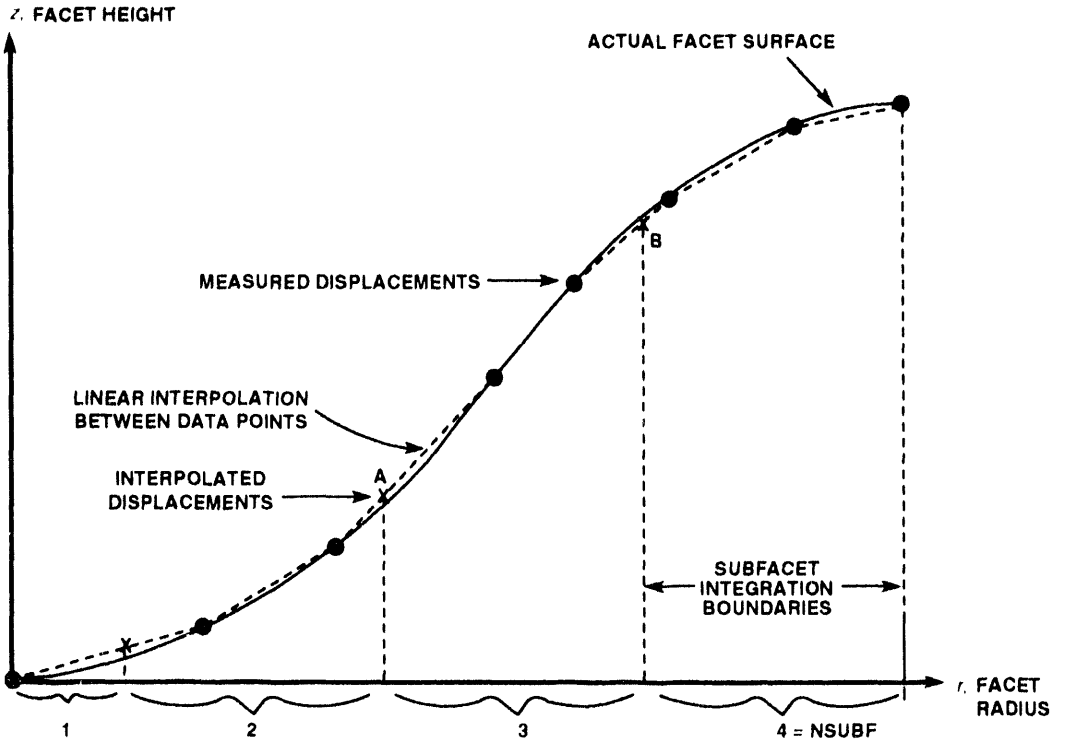

Figure 6.5 Linear Fit to Surface Profile of a Stretched Membrane Facet

For clarity, the geometry of this example was set up so that the X's lie off the facet surface by an appreciable amount. More data points, more evenly spaced measurements, or a concentration of measurements about subfacet boundaries, would all result in interpolated displacements that better approximate the actual facet surface. Also, using cubic interpolation (INTERP=1) would result in a much better fit. To get a quantitative feel, consider again the 14-m diameter spherical dish. Using the 15 data points

of Table 2, heights at the subfacet-bounding radii are listed in Table 4 for both linear and cubic interpolations. A comparison to heights obtained by the equation of a sphere (IOPT=3) is made. Even with this modest number of data points, it is possible with cubic interpolation to accurately portray the actual facet surface. Nevertheless, since the number of data points negligibly affects CIRCE2 execution time, it is advisable to include as many points as possible to maximize accuracy of the representation.

In summary, at least for a circular arc, linear and cubic interpolations with the IOPT=5 option are respectively more accurate than the IOPT=4 option with 2^{nd} and 4^{th} order least-squares regression fits –thereby yielding greater accuracy with less demands on the user.

Table 4. Comparison of IOPT=3, IOPT=5 Options for Spherical Facet Contour.

Point	Radial Position (m)	Height (m) Analytic (IOPT=3)	Height (m) IOPT=5, LIN	Δ%	Height (m) IOPT=5, CUB	Δ%
1	0.00000	0.0000000	0.0000000	0.0%	0.0000000	0.00%
2	0.76987	0.0105858	0.0116962	10.5	0.0105857	0.00
3	1.47998	0.0391407	0.0393127	0.4	0.0391403	0.00
4	2.21040	0.0873833	0.0884825	1.3	0.0873839	0.00
5	2.94584	0.1553936	0.1558326	0.3	0.1553940	0.00
6	3.68243	0.2432041	0.2442671	0.4	0.2432049	0.00
7	4.41987	0.3510437	0.3516670	0.2	0.3510429	0.00
8	5.15776	0.4791451	0.4801613	0.2	0.4791457	0.00
9	5.89606	0.6278152	0.6286009	0.1	0.6278139	0.00
10	6.63439	0.7973347	0.7982948	0.1	0.7973413	0.00
				$\sqrt{\frac{\Sigma(\Delta\%)^2}{10}} = 3.3\%$		$\sqrt{\frac{\Sigma(\Delta\%)^2}{10}} = 0.00\%$

The motivation for IOPT=6 will now be established. Fixing attention on the interpolated boundary points A and B of Figure 6.5, assume for the moment that they lie on the actual facet surface as shown in Figure 6.6. It is desired to obtain a line-weighted-average normal over the reflector surface from A to B. (Weighting which arises from the greater circumferential arc length at B than at A will be neglected here, but can be accounted-for as in the derivation of Equation (B.5) in Appendix B.) In order to reach B from A along any path, the average direction traveled must be along a vector from A to B, whose components are given by the slope of the straight-line segment connecting A and B. Thus, the line-weighted-average tangent vector along the facet surface from A to B parallels the segment AB. The average normal vector must lie perpendicular to the average tangent vector, and thus lies perpendicular to the line segment AB.

Returning to Figure 6.5, in which points A and B lie close to (but in general not on) the actual facet surface, the average normal vector over the 3rd integration interval is approximated to be perpendicular to a straight line drawn through the two points. This normal vector constitutes the geometric normal for IOPT=5,6 and ideal normal for IOPT=5. Likewise, straight-line connections between all the other interpolated boundary points are made, and a piecewise-linear approximation to the actual facet profile results. Source points are taken to be at radii marking the centroids of the corresponding projected subfacets in the x–y facet-coordinate plane. Heights of the source points are linearly interpolated from the heights at the integration boundaries. The IOPT=5,6 options can be substituted for the IOPT=1,3, and 4 options when the facet shape is, respectively, parabolic, spherical, or polynomial. Use of the former options produces no discontinuities in the facet profile whereas, for IOPT=1,3, and 4, discontinuities exist because the geometric normals evaluated at subfacet "centroids" generally differ from the normals evaluated with the above method. Presumably, the IOPT=5 method will be more accurate if, for the order of interpolation chosen, sufficiently many data points are supplied to allow accurate estimation of the facet heights at the integration boundaries.

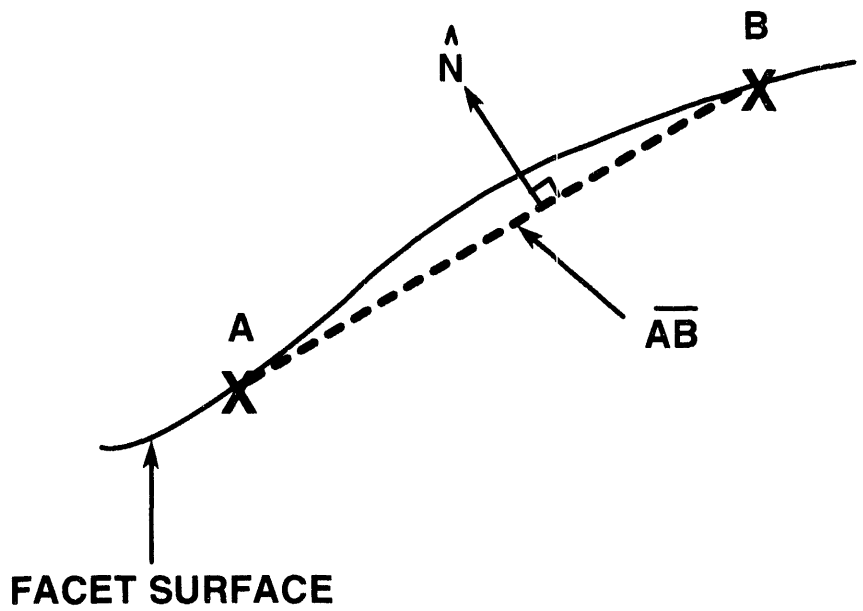

Figure 6.6 Close-up of Section A-B of Figure 6.5.

The IOPT=5 option avoids the problem of discontinuous concentrator profile and frees constraints on the geometry of analytic surfaces that can be analyzed, and it allows measured data to be used directly without a regression analysis. Nevertheless, there are situations that call for user-specification of the ideal surface-normal separately from the geometric normal. For instance, if the user wants to account for the effect of increasing circumferential arc-length with radius, IOPT=6 makes this possible by retaining the IOPT=5 normal as the geometric normal (for profile continuity) while simultaneously allowing the user to specify a more accurate area-weighted surface-normal (as in Appendix B). For nonanalytic (measured) surfaces, in many cases the measure-

ment of surface-normal vs. radius is easier and more accurate than measurement of z-displacement. Often, displacement is not measured directly but is derived iteratively from the slope measurements [17]. If confidence in z-displacement data is low such that derivation of the all-important ideal normal from this data is to be avoided and accurate slope information is available, IOPT=6 works best. With this option, the displacement data is entered as in IOPT=5, but the user separately specifies components of the ideal normal $\hat{N}_0$ at the subfacet centroids. The geometric profile modeled remains straight-line segments between heights at subfacet-bounding radii. (Though the geometry may be modeled with relatively crude displacement data in these cases, the effect on results is minimal because it is really the subfacet normals that the final results are most sensitive to, and the user is presumably inputting "good" values for these.)

A measured or estimated ideal subfacet-normal is separately entered by the user for each of the NSUBF-1 outer integration intervals of the facet. (The innermost subfacet is not a circular sector but a circular disk, as explained in Section 6.2. For this disk, the source-point is assumed to be at the facet vertex (z= r=0.0) and the geometric and ideal normals lie along the z-axis.) Subfacet boundaries are obtained from Equations (6.1) and (6.2). DEKGEN2 specifies the boundary locations when prompting for the r (RCOMP) and z (ZCOMP) components of the ideal normal. Components input do not have to be those of a unit vector. Coordinate axes and correct normal-directions are as shown in Figure 6.5. Example 3 of Chapter 8 illustrates the use of the option IOPT=6 for defining the geometry of a stretched-membrane reflector. Before using IOPT=6, the user is cautioned to have a good grasp of the considerations presented here.

The last option available for describing dish contour is IOPT=7, which employs a user-supplied subroutine to determine the z-displacement and subfacet-normal information. This option is only available for single-facet, continuous-surface concentrators (NFACET=1), but is applicable to rectangular, triangular, and circular projected shapes. It admits a much larger class of concentrator geometries than can be described by rotation of a curve about the facet z-axis. CIRCE2 calls subroutine USERDISH(....) to evaluate facet height and normal-direction given the facet-system (x,y) coordinates of each subfacet centroid. Appendix A lists a sample USERDISH subroutine. This subroutine is the one that CIRCE2 uses by default for IOPT=7, and it must be replaced with a user-supplied subroutine at compile-time if the user wishes to analyze a unique geometry.

7 CONCENTRATOR MODELING

Concentrators comprising one |quasi-|continuous facet (Figure 7.1), or several distinct facets (Figure 7.2) can be modeled with CIRCE2.

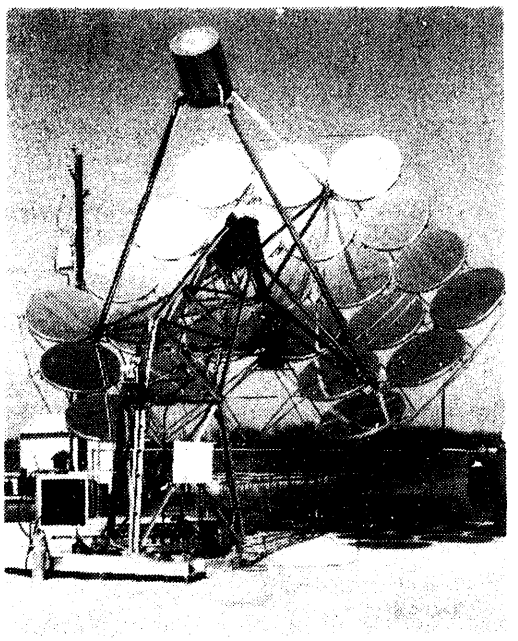

Figure 7.1 Photograph of the General Electric 7-m parabolic dishes located at Shenandoah, Georgia.

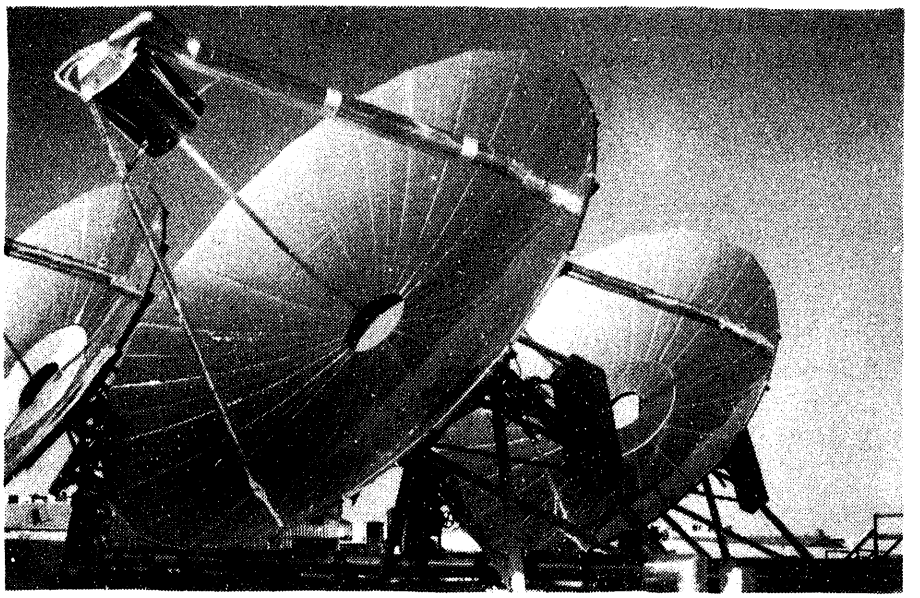

Figure 7.2 Photograph of a Cummins Power Generation CPG-460 Concentrator.

Concentrators with up to 350 facets can be modeled with CIRCE2. The parameter NFACET dictates the number of facets on the concentrator. When a concentrator consists of two or more facets, all facets are assumed to be geometrically similar and to have the same solar-band specular reflectance REFLEC (κ used in Equation 2.5).

When a reflector consists of many facets, it may be beneficial to assemble a free-formatted facet geometry file that can be read into DEKGEN2. This file would include for each facet: the facet identification number IDF, the collector-system coordinates of the facet center, the facet focal length or radius of curvature (FOC), the shading and blockage factor SBM, the aim-point identifier IDAIM, and the facet rotation angle IBETA. A sample file is presented in Example 4 of Chapter 8 (pp. 97), with an annotated guide presented at the bottom of Appendix D.

7.1 Geometry Definition

Concentrator geometry is defined using an absolute X-Y-Z reference frame, referred to as the "**collector coordinate system**". Figure 7.3 helps picture the quantities needed for modeling faceted concentrators. The coordinates (X(IDF),Y(IDF),Z(IDF)) of the vertex of each facet must be specified, where IDF is the identifying index of the facet and IDF ranges from 1 to NFACET. The vertex of a facet marks the origin of the *x–y–z* facet coordinate system from which the facet's geometry is established.

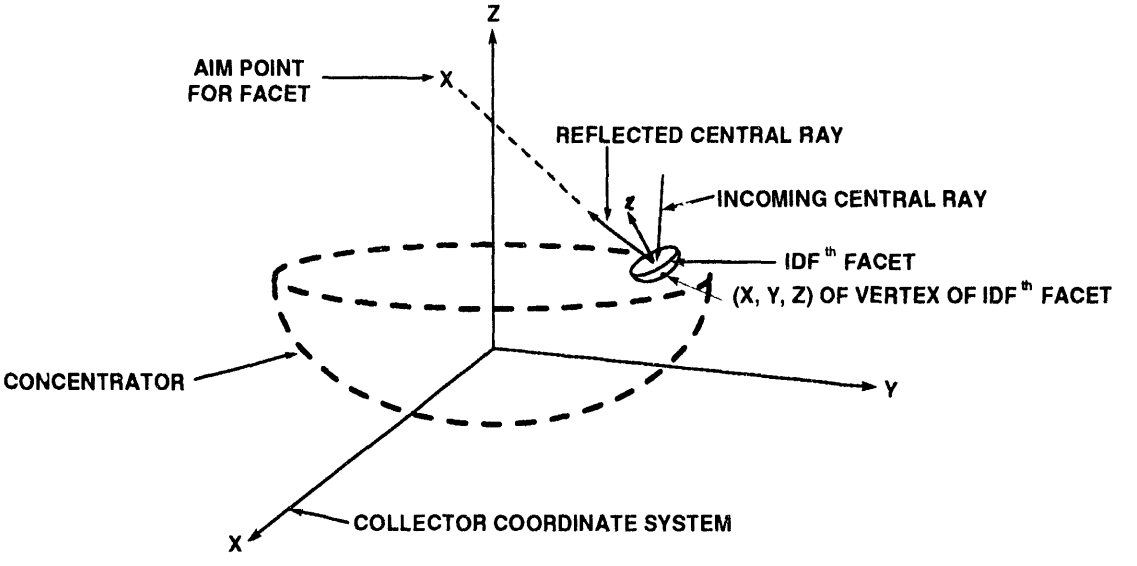

Figure 7.3 Elements of Concentrator Modeling.

The direction of the facet-system *z* axis is established either internally by CIRCE2 or input by the user, depending upon the choice ICPQR. If ICPQR=0 is chosen, the direction of the facet axis is determined such that the reflected central ray from the vertex of

the IDFth facet (assuming it osculates the x-y plane at x=y=z=0) goes through the aim-point assigned to that facet, assuming the sun to be on-axis (i.e., the concentrator tracks the sun perfectly such that incoming central rays are parallel to the collector-system Z-axis). Each facet may have it's own uniquely located aim point, or several may share a common aim point. Thus, the maximum number of aim points that may be defined is equal to the maximum number of facets, 350. NAIM specifies the number of aim points to be input. The location of the IDth aim point (which can be on or off the target) is specified in collector-system coordinates by (XAIM(ID), YAIM(ID), ZAIM(ID)). This information may be entered interactively or stored in a file for DEKGEN2 to read. Example 2 of Chapter 8 (pp. 81) presents a sample aim-point date file. Each facet must be assigned an aim point. If only one aim point is specified (NAIM=1), DEKGEN2 assigns all facets that aim point.

If the user chooses to input the facet normals (ICPQR=1) instead of inputing aim points and letting CIRCE2 calculate the normals (ICPQR=0), he may interactively input the facet identifier (IDF) and the collector-system components (PN, QN, RN) of the vectors (not necessarily unit vectors) that aim the facets. Alternatively, a free-formatted data file that contains this information may be generated for DEKGEN2 to read. Note that for ICPQR=1, aim points are not needed.

The plane containing the facet-system x- and y- axes is established by the orientation of the facet z-axis, which is determined as stated above. For facets of rectangular and triangular projected shape, one more piece of information is required: IBETA, which controls rotational orientation of the facet. Figures 6.3 and 6.4 show the orientation of rectangular and triangular facets relative to the facet-system x-y frame. The orientation of the x-y frame on the plane normal to the z-axis determines the rotational orientation of these (nonaxisymmetric) facets. Rotational orientation of this frame must be defined relative to some deterministic coordinate frame on the plane. The sun-reflector coordinate system (see Section 4.3) provides such a frame.

> The (somewhat cumbersome) method for defining the facet-system x and y directions with respect to global coordinate directions is explained below. In many cases, specification of this information can be avoided. If there is only one subfacet per facet, the rotational orientation of the facet is immaterial since the source-point (see the "Source-Point Location" article of section 6.3) is at the facet-system origin and does not move when the facet is rotated. Even if there are many subfacets per facet, unless the concentrator is made up of a small number (<10) of relatively large facets, facet rotation will have little effect on the calculated flux distribution, and can therefore be neglected. Additionally, for facets of circular projected shape, facet rotation is immaterial. In these instances, a global rotation angle of IBETA=0 degrees is assigned.

If it is felt that facet rotation will have a significant impact upon results, the following process must be undertaken. Figure 7.4 shows the projected shape of a rectangular facet. The sun-reflector coordinate system (Section 4.3) at the projected shape's centroid is also drawn. The facet-system z-axis and the sun-reflector-system ζ-axis coincide and point out of the page. Facet rotation about the z-axis is controlled by rotation of the x-y coordinate frame relative to the sun-reflector ξ-η system. The amount of rotation is specified by the parameter IBETA. IBETA is the counterclockwise positive angle

(measured in degrees) that locates the x- and y- axes of the facet coordinate system relative to the ξ- and η- axes of the sun-reflector system. IBETA ranges from -90 to 90 degrees, inclusive. A similar procedure is used to orient triangular facets. Example 4 in Chapter 8 illustrates a practical application of facet rotation using the parameter IBETA.

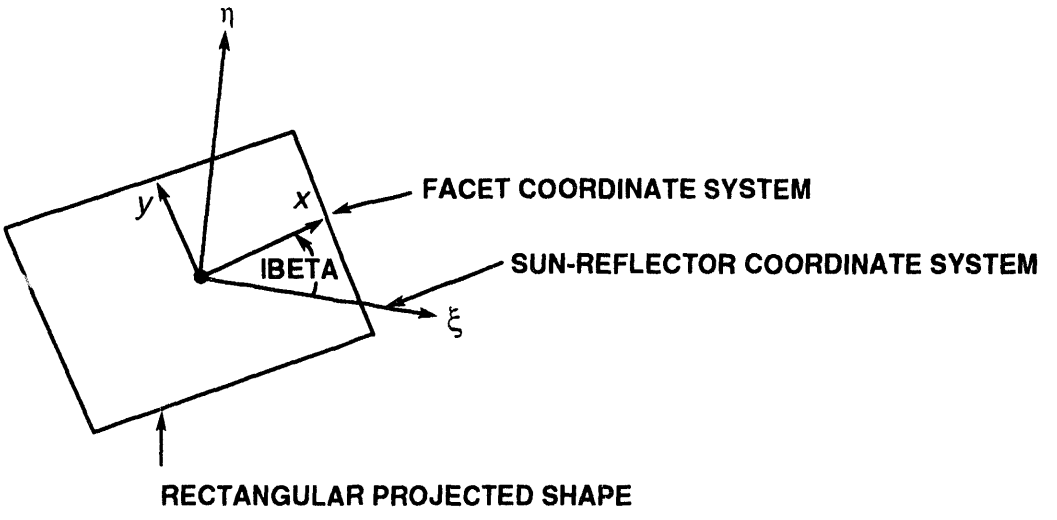

Figure 7.4 Relative Orientation of Sun-Reflector and Facet Coordinate Systems.

7.2 Shading and Blocking

Several options exist to account for: 1) shading of the concentrator by the target, target support structure, and other objects; and 2) blocking of rays on their way to the target after reflection from the concentrator. These options manifest themselves in a shading/blocking factor SBM for each facet. Ultimately, each subfacet of the IDFth facet is assigned the factor of B_j=SBM(IDF) (see Equation ? ?). Hence, the power reflected from every subfacet of the IDFth facet is diminished by the factor (1-SBM(IDF)). Thus, a value of SBM=0 indicates no shading or blocking occurs, and a value of SBM=1 indicates total shading which results in no contribution from the facet. Note: CIRCE2 does not check for facet self-shading and self-blocking. This saves considerable computer time, but it is possible that these may occur for some geometry and sun-position combinations. The user must be aware of the conditions being modeled and use other means (see ISHAD=2 below) to account for self blocking/shading.

For ISHAD=0, shadowing is assumed to be small and is therefore neglected, i.e., SBM=0 for every facet.

For ISHAD=1, shadow factors are computed internally by CIRCE2. The shading algorithm calculates SBM(IDF) as the overlap of a quadrilateral shadow on a quadrilateral "solar projection" of the IDFth facet [Reference 3, Section 7.4]. The solar projection

of a facet is obtained by: 1) first constructing a square projected-shape (in the sense of Section 6.1) for facets of circular and triangular projected-shape by determining a square having the same area as the original projected-shape; and 2) finding the projection of the rectangular projected-shape onto a plane normal to the incident solar central ray and containing the facet vertex. In general, such a projection will be a quadrilateral. A shadow is cast onto this same plane by a flat square plate representing the shading object. The square plate can be located and oriented however the user wishes by the same procedure used to position a flat rectangular target (Section 5.4.1). The shadow is the projection of the plate onto the concentrator, based on the sun's position. Since the square plate can be arbitrarily oriented, the shadow cast onto the plane is in general a nonrectangular quadrilateral. The fraction of the facet-quadrilateral that is overlapped by the shading quadrilateral gives the factor SBM(IDF) or, at the subfacet level it gives B_j. Each facet of the concentrator is checked for overlap in this manner.

In using this option, the user must specify the edge length SHADL of the square plate that casts the shadow. Alternatively, if a circular flat disk models the shading object better, the user may specify the radius SHADR of such a disk. The algorithm in CIRCE2 emulates the circular plate with a square plate of equivalent area. For the special case of a single-facet dish of circular projected shape, a true circular shadow of radius SHADR can be projected onto the center of the facet. The portion of the reflector that is shaded is then assumed not to exist at all, and SBM for the remainder of the facet is assigned a value of unity. This is the way to model a circular receiver's shadow at the vertex of a parabolic or spherical dish, or to model concentrators like the one in Figure 7.1 (that has a hole at its vertex).

For ISHAD=2, the user can specify the shading factor SBM(IDF) for each facet individually.

8 TUTORIAL

This chapter serves as a tutorial to familiarize the user with some of the more important capabilities of the CIRCE2/DEKGEN2 package. Toward this purpose, a variety of illustrative examples are covered in detail, with commentary and interpretation of results as appropriate. Since each example addresses different questions that the user is anticipated to have, it is recommended that the user read all of the examples before employing the software for his specific applications. While studying these examples, Appendix G serves as a quick-reference directory that points to places in the manual where more information about the various input parameters and technical terms can be found.

Numerical results for the following examples were obtained with version g.3 of the software package run on a SUN SPARCstation (SUN Fortran 1.4, level 02 optimization, SunOS 4.1.3 operating system).

EXAMPLE 1 Parabolic Dish Concentrator with a Circular Flat Target

Using DEKGEN2 we will build the sun model and collector system from scratch. Run DEKGEN2 alongside this example to read the actual prompts for which the following responses are given. Type-in the indicated responses at the terminal and follow along. Comments about individual responses are listed at the right, following a semi-colon.

```
% dekg2-g3.x              ; Run version g.3 of the DEKGEN2 code.

RESP:   <ret>             ; Press the "return" key after reading version information

RESP:   <ret>             ; Press the "return" key after reading disclaimer.

RESP:   n                 ; We're building the data file from scratch.

RESP:   EXAMPLE 1 OF CIRCE2 USER'S MANUAL; title of this run

RESP:   0 0 1             ; components of sun vector, VS(I),I=1-3, sun is on-axis
                            with respect to concentrator

RESP:   1000              ; I, solar insolation in W/m^2

RESP:   1                 ; sunshape descriptor, JSUN, we'll build a custom sun
                            model with a table of values

RESP:   N                 ; no tabular sunshape data file exists, we will build one

RESP:   22                ; (NTABL =)22 rows of data for the tabular sunshape, each
                            containing the sun cone angle RHO (in milliradians) in
                            the first column and weighting magnitude SVAL (unitless)
                            in the second column. Data points must be input in order
                            of increasing cone angle.
```

```
RESP:   0.000   2010.6   ; RHO(1), SVAL(1)
RESP:   0.352   2010.6   ; RHO(2), SVAL(2)
RESP:   0.704   2008.0   ; ... etc.
RESP:   1.056   1991.2   ; Note that the first data point must correspond to the
RESP:   1.408   1966.7   ; center of the axisymmetric sun disk (RHO= 0.0).
RESP:   1.760   1935.4   ; Data may be separated by either a comma or a blank
RESP:   2.112   1901.3   ; space.  Magnitudes here are representative when
RESP:   2.464   1864.6   ; assigned units of W/m2-steradian.
RESP:   2.816   1814.1
RESP:   3.168   1738.3
RESP:   3.520   1620.2
RESP:   3.872   1365.2
RESP:   4.224   884.21
RESP:   4.576   83.487
RESP:   4.928   17.796
RESP:   5.280   2.1680
RESP:   5.632   1.5224
RESP:   5.984   1.1320
RESP:   6.336   0.8722
RESP:   6.688   0.7584
RESP:   7.040   0.6845
RESP:   7.216   0.0000   ; Intensity of the sun disk is taken to be zero
                           beyond this cone angle.

RESP: 2                  ; NER, number of concentrator-error distribution func-
                           ions to be input

RESP:   0., 2.5, 2.5     ; TH(1),SIGR(1),SIGS(1) describe the 1-D circular-normal
                           distribution function corresponding to reflector slope
                           errors (see Section 4.3). Units are degrees, milli-
                           radans, milliradians, respectively.

RESP:   0., 1.5, 1.5     ; TH(2),SIGR(2),SIGS(2) describe the 1-D circular-normal
                           distribution function corresponding to mirror specular-
                           ity. Remember that mirror specularity is often expressed
                           by the dispersion of the reflected image instead of as a
                           degree of indeterminacy in surface-normal direction. To
                           convert dispersion-based specularity errors to surface-
                           normal errors for CIRCE2, divide the angular dispersion
                           errors by two before inputting here.

RESP:   1                ; IDIM. In accordance with the convolution strategy of
                           Section 4.6.4, since we know nothing about the relative
                           rms widths of the sunshape or mapped error-cone distri-
                           butions, we could choose the parameter set IDIM=1/IANLYT
                           =0/NEWCONV=3 and proceed with the analysis, being confi-
                           dent in the final result (assuming adequate concentrator
                           and target discretion).  Alternatively, if we want to
```

run parametric studies of some sort, or perform a convergence study on concentrator and target discretization, then we will want to use the parameter set IDIM=1/IANLYT=1/NEWCONV=1 to produce a quick run from which we can determine the relative widths of the sunshape and mapped error-cone distributions, and subsequently optimize the accuracy and speed of the ensuing simulations. We will take this to be the case for our example, and use the parameter set IDIM=1/IANLYT=1/NEWCONV=1 for this investigatory run.

RESP: 1 ; IANLYT=1 dictates that convolutions will be performed analytically. This saves computational resources, but if the rms widths of the mapped error-cone are narrower than the rms width (dispersion) of the sunshape, it is unacceptably accurate and numerical convolution must be used instead. Since we do not at this point know the relative widths, the sole purpose of this run is to determine them.

RESP: 1 ; NEWCONV. A single convolution is all that is required to determine the rms width of the sunshape and typical rms widths of the elliptic-normal mapped error-cone distribution.

RESP: 2 ; INCPICK. We choose the value 2 here because it serves our purposes without requiring estimation of the concentrator-averaged incidence angle $\bar{\mu}$ (though for a parabolic concentrator, this is easily determined via Equation 4.18).

RESP: SAMPLE TABULAR SUNSHAPE MODEL;title for sun and error cone parameters data group

RESP: 1 METER RADIUS FLAT-CIRCULAR TARGET ;title for target parameters data group

RESP: 6 ; ITARSH selection for a flat, circular target

RESP: y ; We want to place the target at the dish focus, which is calculated by Equation (6.3).

RESP: 45 ; This is the dish rim-angle RIMANG (see concentrator parameters data group below).

RESP: 7 ; This is the dish edge-radius DISHRAD in meters.

RESP: <ret> ; The focal length is calculated by DEKGEN2 and printed to the screen. We round the number to 8.45 for our use

here. After recording the number for later use, press the "return" key to continue.

RESP: After reading the message about the default value of INORM, press the "return" key to continue.

RESP: 0.,0.,8.45 ; Xo,Yo,Zo; target center is located at the focal point

RESP: 0, 0 ; ALPHA=BETA=0 for an unrotated, untilted target

RESP: 1 ; RMAX, target radius

RESP: 360 ; THETAMAX, angular span of the target

RESP: 1, 25 ; TPTS,RPTS are the number of grid points in the circumferential and radial directions, respectively, which discretize the circular target. The configuration of the collector system is such that the flux distribution on the target will theoretically be axisymmetric. Dividing the concentrator into a sufficiently large number of subfacets will result in a flux distribution predicted by the numerical model that is essentially axisymmetric. Thus, it is only necessary to determine the flux distribution along one radial line on the target

RESP: 0 ; IAPT=0 dictates that no auxiliary aperture is present.

RESP: 14 METER DIA., 45 DEG. RIM-ANGLE PARABOLIC DISH ; title of concentrator/reflector parameters data group

RESP: 1 ; REFLEC is the specular reflection coefficient for solar radiation. For this investigatory run we will prescribe no reflection losses so that we may verify at the end of the CIRCE2 simulation that all energy is accounted for.

RESP: 1 ; KORD specifies the facet's projected shape, which is circular for a paraboic dish.

RESP: 1 ; IOPT=1 when the facet has a parabolic contour

RESP: 7 ; FLENG is the *radius* of the 14-m diameter parabolic dish.

RESP: 10 ; NSUBF = 10 results in division of the dish into 372 subfacets according to Table 1, Chapter 6. This ought to ensure that the flux distribution on the target is essentially axisymmetric, thus justifying the choice of TPTS=1 above.

```
RESP:   1                ; ISHAD=1 specifies that shading by the target is to be
                           accounted for.

RESP:   Y                ; For the special case when the concentrator is made
                           of one facet, as is the case here, and it is
                           circular, a special shading algorithm that treats
                           the concentrator as having a hole in its center, like
                           that of Figure 7.1, is employed. Read the message
                           printed on the screen by DEKGEN2 to make sure that
                           the analysis is consistent with the collection system
                           you want analyzed.

RESP:   1.0              ; SHADR. The radius of the shading obstruction (in this
                           case the circular target) is 1 meter.

RESP:   1                ; Normally, we would choose ICPQR=0 here, but since
                           the components of the unit normal-vector which
                           orients the dish are obvious, we choose this option
                           to familiarize the user with the process of manual
                           specification of facet-normal data.

RESP:   n                ; We have no previously generated data file.

RESP:   1                ; NFACET=1 for the continuous dish concentrator

RESP:   0, 0, 0, 8.45    ; (X,Y,Z) and FOC, respectively, locate the position of
                           the dish vertex (in collector-system coordinates)
                           and define the focal length of this 45 degree
                           rim-angle parabolic dish (given above when the option to
                           help locate the target was employed).

RESP:   <ret>            ; After reading the message press the "return" key to
                           continue.

RESP:   N                ; We have no previously generated file containing facet
                           normal data.

RESP:   0 0 1            ; These PN,QN,RN vector components indicate that the axis
                           of the parabolic dish points along the Z-axis of the
                           collector coordinate system.
```

Comment: That's it! DEKGEN2 will name the resulting data file "**input**" because it will be used as input data to run CIRCE2. Appendix D lists an annnotated form of this file in which parameter names are listed alongside the various input data. It is helpful to use this appendix as a key when examining a data file.

Comment: When CIRCE2 is run it produces an output file called "**output.**" This file echoes the input data, provides diagnostic and debugging information, and

lists results. The sections at the ends of Examples 2 and 3 contain information that is useful in interpreting **output** files. A condensed version of **output** is also created. This file, named "**flux**", contains a summary of the the most important results. The **flux** file for Example 1 is listed in Appendix E. It provides a numerical benchmark against which users on different computing platforms can compare their results. Finally, a third file called "**messages**" is created which holds special messages pertaining to "unusual occurances" in the analysis. It should be checked at the end of each run.

Comment: To keep track of this analysis we will rename files as follows:

input --> **example1.dat**
output --> **example1.out**
flux --> **example1.flx**
messages --> **example1.msg**

Comment: From the **output** file, we find that the rms width of the sunshape is about 2.09 mrad and that the rms width of the 1-D approximation to the 2-D elliptic-normal mapped error-cone is approximately 5.8 mrad. Thus, we have a relatively wide mapped error-cone. Knowing this, and with a good approximation to $\bar{\mu}$ being 15 degrees by evaluation of Equation (4.18), the guidelines of Section 4.6.4 indicate that the most efficient parameter sets are IDIM=1/IANLYT=1/NEWCONV=1/INCPICK=1/INCANGL=15 degrees for parametric and scoping studies where speed is the primary concern but good accuracy is desired, and IDIM=2/IANLYT=0/NEWCONV=1/INCPICK=1/INCANGL=15 degrees for final results where accuracy is paramount. These sets would be used as appropriate in subsequent analyses of this concentrator.

Comment: Now that a tabular sunshape has been specified, it will be advantageous to edit the **input** file produced by DEKGEN2 to make a sunshape table like that below. Future runs using this sunshape can be expedited by reading in this file (we'll name it "**sun.dat**").

```
1    0.0000     2010.6
2    0.3520     2010.6
3    0.7040     2008.0
4    1.0560     1991.2
5    1.4080     1966.7
6    1.7600     1935.4
7    2.1120     1901.3
8    2.4640     1864.6
9    2.8160     1814.1
10   3.1680     1738.3
11   3.5200     1620.2
12   3.8720     1365.2
13   4.2240     884.21
14   4.5760     83.487
15   4.9280     17.796
```

16	5.2800	2.1680
18	5.9840	1.1320
19	6.3360	0.8722
20	6.6880	0.7584
21	7.0400	0.6845
22	7.2160	0.0000

EXAMPLE 2 Same as EXAMPLE 1, but with a Spherical Dish.

This example is essentially the same as Example 1, but with a spherical dish insted of a parabolic one, and with a user-specified aim point to orient (aim) the dish (ICPQR=0) rather than a user-input vector for the dish-axis direction (ICPQR=1). For purposes of illustration, this example utilizes an aim-point data file that DEKGEN2 reads and appends to the database. Example 3 illustrates interactive input of aim-point data. The collector-system coordinates (in meters) of the center of the target are (0,0,8.45). Wanting the dish'es aim-point to coincide with the center of the target, we create the following aim-point data file, which we name "aimpt.dat":

```
1
1       0.      0.      8.45
```

The first row specifies the number of aim points (NAIM) to be defined, and the following NAIM rows each contain an aim-point identifier ID and its collector-system coordinates XAIM(ID), YAIM(ID), and ZAIM(ID). The aim points must be numbered consecutively from 1 to NAIM (i.e., ID ranges from 1 to NAIM in the file).

We now begin the DEKGEN2 session:

```
% dekg2-g3.x              ; Run version g.3 of the DEKGEN2 code.

RESP:   <ret>             ; Press the "return" key after reading version information

RESP:   <ret>             ; Press the "return" key after reading disclaimer.

RESP:   y                 ; It's faster to modify the old file instead of
                            creating a new one since there are only a few
                            differences between Examples 1 and 2.

RESP:   dir.example1/example1.dat      ;pathname and filename for old data file

RESP:   Y                 ; We must change the title to suit the new database.

RESP:   EXAMPLE 2 OF CIRCE2 USER MANUAL       ; title of this run

RESP:   N                 ; We will keep the sun-parameters data group as is.
                            (The user may have to press the "return" key several
                            times to scroll through the data from the old file.)

RESP:   0                 ; We will also not alter any of the target parameters.

RESP:   y                 ; Since we are going to use a spherical facet instead of
                            a parabolic one as in Example 1, this is where we must
                            start changing the database.
```

```
RESP:  SPHERICAL DISH, SAME FOCAL LENGTH AND PROJECTED AREA AS IN EXAMPLE 1; title

RESP:  1.              ; REFLEC, perfect surface-reflectance assumed

RESP:  1               ; KORD=1 for a facet with a round projected shape

RESP:  3               ; IOPT=3 for facets having spherical contour

RESP:  7               ; For facets of circular projected-shape, FLENG specifies
                         the facet radius. The value here gives this dish the
                         same projected area as the dish in Example 1.

RESP:  10              ; NSUBF is the facet division parameter for circular (and
                         triangular) facets. NSUBF = 10 results in division of
                         the dish into 372 subfacets according to Table 1,
                         Chapter 6. This ought to ensure that the flux distribu-
                         tion on the target is essentially axisymmetric, thus
                         justifying the default choice of TPTS=1 that is the
                         result of using the old target parameters.

RESP:  Y               ; Changes is this data group are also necessitated when
                         changing from a parabolic to a spherical dish.

RESP:  1               ; ISHAD=1 specifies that shading by the target is to be
                         accounted for.

RESP:  Y               ; For the special          en the concentrator is made
                         up of one facet          the case here) and it is also
                         circular, a special shading algorithm which treats
                         the concentrator as having a hole in its center, like
                         that of Figure 7.1, is employed. Read the message
                         printed on the screen by DEKGEN2 to make sure that
                         the analysis is consistent with the collection system
                         you want analyzed.

RESP:  1               ; SHADR. The radius of the shading obstruction (in this
                         case the circular target) is 1 meter.

RESP:  0               ; This choice for ICPQR directs CIRCE2 to internally
                         calculate normals, i.e. "aim" facets, such that rays
                         from an overhead sun reflect off the center/vertex of
                         the facet and strike its specified aim-point.

RESP:  y               ; We do not have a file containing aim-point data and must
                         therefore enter the data interactively.

RESP:  aimpt.dat       ; The file we created that contains the collector-system
                         coordinates of the aim point was name "aimpt.dat".
```

```
RESP:   n                ; We have no previously generated file containing the
                           facet data.

RESP:   1                ; NFACET=1 for a continuous dish concentrator.

RESP:   0, 0, 0, 16.9    ; (X,Y,Z) and FOC are respectively the X,Y,Z
                           collector-system coordinates of the vertex of the facet,
                           and the radius of curvature (R.O.C.) of the spherical
                           facet.  The radius of curvature used here gives this
                           dish the equivalent focal-length of the parabolic dish
                           of Example 1 (R.O.C. = 2f).

RESP:   <ret>            ; Press the "return" key after reading the message about
                           the default value of IBETA for this concentrator.
```

Comment: That's it! The **input** file for CIRCE2 has now been generated. To keep it uniquely identified, **it** should be renamed to something like "**example2.dat**" upon completion of a CIRCE2 analysis.

Comment: Upon running CIRCE2, the following results summary table is produced. It is located at the bottom of the **output** and **flux** files.

```
     **** SUMMARY RESULTS ****
CONCENTRATOR SURFACE AREA =                158.008 m^2
Ap = SOLAR PROJECTED AREA=                 150.796 m^2
Ar = Ap REDUCED BY SHADING AND BLOCKING =150.796 m^2
I = SOLAR INSOLATION =1000.00 W/m^2
NO. OF SUNS IN PEAK = 1671.56
Pideal = MAX INTERCEPTABLE POWER = I*Ap =   0.150796E+06 W
Prefl = PWR REFL FROM CONC. = I*Ar*REFLEC =0.150796E+06 W
Prec = POWER ON RECEIVER (QAGS & QNC79) =   0.150271E+06 W
Ceff = CONCENTRATOR EFFNCY = Prefl/Pideal =100.00%
Reff = RECEVR COLLECTION EFF = Prec/Prefl =  99.65%
TOTAL COLLECTOR SYSTM EFFINCY = Ceff*Reff    99.65%
```

Comment: "CONCENTRATOR SURFACE AREA" is obtained by summing the areas of all the subfacets ($=\Sigma A_j$). "SOLAR PROJECTED AREA" A_p is the sum of all subfacet "solar projections", where a solar projection is obtained by multiplying a subfacet's area A_j by the cosine of the angle between the direction-vector $\hat{V}_s$ of the incoming solar central-ray and the subfacet geometric normal $\hat{N}_g$ (= the ideal normal $\hat{N}_o$ except when IOPT=6). Thus, solar projected area changes for different values of the sun-vector parameters SV(i). A_r is the solar projected area A_p reduced by shading and blocking. Note that even though we have specified a circular shadow of radius 1 m at the vertex of the dish, the values A_r and A_p are the same here. This is because the shading algorithm used for this special shading case effectively removes the part of the facet that is covered by the shadow. Thus, the area A_p is the solar projection of a paraboloid with a hole in it, not of a regular paraboloid. So, in

this case, the reduced area due to shading is already taken into account in the calculation of A_p. In all other cases of shading, the "sunny" portion of the concentrator, A_r, will be less than the solar projection A_p, as expected. "NO. OF SUNS IN PEAK" is the ratio of the maximum of all fluxes calculated at the target points to the solar insolation I. All other quantities are defined in the table.

Comment: For circular targets a table of "optical disk efficiency" (see Section 5.2.3) is produced by CIRCE2. Various collection efficiencies and cumulative distributions are reported. The table corresponding to this example is listed below.

OPTICAL EFFICIENCY FOR APERTURE DISK:

RADIUS (M)	% OF TOT RADIUS	% OF TOT TGT AREA	% OF TOTAL PWR ON TGT	% OF PWR ON UNSHADED DISH
0.00	0.00	0.00	0.00	0.00
0.04	4.17	0.17	5.41	5.39
0.08	8.33	0.69	16.88	16.82
0.12	12.50	1.56	27.32	27.23
0.17	16.67	2.78	35.10	34.98
0.21	20.83	4.34	41.29	41.15
0.25	25.00	6.25	46.65	46.49
0.29	29.17	8.51	51.48	51.30
0.33	33.33	11.11	55.98	55.78
0.38	37.50	14.06	60.13	59.92
0.42	41.67	17.36	63.84	63.61
0.46	45.83	21.01	67.29	67.05
0.50	50.00	25.00	70.83	70.59
0.54	54.17	29.34	74.46	74.20
0.58	58.33	34.03	77.74	77.47
0.62	62.50	39.06	80.38	80.10
0.67	66.67	44.44	82.59	82.31
0.71	70.83	50.17	84.95	84.65
0.75	75.00	56.25	87.83	87.53
0.79	79.17	62.67	91.13	90.82
0.83	83.33	69.44	94.34	94.01
0.88	87.50	76.56	96.92	96.59
0.92	91.67	84.03	98.63	98.29
0.96	95.83	91.84	99.57	99.22
1.00	100.00	100.00	100.00	99.65

EXAMPLE 3 Stretched Membrane Dish and Tilted, Rotated, Off-Axis Flat Semi-Circular Target

This example features a collector system that illustrates some of the coordinate systems in CIRCE2. Figure 8.1 shows the particular system being modelled. The view is from beneath the concentrator, facing its convex side, and looking up toward the target as the concentrator would see it. The lines on the concentrator are solely for aid in visualizing the curved surface and should not be taken as suggestive of the concentrator's division into subfacets. In a "conventional" collector design, the target would lie on the Z-axis of the collector coordinate system. The dish (here the term "dish" is used in the special case where the concentrator is made up of only one facet) would be aimed or directed along this axis such that the facet coordinate system z-axis would coincide with the collector system Z-axis. In this example, however, the systems do not coincide; there is relative rotation between the two. For convenience, the origins of the two systems are the same here, though this does not have to be the case, as will be demonstrated in another example. The aperture and target are chosen to demonstrate the meanings of various parameters. For generality, this particular example uses the IOPT=6 method of geometry description for the stretched-membrane dish, which encompasses the simpler IOPT=5 option. This example, then, also demonstrates the essentials when the choice IOPT=5 is employed.

Suppose that (as in [17]) surface-normal data is measured at certain radii of an axisymmetric stretched-membrane concentrator. Also, assume that the data is amenable to a functional curve fit, or some other interpolation algorithm, which can be used to obtain values of surface-normal r- and z- components (refer to Figure 6.5) as a function of radius. Let radius vs. displacement data, either measured directly or derived from the slope data as in [17], also be available. Then the IOPT=6 option can be used to model the facet. It should be noted that it is necessary for displacement to be known only at discrete points, and there is freedom in the location of those points, whereas the slope vs. radius information must be known as a continuous function of radius if freedom in the subdivision of the facet is to be maintained. This example will illustrate these points.

Suppose that displacements are obtained at 15 radii as listed in Table 2, Section 6.3. From this table let's make the data file called "**displ.dat**" shown below. Recall that the first data point must be $(r,z)=(0,0)$, the last data point must correspond to the outer radius of the dish, and that data must be listed in order of increasing radii. Unequal radial spacing between data points is acceptable.

```
1       0.0     0.00000000E+00
2       0.5     0.44646398E-02
3       1.0     0.17862840E-01
4       1.5     0.40207438E-01
5       2.0     0.71519911E-01
6       2.5     0.11183047E+00
7       3.0     0.16117819E+00
8       3.5     0.21961123E+00
9       4.0     0.28718707E+00
10      4.5     0.36397278E+00
11      5.0     0.45004538E+00
```

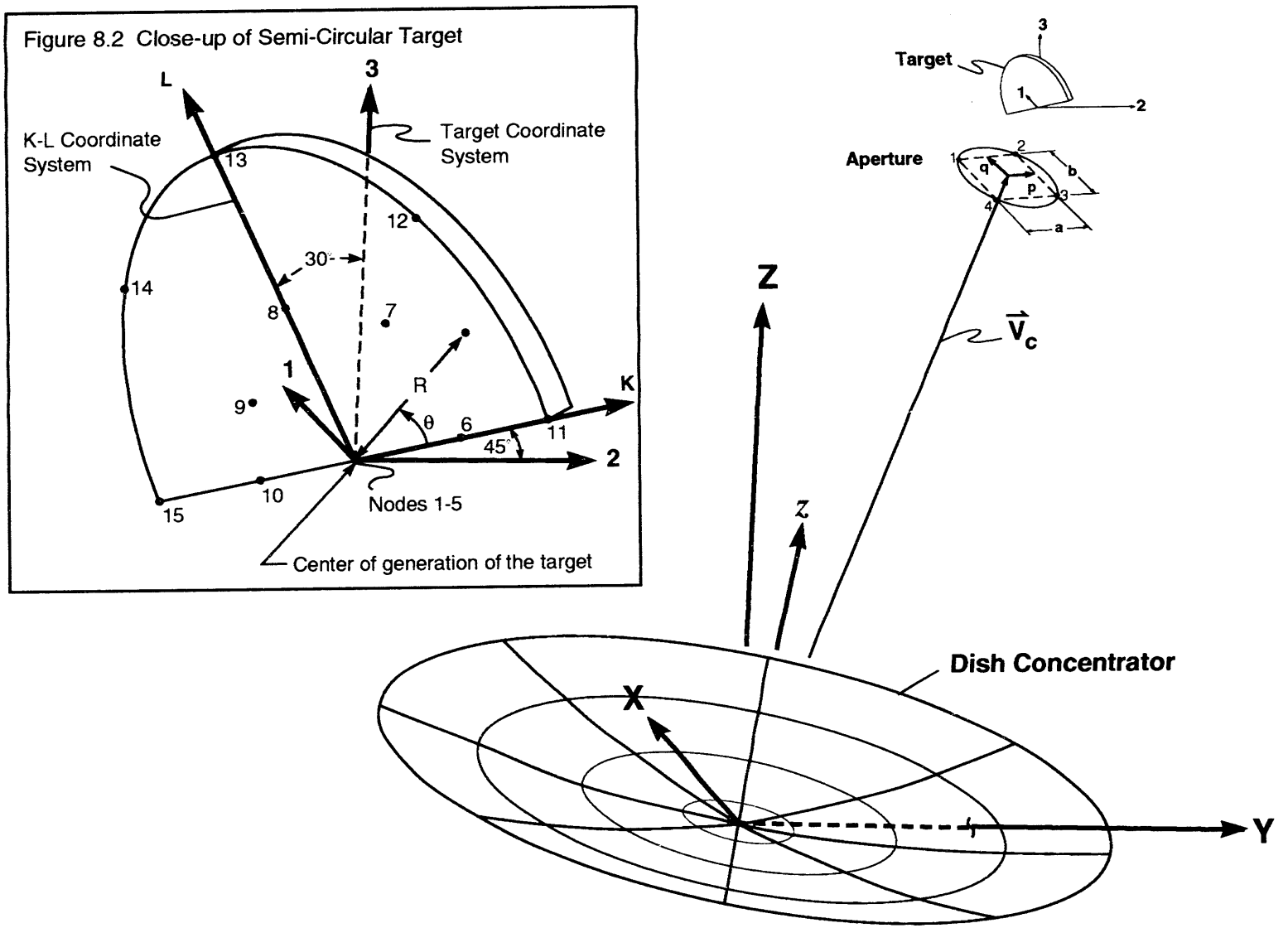

Figure 8.1 Collector System for Example 3

```
12      5.5     0.54549122E+00
13      6.0     0.65041137E+00
14      6.5     0.76491237E+00
15      7.0     0.88911659E+00
```

Now let's begin the DEKGEN2 execution:

```
% dekg2-g.3              ; Run the DEKGEN2 code.

RESP:   <ret>            ; Press the "return" key after reading version information

RESP:   <ret>            ; Press the "return" key after reading disclaimer.

RESP:   n                ; We'll build this data file from scratch since this
                           concentrator will be very different from those in
                           Examples 1 and 2.

RESP:   EXAMPLE 3 OF CIRCE2 USER'S MANUAL     ; descriptive title of this run.

RESP:   0 0 1            ; SV(i), i=1-3 are the components of the direction vector
                           of the sun.  In this case an overhead sun is specified.

RESP:   1000.            ; I, the solar insolation in W/m^2

RESP:   1                ; JSUN=1; we elect to define the sun with a table of data

RESP:   Y                ; Here I want to read in sunshape data from the file
                           generated in Example 1.

RESP: dir.example1/sun.dat ;the name of the file containing the required sun data
                           (The user will have to press the "return" key several
                           times to scroll through the data being read-in. This
                           allows the user to check the incoming data.)

RESP:   2                ; NER=2 concentrator error distributions to be input

RESP:   0,2.5,2.5        ; TH(1),SIGR(1),SIGS(1) same as in Example 1

RESP:   0,1.5,1.5        ; TH(2),SIGR(2),SIGS(2) same as in Example 1

RESP:   1                ; IDIM. We know from Example 1 that the mapped error-cone
                           is wider than the sunshape.  However, since the sun is
                           not on-axis with the dish and the dish is not parabolic,
                           a good estimate for μ̄ (see Section 4.6.3) is not at
                           hand. Then, according to the advice in section 4.6.4,
                           the most appropriate sets of convolution parameters are:
```

IDIM=1/IANLYT=1/NEWCONV=3 for working results and IDIM=1/IANLYT=0/NEWCONV=3 for final results. Assuming that this is a preliminary run, we choose the former parameter-set for this example.

RESP: 1 ; IANLYT.

RESP: 3 ; NEWCONV.

RESP: SUN.DAT tabular sunshape; descriptive title of sun and error parameters

RESP: ROTATED, CANTED, OFF-AXIS FLAT SEMI-CIRCULAR TARGET; title of target data

RESP: 6 ; ITARSH selection for a flat, circular target sector

RESP: N ; In this example we do not need the proposed information.

RESP: <ret> ; Press the "return" key after reading the message.

RESP: -6, 4, 15 ; The origin of the 1-2-3 target coordinate system shown in Figure 8.1 and the insert, Figure 8.2, is at (Xo,Yo,Zo)=(-6,4,15). (The target is drawn with some thickness to add perspective.) Figure 8.2 is a magnified view of the target with the same orientation as in Figure 8.1.

RESP: -45 60 ; ALPHA and BETA are the angles that orient the virtual K-L axis system of the circular target relative to the 1-2-3 target coordinate system. The various coordinate systems and angles are shown in Figure 8.2. The tilt angle BETA tilts the L-axis, and the target with it, 60 degrees up from the 1-axis of the target system. The -45 degree rotation ALPHA swings the tilted L-axis and the K-axis (always constrained to be horizontal) 45 degrees counterclockwise, rotating the target correspondingly.

RESP: 1 ; The semi-circular target has a radius of RMAX=1.0 meter.

RESP: 180 ; THETAMAX. The positive direction of theta is as indicated in Figure 8.2. If the parameter THETAMAX had a 90 degree value, the target sector would extend from the K-axis to the L-axis as in Figure 5.2. Figure 8.2 shows a sector with an angular extent from the positive K-axis to the negative K-axis (semi-circular target) corresponding to THETAMAX = 180 degrees.

```
RESP:   5, 3                ; TPTS,RPTS.  The mesh imposed upon the target by these
                              parameter values is illustrated in Figure 8.2.
                              Note the node numbering convention for circular
                              targets.

RESP:   2                   ; IAPT=2 for circular apertures, such as the one depicted
                              in Figure 8.1.  These are defined by specification of an
                              inscribed square.

RESP:   -5.27   2.663   13.825     ; These are the coordinates, referred to the
RESP:   -4.485  3.84    13.825     ; collector coordinate system, of the four
RESP:   -5.546  4.547   13.213     ; corners of the inscribed square (dashed
RESP:   -6.331  3.37    13.213     ; lines) shown in Figure 8.1.  Appendix F shows
                                   ; how the coordinates were determined.

RESP:   14 METER DIAMETER, 45 DEGREE RIM-ANGLE MEMBRANE DISH; descriptive title

RESP:   0.8                 ; REFLEC, surface reflectance

RESP:   1                   ; KORD=1 for the axisymmetric dish

RESP:   6                   ; IOPT.  The user will specify displacements and normals
                              for this custom-curvature dish.

RESP:   1                   ; This choice for INTERP, indicating cubic interpolation,
                              is not costly and is most accurate.

RESP:   y                   ; We will read in the displacement data prepared earlier.

RESP:   displ.dat           ; We named the displacement data file "displ.dat."
                              (The user will have to press the "return" key
                              to scroll through the data being read-in.  This
                              allows the user to check the incoming data.)

RESP:   10                  ; NSUBF, the parameter controlling division of the facet
                              into subfacets, see Table 1 of Section 6.3.
```

Comment: The ideal normal at the center of any axisymmetric facet points along the facet coordinate system z-axis (refer to Section 6.3). Thus, the subfacet at the center always has a normal whose r- and z- components are Nr=0.0 and Nz=1.0. These are internally assigned in DEKGEN2. To get the r- and z-components for the other subfacets, a variety of options can be exercised as explained in Section 6.3. With IOPT=6, the user is free to specify the effective normal over each subfacet. The method by which this normal is obtained is left to the discretion of the user. Consider the subfacet sector immediately adjacent to the center, whose inner and outer radii are 0.35 and 1.088889 meters, respectively. (These radii are calculated with equations

(6.00) and (6.0) and are written to the computer screen by DEKGEN2.) By some means[1] we determine the radial and normal components of this sector's effective normal to be Nr = -2.569747E-02 and Nz = 0.9996698. These are input below, along with the values for the other 8 angular sectors .

```
RESP:      -0.02569747       0.9996698
RESP:      -0.05208606       0.9986426
RESP:      -0.07848112       0.9969156
RESP:      -0.1048685        0.9944861
RESP:      -0.1312636        0.9913475
RESP:      -0.1576509        0.9874949
RESP:      -0.1840451        0.9829178
RESP:      -0.2104357        0.9776077
RESP:      -0.2368280        0.9715516

RESP:  0                  ; ISHAD. It is obvious from the sun and target positions
                            that the target will not shade the concentrator signif-
                            icantly.

RESP:  0                  ; ICPQR. Remember, the sun is always assumed to be over-
                            head (SV(i) = {0.,0.,1.}) when the ICPQR = 0 option
                            aims facets toward their aim points, even if the
                            user specifies the sun as being off-axis. Since one
                            designs conventional collector systems based upon
                            an on-axis sun, the above option proves to be most
                            helpful in assisting the designer with geometry
                            definition. However, since the designer realizes
                            that the tracking system may not always keep the
                            collector on-axis with respect to the sun, the
                            capability exists in CIRCE2 to specify off-axis sun
                            position to quantify effects of tracking
                            errors. The user may avoid this constraint by choosing
                            ICPQR=1 and aiming the facets "manually."

RESP:  n                  ; There is no pre-existing aim-point data file.

RESP:  1                  ; There will be NAIM=1 aim point for this one-facet con-
                            centrator.

RESP:  -6,4,15            ; XAIM(1),YAIM(1),ZAIM(1). These values will cause the
                            central reflected ray from the dish vertex to strike the
                            target at its center of generation (r=θ=0).

RESP:  n                  ; There is no pre-existing facet data file.
```

[1] For demonstration of the IOPT=6 capability we used displacement data from Table 2 of Section 6.3, which we know is representative of a spherical facet. In carrying out the demonstration, we use the equation of the sphere to determine the r- and z- components of the surface-normal at the required locations.

```
RESP:   1                ; NFACET=1 for this one-facet concentrator.

RESP:   0  0  0          ; X(1),Y(1),Z(1). The vertex of the dish is at the origin
                           of the collector coordinate system.

RESP:   <ret>            ; IBETA=0 for facets of circular projected shape.
```

Comment: Generation of the data file is now complete. Let's look at some of the data output by CIRCE2 upon execution with this data file. The following are excerpts from the **output** file, accompanied by explanatory observations.

output:

FACET	COORDS AT CENTER			UNIT NORMAL VECTOR			FOCAL LEN/	SHADE	AIM	FACET
IDF	X	Y	Z	PN	QN	RN	RAD OF CRV	FACTOR	PNT	ROT'N
1	0.00	0.00	0.00	-0.1849	0.1232	0.9750	0.0000	0.000	1	0

Observation: The components PN, QN, and RN (referred to the collector coordinate system) of the unit normal-vector which orients the dish have been internally calculated (recall ICPQR=0) and are supplied here in what is otherwise an echo of the input data. Similarly, if ISHAD=1 the results that appear here are internally calculated shading factors SBM, and not an echo of the null shading factors input.

output:

```
UNIT VECTOR ORIENTING FLAT TARGET: 0.3536 -0.3536 0.8660
```

Observation: These are the components (referred to the collector coordinate system) of a unit vector representing the direction of the L-axis of the target's virtual K-L coordinate system.

output:

```
FLAT-TARGET ORIENTATION VECTORS VHORIZ, VORTHOG, AND VNORM:
   1      0.7071      0.7071      0.0000
   2      0.3536     -0.3536      0.8660
   3      0.6124     -0.6124     -0.5000
```

Observation: VHORIZ is the unit vector that marks the direction of the K-axis (which is constrained to always be horizontal, *i.e.* in the 1-2 plane of the local target coordinate system, see Figure 5.1a). VNORM is normal to the target, facing in a general downward direction (toward the concentrator). VORTHOG completes the right-handed orthogonal coordinate system.

output:

TARGET DEFINITION

NTAG	XTA	YTA	ZTA	VMTx	VMTy	VMTz
1	-0.6000E+01	0.4000E+01	0.1500E+02	0.6124	-0.6124	-0.5000
2	-0.6000E+01	0.4000E+01	0.1500E+02	0.6124	-0.6124	-0.5000
3	-0.6000E+01	0.4000E+01	0.1500E+02	0.6124	-0.6124	-0.5000
4	-0.6000E+01	0.4000E+01	0.1500E+02	0.6124	-0.6124	-0.5000
5	-0.6000E+01	0.4000E+01	0.1500E+02	0.6124	-0.6124	-0.5000
6	-0.5646E+01	0.4354E+01	0.1500E+02	0.6124	-0.6124	-0.5000
7	-0.5625E+01	0.4125E+01	0.1531E+02	0.6124	-0.6124	-0.5000
8	-0.5823E+01	0.3823E+01	0.1543E+02	0.6124	-0.6124	-0.5000
9	-0.6125E+01	0.3625E+01	0.1531E+02	0.6124	-0.6124	-0.5000
10	-0.6354E+01	0.3646E+01	0.1500E+02	0.6124	-0.6124	-0.5000
11	-0.5293E+01	0.4707E+01	0.1500E+02	0.6124	-0.6124	-0.5000
12	-0.5250E+01	0.4250E+01	0.1561E+02	0.6124	-0.6124	-0.5000
13	-0.5646E+01	0.3646E+01	0.1587E+02	0.6124	-0.6124	-0.5000
14	-0.6250E+01	0.3250E+01	0.1561E+02	0.6124	-0.6124	-0.5000
15	-0.6707E+01	0.3293E+01	0.1500E+02	0.6124	-0.6124	-0.5000

Observation: These are the global (X,Y,Z) coordinates of the target mesh-points and the target normals at these points.

output:

NTAG	FLUX (W/cm^2)
1	0.305531E+01
2	0.305531E+01
3	0.305531E+01
4	0.305531E+01
5	0.305531E+01
6	0.179380E+01
7	0.179078E+01
8	0.171665E+01
9	0.151087E+01
10	0.145495E+01
11	0.134720E+01
12	0.137470E+01
13	0.133304E+01
14	0.106620E+01
15	0.100657E+01

Observation: List of normally-incident flux at the target points.

output:

```
          ***** FLUX DISTRIBUTION ON TARGET (W/cm2) *****
THETA(j)=  0.0000    0.7854    1.5708    2.3562    3.1416
 R(i)
0.0000    3.055E+00 3.055E+00 3.055E+00 3.055E+00 3.055E+00
0.5000    1.794E+00 1.791E+00 1.717E+00 1.511E+01 1.455E+00
1.0000    1.347E+00 1.375E+00 1.333E+00 1.066E+00 1.007E+00
```

Observation: Normally-incident flux upon each of the target points. R is the radial distance (meters) from the center of generation of the target and THETA (in radians) is the polar angle θ. These quantities are illustrated in Figure 8.2.

output:

```
MATRIX INDICATING THE NUMBER OF RAYS CONTRIBUTING TO EACH TARGET POINT
 55        55        55        55        55
 45        51        50        47        40
 27        36        40        31        29
```

Observation: This "**hit map**" indicates the number of subfacets whose reflected central-rays strike a target point. The rows and columns of this matrix correspond to those of the flux-distribution matrix above, *i.e.* they have the same R and θ indices. For example, the point experiencing 51 "hits" is located at R=0.5 meters and θ=0.7854 radians.

output:

```
INTEGRATED FLUX USING QAGS AND QNC79 FOR FLAT TARGETS = 0.243796E+05 W
    POWER MATRIX (HOGAN'S METHOD):     0.128371E+05  0.110340EE+05
        TOTAL POWER ON TARGET(HOGAN'S METHOD)IS 0.238711E+05 WATTS.
```

Observation: The first line lists the results from the sophisticated Legendre-Gauss/Newton-Cotes integration scheme (subroutines QAGS and QNC79) available for flat targets (see Section 5.2.2). Line 2 contains the results of "star pattern" integration over 3x3 sub-matrices of the flux-distribution matrix (see Appendix C). These "power matrix" elements are then summed to obtain total collected power as reported on line 3. The QAGS/QNC79 result is reported in the summary table (see below) when flat targets are involved.

output:

```
      **** SUMMARY RESULTS ****
CONCENTRATOR SURFACE AREA =                156.408 m2
Ap = SOLAR PROJECTED AREA=                 150.090 m2
Ar = Ap REDUCED BY SHADING AND BLOCKING =150.090 m2
I = SOLAR INSOLATION =1000.00 W/m2
NO. OF SUNS IN PEAK =   30.55
Pideal = MAX INTERCEPTABLE POWER = I*Ap =  0.150090E+06 W
```

```
Prefl = PWR REFL FROM CONC. = I*Ar*REFLEC =0.120072E+06 W
Prec = POWER ON RECEIVER (QAGS & QNC79) =  0.243796E+05 W
Ceff = CONCENTRATOR EFFNCY = Prefl/Pideal =80.00%
Reff = RECEVR COLLECTION EFF = Prec/Prefl =20.30%
TOTAL COLLECTOR SYSTM EFFINCY = Ceff*Reff =16.24%
```

Observation: The above is the results summary table located at the bottom of the **output** and **flux** files. The basis of these quantities is explained near the end of Example 2. Note that since the reflectivity REFLEC is 0.8, the reflected power is only 80% of the maximum reflectable power, and the target captures only 20.3% of this, so that the total system efficiency (which is the ratio of the collected power to the maximum reflectable power) is 16.24%.

EXAMPLE 4 Collector System with Hybrid Receiver and Cyclic Symmetry

For conventional collector systems, in many instances symmetry can be exploited to minimize computational time/expense and to get higher resolution of the flux distribution. Figure 7.2 shows a faceted collector system that is symmetric about a plane through the truss arm and receiver. The flux distribution produced on this receiver, if it were on-axis with the sun, would be similarly symmetric. Thus, only half of the receiver need be modelled. This reduces the number of target grid points necessary to fully and uniquely resolve the flux distribution on the receiver.

The collector system to be analyzed in Example 4 is shown in Figures 8.3, 8.4, and 8.5. It features a concentrator consisting of four spherical facets of triangular projected shape. Assume that it is desired to emulate a 10 meter diameter, 25 degree rim-angle parabolic concentrator with the four facets. The projected area of such a concentrator is 78.54 m^2. Let each of the triangular facets have a projected area equal to 1/4 of this value. Then the sides of the equilateral triangles have a length of FLENG = 6.73 meters. The three outer facets will be located symmetrically about the collector Z-axis as shown, their centroids a distance of 2/3 of a facet-height[1] from the axis. Thus, their centroids are located on a radius of R = 3.89 m. The Z-coordinate of the centroids is determined by the parabolic formula $Z = R^2/(4f)$ where f is the focus of the parabolic concentrator being emulated. In this case, from Equation (6.3), the focus is 11.28 meters and Z is calculated to be 0.34 meters. Using the above formulas and the relations $X = Rcos(w)$ and $Y = Rsin(w)$, where w is a polar angle assuming the values of 30, 150, and 270 degrees at the centroids of facets 1, 2, and 3 respectively, one can determine the collector-system coordinates of the facet centroids. Now, assuming that it is desired to maximize the concentration of sunlight at the focus of the concentrator, the radius of curvature (R.O.C.) of each facet should be twice the distance from the facet vertex to the focal point. Thus, $R.O.C._i = 2sqrt(X_i^2 + Y_i^2 + (f - Z_i)^2)$, where i ranges over the four facets. Accordingly, the R.O.C. of facets 1, 2, and 3 is found to be 23.22 m and that of facet 4, its centroid located at (X=0,Y=0,Z=0), is found to be 22.56 meters.

The next consideration in building the concentrator is the facet rotation. Figure 8.4 shows a view from above the concentrator. The facet- and sun-reflector coordinate-systems for each facet are shown. Section 4.3 explains the algorithm by which the $\xi - \eta$ systems are oriented, and Figure 6.4 shows the standard orientation for the x-y axes on a triangular facet. The rotational orientation of the facet is governed by the rotation angle IBETA between the $\xi - \eta$ and the x-y systems. A positive value of IBETA corresponds to counterclockwise rotation of the x-y system relative to the $\xi - \eta$ system (see Figure 7.4). The values of IBETA required to achieve the necessary facet orientations are given in the figure. Note that for facet 4, IBETA=0, causing the facet- and sun-reflector systems to coincide .

Finally, the effects of shading must be taken into account. As will be explained below, the target has a maximum radius of 0.5 meters. It produces a circular shadow that is completely contained within facet 4 of the concentrator. The area of the shadow is 0.79

[1] In the sense of the base and height dimensions of a triangle.

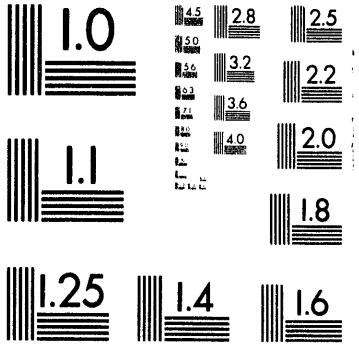
1.0
1.1
1.25
1.4
1.6
1.8
2.0
2.2
2.5
2.8
3.2
3.6
4.0
4.5
5.0
5.6
6.3
7.1

2 of 2

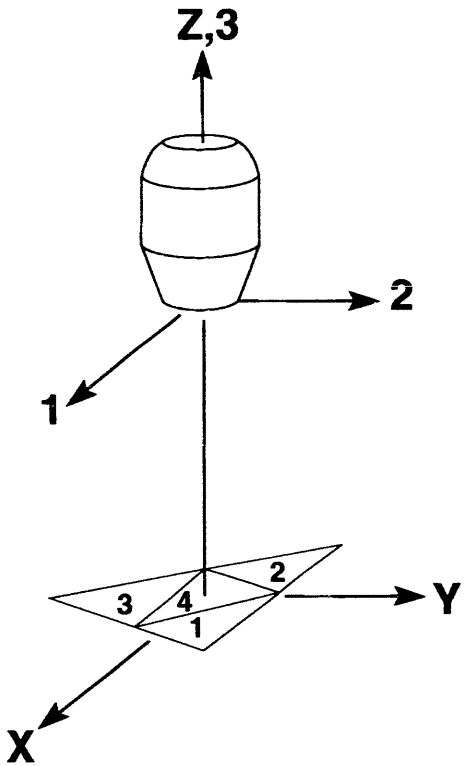

Figure 8.3 Collector system of Example 4

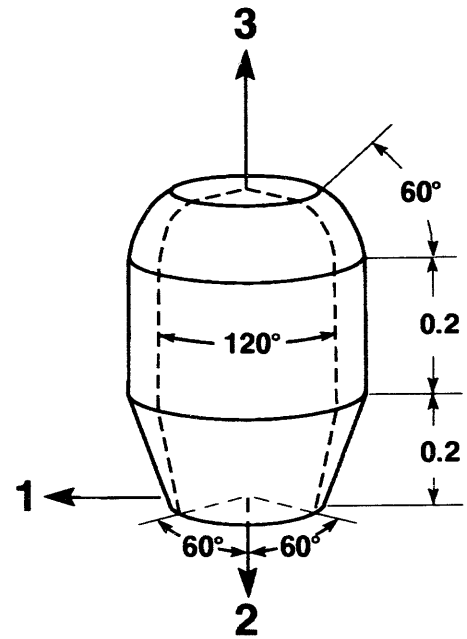

Figure 8.5 Four-component hybrid cavity receiver

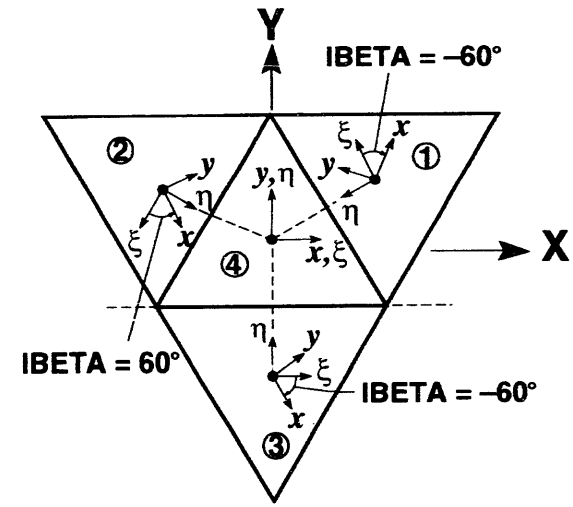

Figure 8.4 Top-view of concentrator made up of four triangular facets

square meters, which is approximately 4% of the area of the facet. Thus, the shading factor for this facet is SBM(4)=0.04.

Using the data file from Example 1 (Appendix D) as a model, the following facet data file, here named **example4.fac**, is produced to be later read into DEKGEN2:

```
4
1          3.3690    1.9450    0.3400    23.22     0.00     1     -60
2         -3.3690    1.9450    0.3400    23.22     0.00     1      60
3          0.0000   -3.8900    0.3400    23.22     0.00     1     -60
4          0.0000    0.0000    0.0000    22.56     0.04     1       0
```

Note that the first line in the data file contains the parameter NFACET, which specifies the number of facets on the concentrator and the number of lines of data to follow.

The receiver is a hybrid receiver built-up from conical, cylindrical, spherical, and flat-circular component shapes. The parameter specifications for the hybrid receiver will make more sense if the reader already understands the commands required to build the individual component shapes. The individual generation of each of these geometries is covered in Sections 5.4.2 to 5.4.5.

With the proposed concentrator, the flux distribution on the axisymmetric cavity receiver has 1/3 cyclic symmetry. That is, when a curve of constant r and z (hybrid receivers are generated with an (r,θ,z) cylindrical coordinate system) on the receiver surface is traversed, the flux distribution is periodic with a period equal to 120 degrees. Therefore, if any continuous 120 degree angular section of the receiver is modeled, it will capture a full period of the flux distribution and is sufficient to uniquely determine the flux distribution over the entire receiver. We will take advantage of this to reduce computational requirements. Of course, if only 1/3 of the receiver is modeled, the total power output by CIRCE2 corresponds to 1/3 of that on the full receiver. Therefore, the total power collected is obtained by multiplying the calculated power by 3. More details on the building of the receiver are given in comment lines beside the responses below. Let's begin by running DEKGEN2:

```
% dekg2-g3.x              ; Run the DEKGEN2 code.

RESP:   <ret>             ; Press the "return" key after reading version information

RESP:   <ret>             ; Press the "return" key after reading disclaimer.

RESP:   N                 ; We'll build this data file from scratch.

RESP:   EXAMPLE 4 OF CIRCE2 USER'S MANUAL; title descriptive of the analysis

RESP:   0 0 1             ; SV(i), i=1-3 are the components of the direction vector
                            of the sun.  In this case an overhead sun is specified.

RESP:   1000              ; I, the solar insolation in W/m^2
```

```
RESP:   1                   ; JSUN=1; we elect to define the sun with a table of data

RESP:   Y                   ; Here I want to read in sunshape data from the file
                              generated in Example 1.

RESP: dir.example1/sun.dat ;the name of the file containing the required sun data
                              (The user will have to press the "return" key several
                              times to scroll through the data being read-in. This
                              allows the user to check the incoming data.)

RESP:   2                   ; NER=2 concentrator error distributions to be input

RESP:   0,2.5,2.5           ; TH(1),SIGR(1),SIGS(1)    --same as in Example 1

RESP:   0,1.5,1.5           ; TH(2),SIGR(2),SIGS(2)    --same as in Example 1

RESP:   2                   ; IDIM. According to the guidelines in Section 4.6.4, for
                              a faceted concentrator with less than 15-20 facets, the
                              best combination of convolution options is the set
                              IDIM=2/IANLYT=0/NEWCONV=2. This combination is very
                              accurate, relatively inexpensive, and requires no
                              knowledge of rms widths of the sunshape and mapped
                              error-cone distributions or of the concentrator-
                              averaged incidence angle μ̄.

RESP:   0                   ; IANLYT.

RESP:   2                   ; NEWCONV.

RESP:   SUN.DAT tabular sunshape;   descriptive title of sun and error parameters

RESP:   120 DEG. ANGULAR SECTION OF A FOUR-COMPONENT HYBRID CAVITY RECEIVER; title

RESP:   -4                  ; ITARSH. This hybrid receiver will be made of 4 differ-
                              ent component geometries: cylindrical, spherical,
                              conical, and flat-circular.

RESP:   y                   ; Though we already know it from the calculations above
                              with equation 6.3, let's check against DEKGEN2's
                              computed focal length.

RESP:   25                  ; RIMANG, the equivalent dish rim-angle of the faceted
                              concentrator.

RESP:   5                   ; DISHRAD, the equivalent dish radius of the faceted
                              concentrator.
```

```
RESP:   <ret>                ; As expected, the focal length of such a concentrator is
                               11.28 meters (rounded). Press "return" after reading.

RESP:   FOUR-COMPONENT HYBRID RECEIVER #Ah5-x10-P  ; descriptive title

RESP:   <ret>                ; Press the "return" key after reading the message.

RESP:   0, 0, 11.28          ; (X_o, Y_o, Z_o). Spillage will be minimized by positioning
                               the receiver such that it's aperture plane is at the
                               concentrator focus.

RESP:   0.3                  ; This is the radius of the receiver aperture, hence the
                               bottom radius of the lowermost component, as Figure 8.5
                               indicates. Frequent reference to this figure will be
                               required for most of the following.

RESP:   120                  ; KEXT=120 indicates that a 1/3 circumferential section of
                               the receiver will be modeled.

RESP:   90                   ; This value of THETAC centers the 120 degree target-
                               section about the 2-3 plane of Figure 8.5. The rela-
                               tive position of the concentrator should result in a
                               flux pattern that is symmetric about this plane.
                               (This value of THETAC will be used in generating each of
                               the component targets individually.)

RESP:   19                   ; KPTS is the number of azimuthal grid-points on the
                               target mesh. The shape of the concentrator results
                               in a substantial flux variation in the
                               azimuthal direction. Since we are only modeling
                               1/3 of the receiver, 19 points should capture the
                               variation adequately.

RESP:   n                    ; CIRCE2 can output a data file (see Section 3.4) that can
                               be read directly into the solar-receiver thermal
                               analysis code AEETES [18]. We have no need for such a
                               file at this time.

RESP:   COMPONENT 1 OF HYBRID RECEIVER: INVERTED CONE FRUSTRUM; component 1 title

RESP:   4                    ; ITYPE. The receiver is built from the aperture up,
begin-
                               ning with the frustrum of an inverted cone as the
                               bottom-most component (see Figure 8.5).

RESP:   0.5                  ; RTOP, the top radius of the conical section (see
                               Figure 5.8).
```

```
RESP:   0.2              ; LEXT, for conical targets it equals the frustrum height

RESP:   7                ; LPTS, for this component, is the number of mesh points
                           to be equally spaced in the slant-direction of the frus-
                           trum. Since a relatively small percentage of insolation
                           will fall on this surface, we will avoid unnecessary
                           resolution here.

RESP:   COMPONENT 2 OF HYBRID RECEIVER: RIGHT-CIRCULAR CYLINDER; component 2 title

RESP:   3                ; ITYPE for component 2. This component, the second from
                           the bottom, has a cylindrical characteristic shape.

RESP:   0.2              ; LEXT for a cylindrical target section is its height ΔZ
                           (see Figure 5.6).

RESP:   15               ; LPTS, the number of grid points to be distributed in a
                           vertical direction along the cylindrical surface. Since
                           we expect more flux and larger variation here, we have
                           doubled the number of grid points from the previous
                           component.

RESP:   COMPONENT 3 OF HYBRID RECEIVER: SPHERICAL CONVERGING SECTION;   title

RESP:   1                ; ITYPE for the spherical component, third from the
                           bottom.

RESP:   0.5              ; RCURV, the radius of curvature of the spherical target
                           (see Figure 5.4).

RESP:   60               ; LEXT, in this case the zenith angle between top and
                           bottom arcs of the spherical section

RESP:   15               ; LPTS, in this case the number of mesh points to be
                           distributed at equal increments of the zenith angle φ.

RESP:   COMPONENT 4 OF HYBRID RECEIVER: TOP CIRCULAR CAP-PLATE;  component 4 title

RESP:   6                ; ITYPE for the flat-circular top component.

RESP:   15               ; LPTS, for this component, the number of mesh points in
                           the radial direction (see Figure 5.2).

RESP:   1                ; INORM for treatment as an internal (cavity) receiver

RESP:   <ret>            ; Designating this receiver as an internal receiver
                           implies a circular aperture. DEKGEN2 automatically
                           generates one using internal logic. Press
```

```
                    the "return" key when ready to proceed.

RESP:  "PARABOLIC" CONCENTRATOR MADE UP OF FOUR SPHERICAL TRIANGULAR FACETS; title

RESP:  1.              ; REFLEC, perfect surface-reflectance is assumed

RESP:  3               ; KORD=3 for facets having a triangular projected shape.
RESP:  3               ; IOPT=3 for facets with spherical contour.

RESP:  6.73            ; FLENG for triangular facets is the edge-length of the
                         facet's projected shape.  This number was derived
                         at the beginning of this example.

RESP:  4               ; NSUBF in the case of a triangular facet is the number
                         of divisions along each edge of the triangular
                         projected-shape.  This will cause the facet to be
                         divided into 4x4=16 equilateral triangles of equal size.

RESP:  2               ; ISHAD.  We have already included the shading factors SBM
                         in the file example4.fac.

RESP:  0               ; This choice for ICPQR dictates that CIRCE2 internally
                         calculate normals such that the reflected central rays
                         from the facet centers strike their respective aim-
                         points.

RESP:  n               ; We do not have a file containing aim-point data and must
                         therefore enter the data interactively.

RESP:  1               ; NAIM.  Recall from above that the common aim point of
                         all facets is to be at the "focus" of the concentrator.

RESP:  0.,0.,11.28     ; XAIM(1),YAIM(1),ZAIM(1) are the collector-system coord-
                         inates of the location of the single aim-point.

RESP:  y               ; We will read-in the facet data file prepared earlier.

RESP:  example4.fac    ; Note the warning message supplied by DEKGEN2.
```

Comment: An annotated **hybrid** file for this example is given below. After using it in the CIRCE2 run we can rename it **"example 4.hyb"** to identify it with this analysis. Note that the circular target sector, component #4, when part of a hybrid receiver is treated as a special case of a cylindrical receiver (see notes in Sections 5.4.2 and 5.4.6).

Annotated **hybrid** file:

```
FOUR-COMPONENT HYBRID RECEIVER #Ah5-x10-P;receiver description
                  ;IAEETES (AEETES file print-option indicator)
COMPONENT 1 OF HYBRID RECEIVER: INVERTED CONE FUSTRUM;title of comp.1
      4                              ;ITYPE (ITARSH target-type)
        2.09440  0.20000  19       7 ;KEXT(rad),LEXT,KPTS,LPTS
        0.00000  0.00000   11.38000  ;(Xo,Yo,Zo)
        0.30000  0.50000    1.57080  ;RBOT, RTOP, THETAC(rad)
COMPONENT 2 OF HYBRID RECEIVER: RIGHT-CIRCULAR CYLINDER ;title of comp.2
      3                              ;ITYPE (ITARSH target-type)
        2.09440  0.20000  19      15 ;KEXT(rad),LEXT,KPTS.LPTS
        0.00000  0.00000   11.58000  ;(Xo,Yo,Zo)
        0.50000  0.00000    1.57080  ;RADIUS,NOT_USED,THETAC(rad)
COMPONENT 3 OF HYBRID RECEIVER: SPHERICAL CONVERGING SECTION;title of comp.3
      1                              ;ITYPE (ITARSH target-type)
        2.09440  1.04720  19      15 ;KEXT(rad),LEXT,KPTS,LPTS
        0.00000  0.00000   11.68000  ;(Xo,Yo,Zo)
        0.50000  1.04720    1.57080  ;RCURV,PHIC(rad),THETAC(rad)
COMPONENT 4 OF HYBRID RECEIVER: TOP CIRCULAR CAP-PLATE;title of comp.4
      6                              ;ITYPE (ITARSH target-type)
        2.09440  0.25000  19      15 ;KEXT(rad),LEXT,KPTS,LPTS
        0.00000  0.00000   12.11301  ;(Xo,Yo,Zo)
        0.00000  0.00000    1.57080  ;NOT_USED,NOT_USED,THETAC(rad)
```

Comment: Below are listed the summary results tables for the individual components of the hybrid receiver and for the receiver as a whole. Adding collected powers and tripling (only 1/3 of the receiver was modeled), the total receiver collection efficiency turns out to be about 99.24%, the other 0.76% of the reflected power falls outside the aperture.

output: (component 1, inverted cone frustrum)

```
      **** SUMMARY RESULTS ****
CONCENTRATOR SURFACE AREA =              78.713 m2
Ap = SOLAR PROJECTED AREA=               77.593 m2
Ar = Ap REDUCED BY SHADING AND BLOCKING =76.809 m2
I = SOLAR INSOLATION =1000.00 W/m2
NO. OF SUNS IN PEAK = 0.00
Pideal = MAX INTERCEPTABLE POWER = I*Ap =  0.775933E+05 W
Prefl = PWR REFL FROM CONC. = I*Ar*REFLEC =0.768088E+05 W
Prec = POWER ON RECEIVER (HOGAN'S METHOD) =0.000000E+00 W
Ceff = CONCENTRATOR EFFNCY = Prefl/Pideal =  98.99%
Reff = RECEVR COLLECTION EFF = Prec/Prefl =   0.00%
TOTAL COLLECTOR SYSTM EFFINCY = Ceff*Reff     0.00%
```

output: (component 2, right circular cylinder)

```
    **** SUMMARY RESULTS ****
CONCENTRATOR SURFACE AREA =                78.713 m2
Ap = SOLAR PROJECTED AREA=                 77.593 m2
Ar = Ap REDUCED BY SHADING AND BLOCKING =76.809 m2
I = SOLAR INSOLATION =1000.00 W/m2
NO. OF SUNS IN PEAK =   17.46
Pideal = MAX INTERCEPTABLE POWER = I*Ap =  0.775933E+05 W
Prefl = PWR REFL FROM CONC. = I*Ar*REFLEC =0.765088E+05 W
Prec = POWER ON RECEIVER (HOGAN'S METHOD) =0.277068E+03 W
Ceff = CONCENTRATOR EFFNCY = Prefl/Pideal =  98.99%
Reff = RECEVR COLLECTION EFF = Prec/Prefl =   0.36%
TOTAL COLLECTOR SYSTM EFFINCY = Ceff*Reff     0.36%
```

output: (component 3, spherical converging section)

```
    **** SUMMARY RESULTS ****
CONCENTRATOR SURFACE AREA =                78.713 m2
Ap = SOLAR PROJECTED AREA=                 77.593 m2
Ar = Ap REDUCED BY SHADING AND BLOCKING =76.809 m2
I = SOLAR INSOLATION =1000.00 W/m2
NO. OF SUNS IN PEAK =  188.37
Pideal = MAX INTERCEPTABLE POWER = I*Ap =  0.775933E+05 W
Prefl = PWR REFL FROM CONC. = I*Ar*REFLEC =0.768088E+05 W
Prec = POWER ON RECEIVER (HOGAN'S METHOD) =0.142109E+05 W
Ceff = CONCENTRATOR EFFNCY = Prefl/Pideal =  98.99%
Reff = RECEVR COLLECTION EFF = Prec/Prefl =  18.50%
TOTAL COLLECTOR SYSTM EFFINCY = Ceff*Reff    18.31%
```

output: (component 4, flat-circular cap plate)

```
    **** SUMMARY RESULTS ****
CONCENTRATOR SURFACE AREA =                78.713 m2
Ap = SOLAR PROJECTED AREA=                 77.593 m2
Ar = Ap REDUCED BY SHADING AND BLOCKING =76.809 m2
I = SOLAR INSOLATION =1000.00 W/m2
NO. OF SUNS IN PEAK =  201.97
Pideal = MAX INTERCEPTABLE POWER = I*Ap =  0.775933E+05 W
Prefl = PWR REFL FROM CONC. = I*Ar*REFLEC =0.768088E+05 W
Prec = POWER ON RECEIVER (QAGS & QNC79) =  0.109197E+05 W
Ceff = CONCENTRATOR EFFNCY = Prefl/Pideal =  98.99%
Reff = RECEVR COLLECTION EFF = Prec/Prefl =  14.22%
TOTAL COLLECTOR SYSTM EFFINCY = Ceff*Reff    14.07%
```

output: (aggregate hybrid receiver)

```
**** SUMMARY RESULTS FOR COMPOSITE HYBRID RECEIVER ****
CONCENTRATOR SURFACE AREA =                78.713 m2
Ap = SOLAR PROJECTED AREA=                 77.593 m2
Ar = Ap REDUCED BY SHADING AND BLOCKING =76.809 m2
I = SOLAR INSOLATION =1000.00 W/m2
NO. OF SUNS IN PEAK =  201.97
Pideal = MAX INTERCEPTABLE POWER = I*Ap =   0.775933E+05 W
Prefl = PWR REFL FROM CONC. = I*Ar*REFLEC = 0.768088E+05 W
Prec = POWER ON RECEIVER                   = 0.254077E+05 W
Ceff = CONCENTRATOR EFFNCY = Prefl/Pideal =  98.99%
Reff = RECEVR COLLECTION EFF = Prec/Prefl =  33.08%
TOTAL COLLECTOR SYSTM EFFINCY = Ceff*Reff    32.74%
```

9 REFERENCES

[1] Wan, C.C., "CAV Code for the Determination of Incident Flux Distribution in an Axisymmetrical Cavity from a Parabolidal Reflector," Ford Aerospace & Communications Corp. Technical Report SCSE-016, July, 1980.

[2] "Concentrator Optical Performance Software (COPS)," user's manual, Honeywell Report DOE/CS/35348-T1 (Vol.2), January, 1980.

[3] Biggs, F., and Vittitoe, C.N., "The HELIOS Model for the Optical Behavior of Reflecting Solar Concentrators," Sandia National Laboratories report SAND76-0347, 1976 ---- 1979 printing available through the National Technical Information Service, U.S. Department of Commerce.

[4] Vittitoe, C.N., and Biggs, F., "A User's Guide to Helios: A Computer Program for Modelling the Optical Behavior of Reflecting Solar Concentrators, Part I: Introduction and Code Input," Sandia National Laboratories report SAND81-1180, printed August, 1981.

[5] Vittitoe, C.N., and Biggs, F., "A User's Guide to Helios: A Computer Program for Modelling the Optical Behavior of Reflecting Solar Concentrators, Part III: Appendices Concerning Helios--Code Details," Sandia National Laboratories report SAND81-1562, printed September, 1981.

[6] Schrenk, G.L., and Gritton, D.G., "Analysis of Solar Reflectors - Mathematical Theory and Methodology for Simulation of Real Reflectors," Allison Division of General Motors Corp., report GMC-AO-EDR3693, December, 1963.

[7] Ratzel, A.C., and Boughton, B.D., "CIRCE.001: A Computer Code for Analysis of Point-Focus Concentrators with Flat Targets," Sandia National Laboratories Report SAND86-1866, printed February, 1987.

[8] Ratzel, A.C., Boughton, B.D., Mancini, T.R., and Diver, R.B., "CIRCE: A Computer Code for the Analysis of Point-Focus Solar Concentrators," *Proceedings of the 1987 ASME-JSME Solar Energy Conference*, Honolulu, Hawaii, March 22-27, 1987.

[9] Romero, V.J., "CIRCE2/DEKGEN2: A Software Package for Facilitated Optical Analysis of 3-D Distributed Solar Energy Concentrators," *Proceedings of the 1992 ASME-JSES-KSES International Solar Energy Conference*, Maui, Hawaii, April 5-9, 1992.

[10] Grether, D., and Hunt, A., "Description of the LBL Reduced Data Base and Standard Profiles," Lawrence Berkely Laboratory, August 9, 1977.

[11] Kuiper, G.P., editor, *The Sun, The Solar System*, University of Chicago Press, Chicago, IL, 1953.

[12] Pettit, R.B., Vittitoe, C.N., and Biggs, F., "Simplified Calculational Procedure for Determining the Amount of Intercepted Sunlight on an Imaging Solar Concentrator," *ASME Journal of Solar Energy Engineering*, Vol. 105, February, 1983.

[13] Rosen, M.A., "The angular Distribution of Diffuse Sky Radiance: An Assessment of the Effects of Haze," *ASME Journal of Solar Energy Engineering*, vol. 113, August, 1991.

[14] Vittitoe, C.N., and Biggs, F., "Six-Gaussian Representation of the Angular-Brightness Distribution for Solar Radiation," *Solar Energy*, vol. 27, no. 6, Pergamon Press, 1981.

[15] Cook, R.D., Malkus, D.S., and Plesha, M.E., *Concepts and Applications of Finite Element Analysis*, 3rd ed., Wiley, 1989

[16] Thompson, J.F., Warsi, Z.U.A., and Mastin, C. W., *Numerical Grid Generation*, Elsevier Science Publishing Co., 1985

[17] "Development of a Stretched-Membrane Dish," Solar Kinetics, Inc., Sandia National Laboratories contractor report SAND88-7031, printed October, 1989.

[18] Hogan, R. E., "AEETES: A Solar Reflux Receiver Thermal Performance Numerical Model," Sandia National Laboratories report SAND91-1280, in progress.

Other Bibliography

Abramowitz and Stegun, eds, *Handbook of Mathematical Functions*, Dover Publications, 9th printing, 1970.

Diver, R.B., and Andraka, C.E., "CAV2 - A PC-Based Computer Program for Predicting Incident Solar Flux Distributions Inside Dish Cavity Receivers," Sandia National Laboratories report SAND86-0927, printed February, 1987.

Ferziger, J. H., *Numerical Methods for Engineering Application*, John Wiley & Sons, 1981.

Hecht, E., and Zajac, H., *Optics*, Addison-Wesley, 4th printing, 1974.

Strang, G., *Linear Algebra and its Applications*, 2nd ed., Chapter 6, Harcourt Brace Jovanovich, Inc., 1980.

APPENDICES

APPENDIX A: Default USERDISH Subroutine (for IOPT=7)

```
      subroutine userdish(x, y, zdispl, unormal)
      dimension unormal(3)

c     x,y       Coordinates in the x-y-z facet system which locate the
c               centroid of the projected subfacet (see section 6.2).
c               These arguments are supplied by the calling routine.
c
c     zdispl    The height, or z-displacement from the x-y plane, of the
c               subfacet centroid (i.e., the source-point location for
c               the subfacet has coordinates {x,y,zdisp} (see section6.3).
c               This quantity must be supplied to the calling routine.
c
c     unormal   The unit vector defining the facet normal direction at
c               the subfacet centroid. This vector must have at least
c               a small component pointing toward the sun (or energy will
c               not be reflected). The components (relative to the x-y-z
c               facet system basis) must be supplied to the calling program.
c
c     This example models the 14 m. dia., 8.45 m. focal-length parabolic dish
c     of Example 1, Chapter 8. For non-axisymmetric facet contour, a 2-D
c     function for z-displacement in terms of the coordinates (x,y or r,theta)
c     in the plane must be determined. It is necessary that the function be
c     single-valued and is highly recommended that it be smooth (have contin-
c     uous first-order partial and second-order mixed partial derivatives) over
c     the domain (projected shape). Bicubic spline interpolation would do nicely
c     (FORTRAN77 source code for this standard technique is presented in,
c     among other standard references, the book "Numerical Recipes: The Art
c     of Scientific Computing," by William H. Press, et. al., Cambridge University
c     Press, 1986). Such interpolation requires the values of the displacement
c     (and, optionally, of the partial derivatives) be supplied at the grid points of
c     a regular rectangular mesh. Either x or r would govern the abscissas of
c     such a mesh, while y or theta would govern the ordinates, depending upon
c     which coordinates accomodate the data best. Since, in the general case, this
c     subroutine asks for interpolated values and not those at the grid points, the
c     construction of the mesh should be guided by availability of data and accuracy
c     considerations, not by facet discretization. If working with measured data, the
c     values at the grid points can be determined by data regression. It is assumed
c     that there is zero displacement at x=y=0, i.e., the "vertex" of the dish is at the
c     origin of the facet coordinate system.

      focus = 8.45
c___Since this particular dish is axisymmetric, angular position (theta)
c___is immaterial, and the height is only a function of the r coordinate.
      zdispl =(x**2 + y**2)/(4.0*focus)
      unormal(1) = -x
      unormal(2) = -y
```

```
      unormal(3) = 2.0*focus
c___The following subroutine normalizes unormal to be a unit vector.
      call unit(unormal)

      return
      end
```

APPENDIX B: Effect of Convolution Options on Numerical Results and Execution Time

The effect of number and type of convolution(s) on CIRCE2 predictions and execution times are quantified here. Hopefully, this study will provide the user with general guidance for choosing appropriate convolution options for his particular application. Results reported here were obtained on a SUN SPARCstation (SUN Fortran 1.4, level O2 optimization, SunOS 4.1.3 operating system, component of execution time devoted to system operations not included) with version g.3 of CIRCE2.

The first set of results illustrates the inaccuracies of analytic convolution when the sunshape distribution is "broader" than the mapped error-cone distribution. As a measure of broadness, we use the rms width (rmsw) of the sunshape distribution, *i.e.* its dispersion, and the rms widths, *i.e* standard deviations, in the principal directions of the mapped error-cone. These quantities are reported in the CIRCE2 **output** results file (in general not being known until the completion of an analysis).

Concentrator #1 has geometry similar to that of Example 1, Chapter 8: a continuous-surface parabolic dish having a rim angle of 45 degrees and a rim diameter of 14 meters. It is divided into 372 subfacets (NSUBF=10). One circular-normal error of rms widths SIGR = SIGS = 0.5 milliradians (mrad) is specified, which results in a much narrower error cone than in Example 1. We use an overhead sun with the same tabular sunshape as in the example, and find apostieri that it has an rmsw of 2.09 mrad, and that a typical[1] 2-D mapped error-cone has rmsw of 1 mrad (as does its 1-D equivalent if IDIM=1 has been selected). Thus, the sunshape distribution is about twice as "wide" as (though correspondingly more shallow than) the mapped error-cone distributions. We say that the mapped error-cone is "relatively" narrow, meaning "narrow relative to the sushape". A 1m. dia. flat-circular target is placed at the focal point of the parabola. A grid of 25 points equally spaced along a target radial line is used to sample the (azimuthally symmetric) flux distribution. (The small number of target grid points permits high sensivity of execution-time to convolution operations, thereby allowing isolation of the relative costs of the various convolution options. Moreover, it is really only the first point, at the center of the target, that is relevant for the figure of merit (peak flux) used in this investigation.)

Eight cases are run, encompassing all the combinations of the convolution options IDIM, IANLYT, and NEWCONV possible for a single-facet concentrator. The pertinent results are displayed in Table B.1. The accuracy of the results is judged by conformance of the peak flux on the target to the result obtained for the "base case" of 2-D numerical convolution at each subfacet (IDIM=2, IANLYT=0, NEWCONV=3), which is assumed to

[1] As explained in section 4.6.3, the rms widths of the mapped error-cone vary at different points on the concentrator, but they do not vary by more than about 10% from the vertex to the rim of this dish over a wide, realistic range of input error-cones.

be most accurate. (This figure of merit isolates the effects of the reflected solar image calculation(s), as opposed to total collected power, which exhibits interdependencies between the effective sunshape(s) and the target grid.)

Table B.1. Effect of Number and Type of Convolutions for Concentrator 1 ("Narrow" Error Cone)

Dimensionality	Convolution Type	Times Convolved	Peak Flux (# of Suns)	Δ% from Base Case	CPU time (sec.)	Savings Factor
2-D	numerical	372	30,139	Base Case	3490	1
2-D	analytic	372	45,724	+52%	3.6	969
2-D	numerical	1	30,108	-0.1%	11.5	303
2-D	analytic	1	45,420	+50.7%	1.7	2053
1-D	numerical	372	29,863	-0.9%	83.6	42
1-D	analytic	372	45,372	+50.5%	3.1	1126
1-D	numerical	1	29,772	-1.2%	1.7	2053
1-D	analytic	1	45,074	+49.6%	1.4	2493

The most obvious and striking result of the study is the very large difference in peak flux when analytic vs. numerical convolution is employed. Irrespective of the other parameters, the result is about 50% high (as a percentage of the base-case peak flux) whenever analytic convolution is used. This difference dwarfs the variations due to different selections of the other convolution parameters, and implies that *analytic convolution (IANLYT=1) is* ***unacceptable*** *when the mapped error-cone is narrower than the sunshape.*

Now, from within the group of runs involving numerical convolution, we notice that "full" convolution (convolution at every subfacet, NEWCONV=3) is prohibitively expensive for the incremental increase in accuracy it provides. One 2-D numerical convolution provides accuracy to within 0.1% of full convolution in less than 1/300 the CPU time. This option is also more accurate and less costly than the 1-D approximation with full convolution. The remaining case of one 1-D numerical convolution is 12X less accurate. In summary, it may reasonably be concluded that, at least *for the case of a relatively narrow error-cone, the optimal combination is a single numerical convolution with a 2-D mapped error-cone (NEWCONV=1, IANLYT=0, IDIM=2).*

Returning to Table B.1, we see that the differences between full (372 times) and minimal (1 time) convolution, all other things being equal, is relatively small (0.7% at most over the four pairs of runs). Combined with the fact that minimal convolution requires from 2 to 300 times less CPU than corresponding runs with full convolution, the

optimal condition[2] under which to perform the single convolution becomes an important issue. Though a 0.7% error corresponding to μ=0 is not very large, if we can considerably reduce it with little effort, then we can eliminate under most any conditions the need (and accompanying expense) of multiple effective sunshape calculations.

It would appear that the optimal incidence angle $\bar{\mu}$ under which to perform the mapping would be the surface-area-weighted angle of incidence for sunrays striking the concentrator:

$$\bar{\mu} = \frac{1}{A}\int_S \mu dS = \frac{1}{A}\int_S acos\,(\hat{N}_0 \bullet \hat{V}_s)\,dS \qquad \text{(B.1)}$$

where S represents the concentrator surface, A the concentrator surface-area, $\hat{N}_o$ the surface normal, $\hat{V}_s$ the unit vector pointing toward the sun, and *acos*( ) the inverse-cosine function. Unfortunately, the integral does not appear to evaluate, for standard parabolic and spherical geometries, to a useful (simple) form. However, a good approximation to $\bar{\mu}$ may be obtained for our present application in the following manner: We take advantage of the fact that the on-axis sun allows $\hat{V}_s$ to be written as $\hat{z}$, the unit vector in the direction of the dish axis, and that the axisymmetric character of the dish allows us to write the surface-normal as a function of two space coordinates (r and z), instead of three. Converting the unit-normal from Cartesian components (see Appendix A) to r-z components, we get

$$\hat{N}_o = \frac{-r\hat{r} + 2f\hat{z}}{\sqrt{r^2 + 4f^2}} \qquad \text{(B.2)}$$

where $\hat{r} = cos\vartheta\hat{x} + sin\vartheta\hat{y}$, ϑ=*atan(y/x)*, and $r = \sqrt{x^2 + y^2}$.

The incident angle μ then becomes simply the inverse-cosine of the z-component of $\hat{N}_o$. We may then approximate $\bar{\mu}$ as the inverse-cosine of the z-component of the average[3] normal over the parabolic dish.

2. The results in Table B.1 where NEWCONV=1 were obtained using the choice INCPICK=2, which directs CIRCE2 to use, in the effective sunshape calculation, the angle of incidence μ at the vertex of the first facet listed in the data file. For this concentrator the resulting angle was μ=0 degrees. Alternatively, CIRCE2 allows the freedom to input a value of μ (the parameter INCANGL introduced in Section 4.6.3) through which the error-cone is mapped before performing the ensuing convolution with the incident sunshape. Thus, μ constitues a free variable under which to optimize the single calculated effective sunshape used in the analysis.

3. It is recognized that, over an axisymmetric surface, the area-averaged x- and y- components of the surface-normal are zero. However, this does not imply that the average r-component of such a vector is zero (and therefore the average z component unity) because r depends upon the square of the x and y components, and though both may average to zero, their squared values do not.

An approximation to the average normal-vector over a generic paraboloid of rim-radius R and focus f may be obtained by the following process: The average z- and r-components over the concentrator surface turn out to be:

$$\bar{N}_z(R,f) = \frac{1}{A}\int_S (\hat{N}_o \bullet \hat{z})\, dS = \frac{1}{A}\int_0^R (\hat{N}_o \bullet \hat{z})\, \frac{2\pi r dr}{\hat{N}_o \bullet \hat{z}} = \frac{\pi R^2}{A(R,f)} \tag{B.3}$$

and

$$\bar{N}_r(R,f) = \frac{1}{A}\int_S (\hat{N}_o \bullet \hat{r})\, dS = \frac{1}{A}\int_0^R (\hat{N}_o \bullet \hat{r})\, \frac{2\pi r dr}{\hat{N}_o \bullet \hat{z}} = -\frac{\pi R^3}{3f \cdot A(R,f)} \tag{B.4}$$

The average unit surface-normal, $\hat{N}_{avg}(R,f)$, is defined here as:

$$\hat{N}_{avg}(R,f) = \frac{\bar{N}_r(R,f)\,\hat{r} + \bar{N}_z(R,f)\,\hat{z}}{\sqrt{\bar{N}_r^2 + \bar{N}_z^2}} \tag{B.5}$$

Thus, for an on-axis sun, the approximate surface-averaged incidence angle over a parabolic concentrator of rim-radius R and focus f is

$$\bar{\mu}(R,f) \approx acos\,(\hat{N}_{avg} \bullet \hat{z}) = acos\,(\,[1 + [R/(3f)]^2]^{-1/2}\,) \tag{B.6}$$

For the concentrator at hand, Equation (B.6) yields $\bar{\mu} \approx 15$ degrees. Supplying this value for the representative incident-angle parameter INCANGL via the INCPICK=1 option of CIRCE2, the following results are obtained:

Table B.2. Concentrator 1, NEWCONV=1/INCPICK=1/INCANGL=15

Dimen-sionality	Convolution Type	Times Convolved	Peak Flux (# of Suns)	Δ% from Base Case	CPU time (sec.)	Savings Factor
2-D	numerical	1	30,137	-0.007%	11.5	303
2-D	analytic	1	45,707	+51.7%	1.7	2053
1-D	numerical	1	29,857	-0.9%	1.7	2053
1-D	analytic	1	45,356	+50.5%	1.4	2493

The average difference in peak flux between the single-convolution runs in Table B.1 (where INCPICK=2) and their full-convolution (372 times) counterparts is 0.45%. The average difference in peak flux between the runs in Table B.2 and their full-convolution counterparts in Table B.1 is 0.027%. This is a decrease by more than a factor of 16. Individually, in all cases the error drops by over an order of magnitude. This benefit, small in absolute terms because of the small magnitude of the original errors here, becomes more pronounced as the width of the error-cone increases. For instance, a similar investiga-

tion with Concentrator 2 (see below) reduces errors from an average of 3.3% to an average of 0.2% (a factor of 16 reduction), with individual errors falling by no less than a factor of 10. So, we see that in the more common case of a relatively wide error cone, we can reduce from a few percent to a few tenths of a percent the difference between calculating the reflected solar image at every subfacet (NEWCONV=3) and calculating it only once (NEWCONV=1) at a representative angle of incidence. Since the case of a new sunshape calculated at the vertex of each facet (NEWCONV=2) is enveloped here, the following holds in general: *We can reduce to insignificant the difference between calculating the reflected solar image at many places on the concentrator (NEWCONV=2,3) and at only one location (NEWCONV=1) by supplying, via the INCPICK=1 option, an appropriate angle INCANGL at which to perform the effective-sunshape calculation. Rigorously, such an angle is the concentrator-averaged angle of incidence of sun rays, μ. In practice, an effective approximation to μ may be calculated as the inverse-cosine of the component (in the direction of the solar central-ray) of the area-weighted unit surface-normal.*

To summarize our findings thus far, the conclusion still holds that for the case of a relatively narrow error cone, the optimal combination is a single numerical convolution with a 2-D mapped error cone (NEWCONV=1, IANLYT=0, IDIM=2). We may improve upon this by saying that if one can easily obtain an approximation to the surface-averaged incident angle μ, we should take advantage of the extra knowledge by invoking the option INCPICK=1 and assigning the parameter INCANGL this value. In our investigation above, when we did this we reduced the percent deviation from full 2-D numerical convolution from 0.1% to 0.007% at no added CPU cost.

We now proceed to the analysis of Concentrator #2, which is identical to Concentrator 1 except that its error-cone is approximately 3 times broader. Two individual circular-normal errors of rms widths SIGR(1) = SIGS(1) = 2.5 mrad and SIGR(2) = SIGS(2) = 1.5 mrad contribute to the error cone. The rms widths in the principal directions of the mapped error-cones vary over the dish by less than +/- 5% about a representative value of 5.7 mrad. Thus, an error-cone 3X wider than in Concentrator 1 translates into a typically 5.7X wider *mapped* error-cone. Since the sunshape has an rms width of about 2 mrad, we would classify the mapped error-cone distribution as a relatively wide one. Table B.3 lists the results of eight cases run that encompass all the combinations of the convolution options IDIM, IANLYT, and NEWCONV. In accordance with the above findings, the parameters INCPICK=1 and INCANGL=15 degrees were specified for the single-convolution runs.

Table B.3. Effect of Number and Type of Convolutions for Concentrator 2 ("Wide" Error Cone)

Dimensionality	Convolution Type	Times Convolved	Peak Flux (# of Suns)	Δ% from Base Case	CPU time (sec.)	Savings Factor
2-D	numerical	372	6459	Base Case	2550	1
2-D	analytic	372	6553	+1.5%	3.3	773
2-D	numerical	1	6444	-0.2%	9.3	274
2-D	analytic	1	6538	+1.2%	1.9	1342

Table B.3. Effect of Number and Type of Convolutions for Concentrator 2 ("Wide" Error Cone) (Continued)

1-D	numerical	372	6402	-0.9%	69.6	37
1-D	analytic	372	6541	+1.3%	2.9	879
1-D	numerical	1	6388	-1.1%	2.0	1275
1-D	analytic	1	6527	+1.0%	1.4	1821

It is immediately seen that the agreement between numerical and analytical convolution is much better than in the narrow error-cone simulations of Table B.1. The discrepancies have dropped from an average of about 50% high in those simulations to about 1.5% high in these. At the same time, analytical convolution is between 1.4 and 772 times faster than its numerical counterpart. Surprisingly, 1-D analytic convolution is more accurate than 2-D analytic convolution, and a single analytic convolution (either 1-D or 2-D) at the representative incidence angle of $\bar{\mu}$=15 degrees is better than convolution at every subfacet[4]. These outcomes resonate to make the combination of parameters (IDIM=1,IANLYT=1,NEWCONV=1,INCPICK=1,INCANGL=$\bar{\mu}$) very attractive; full 2-D numerical convolution results were matched within 1% at a savings of over 1800X. *The optimum choice, however, in terms of relative accuracy and execution time, appears to be a single 2-D numerical convolution at the representative incidence angle* $\bar{\mu}$ *(IDIM=2,IANLYT=0,NEWCONV=1,INCPICK=1,INCANGL=*$\bar{\mu}$*).* (This was exactly the same conclusion reached for Concentrator 1 above with a relatively narrow error cone.) This option requires 1/274 the run-time of full 2-D numerical convolution and displays accuracy within 0.2%. Since the total cost is minimal (only 9.3 CPU-seconds), the additional accuracy comes cheaply.

The complexion of the study changes sharply, however, when for NEWCONV=1 the angle μ through which the error-cone is mapped is not representative of $\bar{\mu}$. Table B.4 presents results of simulations where the combination NEWCONV=1/INCPICK=2 is used[2]. We see that now the optimal choice is full 1-D numerical convolution; a speedup of over 36X is realized vs. full 2-D numerical convolution, with a peak flux that matches to within 1%. A good, slightly less-accurate but much faster alternative is full 1-D analytic convolution, for which a speedup of nearly 880X is realized vs. full 2-D numerical convolution, with a peak flux that deviates by only 1.3%. We can conclude that *if a fairly good approximation to* $\bar{\mu}$ *is not available, the optimal combination of convolution parameters for a relatively wide error cone is IDIM=1/IANLYT=0/NEWCONV=3. Or, just slightly less accurate but much faster, analytic convolution may be used in the combination IDIM=1/IANLYT=1/NEWCONV=3.*

4. These are not general trends. They are reversed in the outcomes reported in Table B.4, where the choice INPICK=2 is used and the single convolution takes place at an angle of incidence of 0 degrees[2].

Table B.4. Concentrator 2, NEWCONV=1/INCPICK=2

Dimen-sionality	Convolution Type	Times Convolved	Peak Flux (# of Suns)	Δ% from Base Case	CPU time (sec.)	Savings Factor
2-D	numerical	1	6254	-3.2%	9.4	271
2-D	analytic	1	6340	-1.8%	1.8	1417
1-D	numerical	1	6193	-4.1%	2.0	1275
1-D	analytic	1	6334	-1.9%	1.4	1821

From the results of this study we may reach another general conclusion: *the most robust*[5] *method of convolution is full 1-D numerical convolution (IDIM=1,IANLYT=0, NEWCONV=3).* For both concentrators (wide-cone and narrow-cone), this combination led to peak fluxes that were within 1% of those calculated with full 2-D numerical convolution, in typically 1/40 the run-time. Additionally, this approach does not require an estimate for $\bar{\mu}$, making it automatic to use. However, as we have seen, if a good estimate for $\bar{\mu}$ is available, then single 2-D numerical convolution becomes robust for applications involving relatively wide error-cones[6]). In this case, it is much more cost-effective to use single 2-D numerical convolution. In fact, over the two concentrators, with the value we derived of $\bar{\mu} \approx 15$ degrees, we found an average deviation of about 0.1% in peak flux from full 2-D numerical convolution, with average run-time reduced by a factor of 290X. We may conclude: *provided a good estimate for $\bar{\mu}$ is available, single 2-D numerical convolution is the best overall method of convolution.*

5. Of course, the most robust method of convolution is really full 2-D numerical convolution, but since this is impractically expensive in most cases, it is discounted from consideration here.

6. We have already determined that it is the best choice for relatively narrow error-cones, whether a good estimate for $\bar{\mu}$ is available or not.

APPENDIX C: Hogan's Improved Method for Integrating Flux Distributions on Axisymmetric Receivers.

Sandia National Laboratories
Albuquerque, New Mexico 87185

date: February 19, 1991

to: R. B. Diver, 6217

from: R. E. Hogan and V. J. Romero, 1513

subject: Improved CIRCE2 Integrator for Axisymmetric Geometries

Introduction

The CIRCE computer code[1] for predicting incident solar flux distributions from point-focus concentrators has received extensive use in the solar community. It was developed originally to predict flux distributions on flat targets. Recently, CIRCE was modified to permit prediction of incident solar flux distrbutions on non-planar and axisymmetric geometries. The enhanced version of the code is now commonly referred to as CIRCE2.

During the development of a numerical model for reflux solar receivers, the use of CIRCE2 in predicting the total power incident upon the Sandia reflux pool-boiler receiver pointed out a deficiency in the integrated power computation for axisymmetric geometries. In particular, the power computed by CIRCE2 on an axisymmetric target is dependent on the limits of integration. This memo describes the difficulties we encountered using CIRCE2 for axisymmetric geometries and describes our solution.

CIRCE for Flat Targets

The original CIRCE computer code was developed to predict solar flux distributions on flat targets. Figure 1 shows the form of the array of computed fluxes for a circular target contained in the CIRCE output file. To calculate the power incident on the target, an approximation for the integral of these fluxes over the target area is computed using a Jacobian mapping of the circular target geometry into a rectangular domain. The integral over the target is then evaluated as a summation of the integrals approximated using 3x3 (9 functional values) rectangular sub-areas. Figure 1 also shows a typical sub-area to which an integrating formula can be applied to approximate the value of the integral. The two different sub-area integrating formulas used in CIRCE to approximate this integral are

$$I_1 = \frac{A}{36}\left\{16 f_{center} + \sum f_{corners} + 4\sum f_{midsides}\right\} \qquad (1)$$

[1]Ratzel, A. C. and Boughton, B. D., *CIRCE.001: A Computer Code for Analysis of Point-Focus Concentrators with Flat Targets*, SAND86-1866, February 1987.

and

$$I_2 = \frac{A}{48}\left\{20 f_{center} + \sum f_{corners} + 6\sum f_{midsides}\right\}, \qquad (2)$$

where f is the integrand and A is the area of the rectangular sub-area. For this geometry, $f_{i,j} = F_{i,j} r_i$ and $A = 4\Delta r \Delta\theta$, because of the circular mapping. Equation (1) is referred to in the CIRCE output as "Method 1" and Eq. (2) is "Method 2." These are also given in the Helios manual as Eqs. (7.1-4b) and (7.1-5b), respectively [2]. They are used to compute the power on all targets that can be analyzed in CIRCE2. For flat targets only, a highly accurate Legendre-Gauss/Newton-Cotes integration package[1] (hereafter referred to as the Legendre-Cotes method) is also employed. Method 1 results from applying Simpson's rule for integration in each direction and is referred to as the "Product Simpson's Rule Formula." Currently in CIRCE, the numerical "error" in the power is calculated as the difference in the power calculated using Eqs. (1) and (2).

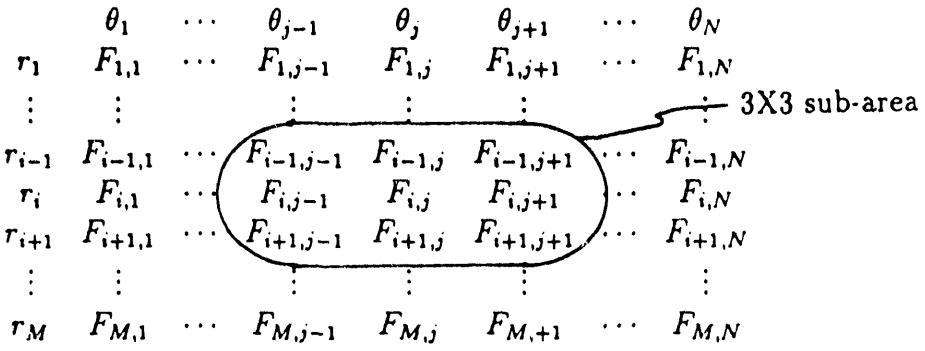

Figure 1. Form of flux array in typical CIRCE output and 3X3 sub-area array for an axisymmetric target.

Enhanced CIRCE for Axisymmetric Targets – CIRCE2

For an axisymmetric target, the incident solar fluxes are circumferentially periodic over 2π. If either of the integrating schemes, Eqs. (1) or (2), is used to calculate the power on an axisymmetric geometry, the computed power is dependent on the limits of integration. For instance, the power integrated from 0 to 360° is, in general, not equal to the power integrated from δ to $360+\delta$° with either Eqs. (1) or (2). The integrated power on the axisymmetric target should be independent of the limits of circumferential integration.

To illustrate this problem, apply Eqs. (1) and (2) to the (r,θ) array of functional values (product of flux and radius) on an axisymmetric target as shown in Fig. 2. Since the geometry is axisymmetric and the flux distribution is circumferentially periodic, the

[2] Biggs, F. and Vittitoe, C. N., *The Helios Model for the Optical Behavior of Reflecting Solar Concentrators*, SAND76-0347, March 1979.

	θ_1	θ_2	θ_3	θ_4	θ_5
r_1	$f_{1,1}$	$f_{1,2}$	$f_{1,3}$	$f_{1,4}$	$f_{1,5}$
r_2	$f_{2,1}$	$f_{2,2}$	$f_{2,3}$	$f_{2,4}$	$f_{2,5}$
r_3	$f_{3,1}$	$f_{3,2}$	$f_{3,3}$	$f_{3,4}$	$f_{3,5}$
r_4	$f_{4,1}$	$f_{4,2}$	$f_{4,3}$	$f_{4,4}$	$f_{4,5}$
r_5	$f_{5,1}$	$f_{5,2}$	$f_{5,3}$	$f_{5,4}$	$f_{5,5}$

Figure 2. Form of CIRCE2 flux array for an axisymmetric target with four intervals in both r and θ coordinates.

values for θ and flux at the starting and ending points, $i = 1$ and $i = 5$, respectively, are the same. Thus, $\theta_5 = \theta_1, f_{1,5} = f_{1,1}, f_{2,5} = f_{2,1}$, etc. Figure 3 shows this periodic distribution written with repeating subscripts using $f_{1,1} = f_{1,5}$. In Fig. 3, the functional values are repeated in the circumferential coordinate direction to aid in applying Eq. (1) with different integration limits. Using Eq. (1), CIRCE2 Method 1 integration scheme, and integrating from θ_1 to θ_1 as shown in Fig. 3, the expression for the integral is

$$\begin{aligned} I^1_{\theta_1-\theta_1} = \frac{A}{36} \{ & 2f_{1,1} + 4f_{1,2} + 2f_{1,3} + 4f_{1,4} \\ & +8f_{2,1} + 16f_{2,2} + 8f_{2,3} + 16f_{2,4} \\ & +4f_{3,1} + 8f_{3,2} + 4f_{3,3} + 8f_{3,4} \\ & +8f_{4,1} + 16f_{4,2} + 8f_{4,3} + 16f_{4,4} \\ & +2f_{5,1} + 4f_{5,2} + 2f_{5,3} + 4f_{5,4} \}, \end{aligned} \tag{3}$$

where $A = 4\Delta r \Delta\theta$ for a cylindrical target due to the mapping of the cylindrical geometry onto a rectangular domain.

Again using Eq. (1), CIRCE2 Method 1, and integrating from θ_2 to θ_2, the expression for the integral is

$$\begin{aligned} I^1_{\theta_2-\theta_2} = \frac{A}{36} \{ & 4f_{1,1} + 2f_{1,2} + 4f_{1,3} + 2f_{1,4} \\ & +16f_{2,1} + 8f_{2,2} + 16f_{2,3} + 8f_{2,4} \\ & +8f_{3,1} + 4f_{3,2} + 8f_{3,3} + 4f_{3,4} \\ & +16f_{4,1} + 8f_{4,2} + 16f_{4,3} + 8f_{4,4} \\ & +4f_{5,1} + 2f_{5,2} + 4f_{5,3} + 2f_{5,4} \} \end{aligned} \tag{4}$$

For these integrals to always be equal, assuming arbitrary fluxes, the coefficients of corresponding $f_{i,j}$'s in Eqs. (3) and (4) must be identical. Clearly, these coefficients are not equal and the values of the integrals are different. Consequently, the integrals

	θ_1	θ_2	θ_3	θ_4	θ_1	θ_2	$\cdots$
r_1	$f_{1,1}$	$f_{1,2}$	$f_{1,3}$	$f_{1,4}$	$f_{1,1}$	$f_{1,2}$	$\cdots$
r_2	$f_{2,1}$	$f_{2,2}$	$f_{2,3}$	$f_{2,4}$	$f_{2,1}$	$f_{2,2}$	$\cdots$
r_3	$f_{3,1}$	$f_{3,2}$	$f_{3,3}$	$f_{3,4}$	$f_{3,1}$	$f_{3,2}$	$\cdots$
r_4	$f_{4,1}$	$f_{4,2}$	$f_{4,3}$	$f_{4,4}$	$f_{4,1}$	$f_{4,2}$	$\cdots$
r_5	$f_{5,1}$	$f_{5,2}$	$f_{5,3}$	$f_{5,4}$	$f_{5,1}$	$f_{5,2}$	$\cdots$

Figure 3. Periodic form of flux array for an axisymmetric target with four intervals in both r and θ coordinates.

are dependent on the choice of integration limits. By subtracting Eqs. (3) and (4), an expression for the difference, or error, E_1, in the power can be computed

$$\begin{aligned} E_1 = I^1_{\theta_1-\theta_1} - I^1_{\theta_2-\theta_2} = \frac{A}{18} \{ & (-f_{1,1} + f_{1,2} - f_{1,3} + f_{1,4}) \\ & +4(-f_{2,1} + f_{2,2} - f_{2,3} + f_{2,4}) \\ & +2(-f_{3,1} + f_{3,2} - f_{3,3} + f_{3,4}) \\ & +4(-f_{4,1} + f_{4,2} - f_{4,3} + f_{4,4}) \\ & +(-f_{5,1} + f_{5,2} - f_{5,3} + f_{5,4})\} \end{aligned} \tag{5}$$

For an arbitrary flux distribution, the difference in power computed with different integration limits is nonzero. Equation (5) suggests this difference could be zero when the fluxes are all equal for each discrete r coordinate. Also, if the field were uniform, then the integrals are independent of integration limits. A similar conclusion is obtained if Eq. (2) (CIRCE2 Method 2) is used to evaluate the integrals in a similar analysis, though the error term E_2 is different.

If the values of the integrals (3) and (4) differ, then what is the appropriate value of the integrated power on the target for Method 1? The proposed approach is to take the average of Eqs. (3) and (4) which results in the expression:

$$\begin{aligned} \overline{I^1} = \frac{1}{2}(I^1_{\theta_1-\theta_1} + I^1_{\theta_2-\theta_2}) = \frac{A}{12} \{ & (0.5f_{1,1} + f_{1,2} + f_{1,3} + f_{1,4} + 0.5f_{1,1}) \\ & +4(0.5f_{2,1} + f_{2,2} + f_{2,3} + f_{2,4} + 0.5f_{2,1}) \\ & +2(0.5f_{3,1} + f_{3,2} + f_{3,3} + f_{3,4} + 0.5f_{3,1}) \\ & +4(0.5f_{4,1} + f_{4,2} + f_{4,3} + f_{4,4} + 0.5f_{4,1}) \\ & +(0.5f_{5,1} + f_{5,2} + f_{5,3} + f_{5,4} + 0.5f_{5,1})\} \end{aligned} \tag{6}$$

The result shown in Eq. (6) is quite interesting because it represents an extended trapazodial integration in the θ coordinate and a Simpson's rule integration in the r coordi-

nate. Equation (6) is also obtained by averaging the integrating scheme given by Eq. (2) (CIRCE2 Method 2) in a similar manner.

Numerical Results

To illustrate the application of the proposed method, the integrated power computed with Eqs. (1) and (2) with different integration limits is compared with the power computed using the proposed method, Eq. (6). For this comparison, the solar flux distribution incident on a 1 m radius circular flat target from a single off-axis (canted) facet reflector is chosen as an example. This example is part of a 3-facet reflector system presented as an example problem (Example 2, pg. 28, Reference 1) in the CIRCE manual. A flat target was chosen because it permits the comparison of computed results with the highly sophisticated Legendre-Coates integration algorithm.

A comparison of the computed integrated powers is presented in Table 1. To compute these CIRCE2 results, the circular target was divided into 10 circumferential and 50 radial intervals. The computed power for Method 1 and Method 2 agree well for the same limits of integration. However, for different limits of integration, the computed power differs by approximately 6% for this example. Compared to the power computed with the Legendre-Coates integration, the power computed with either Method 1 or Method 2 differ by ±3%, depending upon the limits of integration. The magnitude of these errors are unique to the incident solar flux distribution for this example. However, the agreement between the power computed with the proposed method and with the Legendre-Coates method is excellent.

Integration Limits (°)	CIRCE2 Method 1 Eq. (1)	CIRCE2 Method 2 Eq. (2)	Proposed Method Eq. (6)	Legendre-Coates Method
0-0	49627	49627	48299	48298
36-396	46969	46969	48299	48297

Table 1. Comparison of computed integrated power (W) for CIRCE2 and proposed integrating method.

These results suggest several general conclusions on the accuracy of these integration methods when applied to flat axisymmetric targets.

1. The CIRCE2 error estimate computed as the difference of Methods 1 and 2 is an inappropriate error indicator for axisymmetric targets.
2. The power computed with either Method 1 or Method 2 is different than the power computed with the Legendre-Coates integration method.
3. The power computed with either Method 1 or Method 2 is dependent on the limits of integration.
4. The power computed with the proposed method is identical to the power computed with the Legendre-Coates integration method.
5. The power computed with the proposed method is independent of the limits of integration.

Comparisons for axisymmetric non-planar (conical and spherical) geometries also show the computed power using Methods 1 and 2 depend on the limits of integration. Since there is no Legendre-Cotes integraton scheme for non-flat targets in CIRCE2, a direct comparison cannot be made between these methods. However, it is reasonable to assume that, just as for flat targets, the Legendre-Cotes method and the proposed method proposed will yield essentially identical results, which are independent of the limits of integration, and which are superior to results obtained using either Methods 1 or 2.

For flat rectangular targets or angular sub-sections of axisymmetric targets, the flux distributions are rarely periodic with respect to the grid and the question of integration limit dependence is not applicable. However, for these targets, it is informative to compare integrated power predicted with these methods. Table 2 shows the computed powers for a 0.304 m x 0.304 m square target on Test Bed Concentrator No. 1 with an 11x11 grid of points. In this example, the results of Methods 1 and 2 are high by approximately the same amount as the proposed method is low when compared to the Legendre-Cotes results. Thus, it apears that, for any target type CIRCE2 is capable of analyzing, the proposed integration method is at least as accurate, and for axisymmetric geometries more accurate, than Methods 1 and 2. Moreover, the proposed method produces results that agree with the Legendre-Cotes scheme while being far less complex to code and much less computer-intensive. This makes possible an easy upgrade to the routines in CIRCE2 without implementing the complex Legendre-Cotes package for non-planar axisymmetric targets.

CIRCE2 Method 1 Eq. (1)	CIRCE2 Method 2 Eq. (2)	Proposed Method Eq. (6)	Legendre-Coates Method
76258	76253	76035	76162

Table 2. Comparison of computed integrated power (W) for CIRCE2 and proposed integrating method for square target.

Conclusions and Recommendations

We have shown that the integrated power obtained using the Method 1 and 2 integration schemes in CIRCE2 is dependent on the limits of integration when applied to axisymmetric geometries. An integrating scheme for axisymmetric geometries has been proposed whose result is independent of the limits of integration. Results computed with the proposed method agree well with results from the sophisticated Legendre-Coates intergration scheme for the examples cited.

It is recommended that the proposed integration scheme be implemented into CIRCE2 in place of Methods 1 and 2, and that the Legendre-Cotes scheme be retained as a check for integrated power on flat targets. This modification should be included before the code is frozen later this year.

reh

Key Words: **2216.330, Solar, CIRCE2, Axisymmetric Receivers**

Copy to:
1500 E. H. Barsis
1510 J. C. Cummings
DKG 1511 D. K. Gartling
1512 A. C. Ratzel
1513 J. C. Cummings, acting
1513 R. E. Hogan
1513 V. J. Romero
1513 Dayfiles (2)
1514 H. S. Morgan
6216 C. E. Tyner
6216 T. R. Mancini
6217 P. C. Klimas
6210 J. T. Holmes, acting

APPENDIX D: Annotated "input" File of Example Problem #1

```
EXAMPLE 1 OF CIRCE2 USER'S MANUAL                    ; TITLE
SAMPLE TABULAR SUNSHAPE MODEL                        ; TITLE
    0.000000   0.000000   1.000000                   ;SV(i),i=1 to 3 (a unit vector)
       1    1000.000                                 ;JSUN, I
       22                                            ;NTABL
         1     0.0000     0.20106E+04                ;  1    RHO(1)      SVAL(1)
         2     0.3520     0.20106E+04                   .       .           .
         3     0.7040     0.20080E+04                   .       .           .
         4     1.0560     0.19912E+04
         5     1.4080     0.19667E+04
         6     1.7600     0.19354E+04
         7     2.1120     0.19013E+04
         8     2.4640     0.18646E+04
         9     2.8160     0.18141E+04                   .       .           .
        10     3.1680     0.17383E+04                   .       .           .
        11     3.5200     0.16202E+04                   K    RHO(K)      SVAL(K)
        12     3.8720     0.13652E+04                   .       .           .
        13     4.2240     0.88421E+03                   .       .           .
        14     4.5760     0.83487E+02
        15     4.9280     0.17796E+02
        16     5.2800     0.21680E+01
        17     5.6320     0.15224E+01
        18     5.9840     0.11320E+01
        19     6.3360     0.87220E+00
        20     6.6880     0.75840E+00                   .       .           .
        21     7.0400     0.68450E+00                   .       .           .
        22     7.2160     0.00000E+00                ;NTABL  RHO(NTABL)  SVAL(NTABL)
       2       1      1     1                        ;NER, IDIM, IANLYT, NEWCONV
         0.000000    2.500000    2.500000            ;TH(1) SIGR(1) SIGS(1)
         0.000000    1.500000    1.500000            ;TH(2) SIGR(2) SIGS(2)
       2                                             ;INPICK
1 METER RADIUS FLAT-CIRCULAR TARGET                  ;TITLE
       6                                             ;ITARSH
         6.28319    1.00000    1    25               ;THETAMAX(rad), RMAX, TPTS, RPTS
         0.00000    0.00000    8.45000               ;(Xo, Yo, Zo)
         0.00000    0.00000    0.00000               ;ALPHA, BETA, NOT_USED_HERE
       0                                             ;IAPT
       0                                             ;INORM
14 METER DIA., 45 DEG. RIM-ANGLE PARABOLIC DISH      ;TITLE
       1     1     1.000                             ;KORD, IOPT, REFLEC
       7.0000     10                                 ;FLENG, NSUBF
       1      1                                     ;ISHAD, ICPQR
         0.00000      0.00000      0.00000          ;SHADING-OBJECT PARAMETERS
         0.00000      0.00000      1.00000          ;    "       "       "
       1                                             ;NFACET
   1    0.0000    0.0000    0.0000    8.4500     0.000      0           0
 {IDF   X(IDF)    Y(IDF)    Z(IDF)    FOC(IDF) SBM(IDF)  IDAIM(IDF)  IBETA(IDF)}
       1    0.00000     0.00000     1.00000          ;IDF, PN(IDF), QN(IDF), RN(IDF)
```

APPENDIX E: Output "flux" File from Example Problem #1

```
**************************************************************************
  EXAMPLE 1 OF CIRCE2 USER'S MANUAL
**************************************************************************

                    **** FLUX DISTRIBUTION ON TARGET (W/cm^2) ****

  THETA(j)=    0.0000
    R(i)
 0.0000      6.334E+02
 0.0417      4.992E+02
 0.0833      2.469E+02
 0.1250      8.026E+01
 0.1667      1.856E+01
 0.2083      3.372E+00
 0.2500      5.192E-01
 0.2917      6.828E-02
 0.3333      7.532E-03
 0.3750      5.529E-04
 0.4167      0.000E+00
 0.4583      0.000E+00
 0.5000      0.000E+00
 0.5417      0.000E+00
 0.5833      0.000E+00
 0.6250      0.000E+00
 0.6667      0.000E+00
 0.7083      0.000E+00
 0.7500      0.000E+00
 0.7917      0.000E+00
 0.8333      0.000E+00
 0.8750      0.000E+00
 0.9167      0.000E+00
 0.9583      0.000E+00
 1.0000      0.000E+00


MATRIX INDICATING THE NUMBER OF RAYS CONTRIBUTING TO EACH TARGET POINT:

     371
     371
     371
     371
     371
     371
     371
     154
```

56
14
0
0
0
0
0
0
0
0
0
0
0
0
0
0
0

OPTICAL EFFICIENCY FOR APERTURE DISK:

RADIUS (M)	% OF TOT RADIUS	% OF TOT TGT AREA	% OF TOTAL PWR ON TGT	% OF PWR ON UNSHADED DISH
0.00	0.00	0.00	0.00	0.00
0.04	4.17	0.17	20.02	20.03
0.08	8.33	0.69	59.03	59.07
0.12	12.50	1.56	86.15	86.20
0.17	16.67	2.78	96.70	96.76
0.21	20.83	4.34	99.39	99.45
0.25	25.00	6.25	99.91	99.97
0.29	29.17	8.51	99.99	100.05
0.33	33.33	11.11	100.00	100.06
0.38	37.50	14.06	100.00	100.06
0.42	41.67	17.36	100.00	100.06
0.46	45.83	21.01	100.00	100.06
0.50	50.00	25.00	100.00	100.06
0.54	54.17	29.34	100.00	100.06
0.58	58.33	34.03	100.00	100.06
0.62	62.50	39.06	100.00	100.06
0.67	66.67	44.44	100.00	100.06
0.71	70.83	50.17	100.00	100.06
0.75	75.00	56.25	100.00	100.06
0.79	79.17	62.67	100.00	100.06
0.83	83.33	69.44	100.00	100.06
0.88	87.50	76.56	100.00	100.06
0.92	91.67	84.03	100.00	100.06
0.96	95.83	91.84	100.00	100.06
1.00	100.00	100.00	100.00	100.06

**** SUMMARY RESULTS ****

CONCENTRATOR SURFACE AREA = 157.202 M^2
Ap = SOLAR PROJECTED AREA = 150.796 M^2
Ar = Ap REDUCED BY SHADING AND BLOCKING = 150.796 M^2
I = SOLAR INSOLATION = 1000.00 W/M^2
NO. OF SUNS AT PEAK = 6333.65
Pideal = MAX INTERCEPTABLE POWER = I*Ap = 0.150796E+06 W
Prefl = PWR REFL FROM CONC. = I*Ar*REFLEC = 0.150796E+06 W
Prec = POWER ON RECEIVER (QAGS & QNC79) = 0.150885E+06 W
Ceff = CONCENTRATOR EFFNCY = Prefl/Pideal = 100.00%
Reff = RECEVR COLLECTION EFF = Prec/Prefl = 100.06%
TOTAL COLLECTOR SYSTM EFFINCY = Ceff*Reff = 100.06%

APPENDIX F: Corner Locations for a Rectangular Aperture

This appendix describes the procedure used to calculate the collector-system coordinates of the corners of a rectangular aperture. The algorithm is applied to the construction of the circular aperture in Example 3 of Chapter 8, which may be defined by an inscribed square aperture frame.

The aperture is shown in Figure 8.1. Recall from section 5.4 that the corner points are numbered in a clockwise manner when viewed from the concentrator. The numbering starts in the upper-left corner and proceeds clockwise to the lower-left corner as depicted in Figures 5.10 and 8.1. Additionally, the line-segment connecting corners 1 and 2 must be horizontal, as must be the segment between corners 3 and 4. (That is, the Z-coordinates of corners 1 and 2 must be equivalent, and corners 3 and 4 must also have a mutual Z-coordinate.) However, the plane of the aperture does not have to be horizontal. (Example 3 involves an aperture that is tilted with respect to the global X-Y-Z system.) In most cases, the aperture is usually centered about the collector Z-axis and resides in a horizontal plane normal to this axis. In such cases the coordinates of the aperture corners are fairly obvious. However, the following procedure may be used to calculate the corner-point coordinates for tilted apertures (it is assumed that the user can supply location and orientation information for the aperture plane.)

Referring to the aperture frame depicted in Figure 8.1, let the center of the aperture of dimensions a x b be specified by some vector $\vec{V}_c$ originating at the collector coordinate-system origin, which in this example also coincides with the origin of the facet coordinate system. (In some cases, the user may know directly the components of $\vec{V}_c$, but in other cases they may have to be calculated based upon other known information as illustrated here.) For simplicity in this example, let the vector point to the target coordinate-system origin. (If the vector is to point to some grid point on the target, the grid's coordinates can be found by performing a minimal run of CIRCE2 (no aperture specified, NFACET=1,NSUBF=1, IDIM=1, IANALYT=1, NEWCONV=1) and obtaining the target grid coordinates from the **output** file.) From Example 3 of Chapter 8, we know that the coordinates of the target-system origin are (-6,4,15). Thus, a unit vector in the direction of $\vec{V}_c$ is:

$$\hat{d} = (-6\hat{X} + 4\hat{Y} + 15\hat{Z})/\text{sqrt}((-6)^2 + 4^2 + 15^2)$$

where $\hat{X}$, $\hat{Y}$, and $\hat{Z}$ are the unit vectors in the collector-system X, Y, and Z directions, respectively.

The vector $\vec{V}_c$ can be obtained by multiplying the above unit vector by the scalar D (distance from the collector-system origin to the aperture). Here we will take this distance to be 15 meters (approximately 1.6 meters in front of the target). Thus,

$$\vec{V}_c = (-6\hat{X} + 4\hat{Y} + 15\hat{Z})\text{x}15/\text{sqrt}(277).$$

The orientation of the aperture plane is defined by specification of the unit normal $\hat{r}$, which is perpendicular to the plane and faces in the general direction of the concentrator. (It is assumed that the user has the components r1, r2, and r3 of the $\hat{r}$ vector, along the

collector-system X-, Y-, and Z- axes, respectively.) A p-q-r orthogonal cartesian coordinate system can now be defined subject to the constraint that the p-axis is horizontal (has no Z-component just like the lines connecting corners 1,2 and 3,4). Here, the p- and q- axes lie in the aperture plane and are related to the r-axis of the right-handed system by the vector equation $\hat{r} = \hat{p} \times \hat{q}$. This yields 3 equations for the six unknowns p1, p2, p3, q1, q2, and q3. Another equation becomes available by requiring the p- and q- axes to be perpendicular: $\hat{p} \bullet \hat{q} = 0$. To make this a conventional coordinate system we will want the magnitudes of p and q to equal unity, which requires a fifth equation specifying one of them to have unit magnitude, the other then also being constrained to have unit magnitude if the cross product of these orthogonal vectors is to yield a unit vector $|\hat{r}|$. To uniquely specify the rotational orientation of the p-q system about $\hat{r}$, one component of either of their direction vectors must be specified. From the constraint that the p-axis be horizontal, we get the sixth equation: p3 = 0. After some manipulation, the pertinent equations for the other components of $\hat{p}$ and $\hat{q}$ are, in their most useful form,

$$q3 = (+)\ \mathrm{sqrt}|(r1)^2 + (r2)^2|$$

$$q1 = -r1 \times r3/q3$$

$$q2 = -r2 \times r3/q3$$

$$p1 = -r2/q3$$

$$p2 = r1/q3$$

For simplicity in this example, the aperture plane is taken to be normal to $\dot{V}_c$. That is, $\hat{r} = -\hat{d}$. The above equations then yield: q3 = sqrt(52/277), q1 = 90/sqrt(52*277), q2 =-60/sqrt(52*277), p1 = 4/sqrt(52), p2 = /sqrt(52), and p3 = 0.

Referring to Figure 8.1, we will now calculate the vector which, when added to $\dot{V}_c$, points to corner 2 of the aperture frame. In general, it is seen that the vector to corner n of the aperture frame is given by:

$$\begin{aligned}
\dot{V}(n) &= Vn_p\hat{p} + Vn_q\hat{q} \\
&- Vn_p(p1\hat{X} + p2\hat{Y}) + Vn_q(q1\hat{X} + q2\hat{Y} + q3\hat{Z}) \\
&= (Vn_p \cdot p1 + Vn_q \cdot q1)\hat{X} \\
&\quad + (Vn_p \cdot p2 + Vn_q \cdot q2)\hat{Y} \\
&\quad + (Vn_q \cdot q3)\hat{Z}
\end{aligned}$$

From Figure 8.1, for corner 1, $Vn_p = V1_p = -a/2$ and $Vn_q = V1_q = b/2$; for corner 2, $Vn_p = V2_p = a/2$ and $Vn_q = V2_q = b/2$; etc. Now, for our application (the circular aperture of Example 3, Chapter 8), we have the special case of a square aperture frame inscribed within the circular aperture. Thus, $a = b = \sqrt{2}R$, where R is the radius of the circular aperture. A radius of 1.0 meter yields $a = b = 1.4142$ meters. Thus, the vector from the origin of the p-q-r system to corner point 2 becomes, using $V2_p = 0.7071$ and $V2_q = 0.7071$: $\dot{V}(2) = 0.923\hat{X} + 0.235\hat{Y} + 0.306\hat{Z}$. As a check, note that the length of $\dot{V}(2)$ is

unity, as it should for this example. By an analogous procedure, the vector to corner 1 is found to be: $\vec{V}(1) = 0.138\hat{X} + -0.942\hat{Y} + 0.306\hat{Z}$. Then, the relations $\vec{V}(3) = -\vec{V}(1)$ and $\vec{V}(4) = -\vec{V}(2)$ are employed. Finally, the collector-system coordinates of the nth corner point are given by the vector sum $\vec{V}_c + \vec{V}(n)$. For corner 2 this becomes: $\vec{V}_c + \vec{V}(2) = (-5.408 + 0.923)\hat{X} + (3.605 + 0.235)\hat{Y} + (13.519 + 0.306)\hat{Z}$. Thus, the response to the DEKGEN2 prompt in Example 3 for the coordinates of corner 2 of the aperture becomes: -4.485, 3.84, 13.825. The responses for the other corners are derived similarly.

APPENDIX G: Quick-Reference Directory

G.1 Glossary Index

G.2 Parameters Used in DEKGEN2

Sun and Error Parameters

Keyword	Description	Units	Page #
DIPSUN	Characteristic width of a 1-D circular-normal sunshape	[milliradians]	28
I	Solar flux intensity	[W/m^2]	20, 25
IANLYT	Specifies analytic or numerical convolution of effective sunshape		34
IDIM	Identifier for dimensionality of effective sunshape		33
INCANGL	Concentrator-averaged incidence angle	[degrees]	36
INCPICK	Qualifier for NEWCONV = 1 option		36
JSUN	Sunshape-type specifier and manner of input		27
NER	Number of reflector errors		30
NEWCONV	Controls number and location of effective sunshape calculations		35
NTABL	Number of values in sunshape table		28
RHOEDGE	Radius of pillbox sun	[milliradians]	28
RHO	Angle with respect to sun central ray	[milliradians]	28
SIGR	Princ. axis standard deviation of elliptic-normal error distribution	[milliradians]	29-30
SIGS	Princ. axis standard deviation of elliptic-normal error distribution	[milliradians]	29-30
SVAL	sunshape magnitude function		28
SV(i)	Components of a vector pointing toward the sun	any	25
TH	Rotation angle for elliptic-normal error distribution	[degrees]	30

Target/Receiver Parameters

Keyword	Description	Units	Page #
AC(i,j)	aperture-corner locations in collector-system coordinates	[m]	51
ALPHA	flat target rotation angle	[degrees]	42
BETA	flat target tilt angle	[degrees]	42
IAPT	Aperture designator		51
INORM	designator for receiving side of target surface		51
ITARSH	Target shape identifier		42
KEXT	Target dimension in parametric K-direction of target	[dependent]	42-50
KPTS	Number of subdivisions in K-direction		42-50
LEXT	Target dimension in parametric L-direction of target	[dependent]	42-50
LPTS	Number of subdivisions in L-direction		42-50
NTART	Total number of target grid-points (to be specified for ITARSH=2)		41
PHIC	ϕ (polar) coordinate to target center-point	[degrees]	46
RADIUS	radius of cylindrical target section	[m]	47
RBOT	bottom radius of conical target section	[m]	48

RCURV	radius of curvature of spherical target section	[m]	46
RMAX	radius of circular target sector	[m]	43
RPTS	number of grid points in the radial direction of circular target		43
RTOP	top radius of conical target section	[m]	48
THETAC	θ (azimuthal) coordinate at target center-point	[degrees]	46-49
THETAMAX	total angular span of circular target sector	[degrees]	43
TPTS	number of grid points in theta (azimuthal) direction of circular target		43
VMTx(i)	X-component (in the collector-system basis) of normal at target point i		41
VMTy(i)	Y-component (in the collector-system basis) of normal at target point i		41
VMTz(i)	Z-component (in the collector-system basis) of normal at target point i		41
XTA(i)	collector-system X-coordinate of target point i	[m]	41
YTA(i)	collector-system Y-coordinate of target point i	[m]	41
ZTA(i)	collector-system Z-coordinate of target point i	[m]	41
(Xo, Yo, Zo)	collector-system coordinates of target coordinate-system origin	[m]	18, 39

Reflector/Facet Parameters

Keyword	Description	Units	Page #
ASUB(k)	Coefficient of the kth term in the polynomial series for IOPT=4		61
DISHRAD	Parabolic-dish radius	[m]	60
ELENX	X extent of rectangular facet	[m]	56, 58
ELENY	Y extent of rectangular facet	[m]	56, 58
FLENG	Radius of circular facet or edge-length of triangular facet	[m]	56
FOC	Focal length of parabolic facet or radius of curvature for spherical facet	[m]	60
INTERP	Designator for order of interpolation for IOPT=5, 6		64
IOPT	Identifier for facet contour		59
KORD	Identifier for facet projected-shape		55
NSUBF	circular and triangular facet subdivision parameter		56
NTERMS	Number of terms in the polynomial series for IOPT=4		61
NX	Number of subdivisions in x direction for rectangular facet		58
NY	Number of subdivisions in y direction for rectangular facet		58
RCOMP(j)	Radial component of ideal normal at point-j of facet for IOPT = 6		67
RIMANG	Parabolic dish rim-angle	[degrees]	60
ZCOMP(j)	Height (value of z) at point j of facet for IOPT = 6		67

Concentrator Parameters

Keyword	Description	Units	Page #
IBETA(IDF)	rotation angle for facet IDF	[degrees]	70-71
ICPQR	Designator for whether facets are aimed by user or internally by CIRCE2		69-70
ISHAD	Designator for how shading/blocking is to be handled		71
NAIM	Number of facet aim-points to be defined if ICPQR = 0		70
NFACET	Number of facets comprising the concentrator		69
PN(IDF)	X-component (in the collector-system basis) of facet IDF's axis		70
QN(IDF)	Y-component (in the collector-system basis) of facet IDF's axis		70
RN(IDF)	Z-component (in the collector-system basis) of facet IDF's axis		70
REFLEC	Solar specular reflectivity of facet		69
SBM(IDF)	Shading/blocking factor for facet IDF (input for ISHAD=2)		71
SHADL	Edge-length for square shadow if ISHAD = 1	[m]	72
SHADR	Radius for circular shadow if ISHAD = 1	[m]	72
X,Y,Z (IDF)	Collector-system coordinates of center/vertex of IDFth facet	[m]	69
XAIM(ID)	Collector-system X-coordinate of IDth aim-point	[m]	70
YAIM(ID)	Collector-system Y-coordinate of IDth aim-point	[m]	70
ZAIM(ID)	Collector-system Z-coordinate of IDth aim-point	[m]	70

DISTRIBUTION:

U.S. Department of Energy (2)
Forrestal Building
Code CE-132
1000 Independence Avenue, SW
Washington, DC 20585
Attn: G. Burch
S. Gronich

U.S. Department of Energy
Forrestal Building
Code CE-13
1000 Independence Avenue, SW
Washington, DC 20585
Attn: R. Annan

U.S. Department of Energy (2)
Albuquerque Operations Office
P.O. Box 5400
Albuquerque, NM 87115
Attn: G. Tennyson
N. Lackey

U.S. Department of Energy
San Francisco Operations Office
1333 Broadway
Oakland, CA 94612
Attn: R. Hughey

Allied-Signal Aerospace Company
AiResearch, Los Angeles Division
Dept. 93055, M/S T-41
2525 West 190th St.
Torrance, CA. 90509-2960
Attn: J. Borghese

Arizona Solar Energy Office
Dept. of Commerce
1700 W. Washington, 5th Floor
Phoenix, AZ 85007
Attn: F. Mancini

Battelle Pacific Northwest Laboratory
P.O. Box 999
Richland, WA 99352
Attn: D. Brown
R. Carola

California Polytechnic
University Dept. of Mechanical Engineering
3801 West Temple Avenue
Engineering
Pomona, CA 91768
Attn: W. Stine

Clever Fellows
Innovation Consortium, Inc.
R.D. 1, Box 410, River Road
Melrose, NY 12121
Attn: J. A. Corey

Cummins Power Generation, Inc
MC 60125
P.O. Box 3005
Columbus, IN 47202-3005
Attn: R. Kubo

Cummins Power Generation, South
150 Tennehill Drive
Abilene, TX 79602
Attn: M. McGlaun

Detroit Diesel Corp.
13400 Outer Drive West
Detroit, MI 48239-4001
Attn: P. Perdue

Dynatherm Corporation
1 Beaver Court
P.O. Box 398
Cockeysville, MD 21030
Attn: D. Wolf

Electric Power Reasearch Institute
P.O. Box 10412
Palo Alto, CA 94303
Attn: E. Demeo

Energy Technology Engr. Center
Rockwell International Corp.
P.O. Box 1449
Canoga Park, CA 91304
Attn: W. Bigelow
R. LeChevalier

Florida Solar Energy Center
300 State Road, Suite 401
Cape Canaveral, FL 32920
Attn: Library

Georgia Power
7 Solar Circle
Shenandoah, GA 30265
Attn: W. King

Hydrogen Engr. Associates
4738 East Rancho Dr., Suite 1000
Phoenix, AZ 85018
Attn: H. Braun

Institute of Gas Technology
34245 State Street
Chicago, IL 60616
Attn: Library

Jet Propulsion Laboratory
4800 Oak Grove Drive
Pasadena, CA 91109
Attn: M. Alper

Karl Thomas Feldman, Jr. Ph.D., P.E.
Mechanical Engineering Consultant
1704 Stanford Dr. NE
Albuquerque, NM 87106

Lawrence Berkeley Laboratory
MS 90-2024
One Cyclotron Road
Berkeley, CA 94720
Attn: A. Hunt

Los Alamos National Laboratory
MS-E13
Los Alamos, NM 87545
Attn: M. Merrigan

McDonnell-Douglas Astronautics Company
5301 Bolsa Avenue
Huntington Beach, CA 92647-2048
Attn: R. L. Gervais,
R. Drubka

Mechanical Technology, Inc.
968 Albany Shaker Road
Latham, NY 12110
Attn: G. Dochat
J. Wagner

NASA Lewis Research Center (3)
21000 Brook Park Road
Cleveland, OH 44135
Attn: R. Shaltens
J. Schrieber
M. Dustin

National Renewable Energy Laboratory (6)
1617 Cole Boulevard
Golden, CO 80401
Attn: T. Williams
L. M. Murphy
G. Jorgensen
T. Wendelin
A. Lewandowski
M. Bohn

Northern Research and Engineering Corp.
39 Olympia Avenue
Woburn, MA 01801-2073
Attn: J. Kesseli

Power Kinetics, Inc.
415 River Street
Troy, NY 12180-2822
Attn: W. E. Rogers

Research International
18706 142nd Avenue NE
Woodinville, WA 98072
Attn: E. Saaski

Rockwell International – Rocketdyne Div.
6633 Canoga Ave.
Canoga Park, CA 91304
Attn: L. Pidcoke
T. Camaret

Science Applications International
Corporation
15000 W. 6th Ave, Suite 202
Golden, CO 80401
Attn: K. Beninga,
Mgr. of Energy Projects Div.

Solar Energy Industries Assoc.
777 North Capitol St. NE, Suite 805
Washington, D.C. 20002
Attn: S. Sklar
K. Sheinkopf

Solar Kinetics, Inc.
P.O. Box 540636
Dallas, TX 75354-0636
Attn: J. A. Hutchison
P. Schertz

Solar Research Corp. PTY Ltd.
6 Luton Lane
Hawthorn, Victoria, 3122 AUSTRALIA
Attn: N. Kaila

Solar Thermal Research Laboratory
U. of Waterloo Dept. of Mech. Engr.
Waterloo, Ontario, CANADA N2L 3G1
Attn: A. P. Brunger

Space Power Institute
231 Leach Center
Auburn University, AL 36849-5320
Attn: T. Overfelt

Stirling Technology Company
2952 George Washington Way
Richland, WA 99352
Attn: M. A. White

Stirling Thermal Motors
2841 Boardwalk
Ann Arbor, MI 48104
Attn: L. Johansson
R. Meijer

Stirling Machine World
1823 Hummingbird Court
West Richland, WA 99352-9542
Attn: B. Ross

Sunpower, Inc.
6 Byard Street
Athens, OH 45701
Attn: W. Beale

Systems Consultants
11723 Goshen Ave., Suite 101
Los Angeles, CA 90049
Attn: B. David

Thermacore, Inc.
780 Eden Road
Lancaster, PA 17601
Attn: D. Ernst

University of Houston
Solar Energy Laboratory
4800 Calhoun
Houston, TX 77704
Attn: J. Richardson

University of Minnesota
Dept. of Mechanical Engineering
111 Church St., SE
Minneapolis, NM 55455
Attn: E. A. Fletcher

Australian National University
Department of Engineering
Physics
P.O. Box 4
Canberra ACT 2600 AUSTRALIA
Attn: S. Kaneff

Energy Research Centre
R. S. Phy. Sc.
Australian National University
Canberra ACT 2601 AUSTRALIA
Attn: K. Inall

DLR
Pfaffenwaldring 38-40
7000 Stuttgart 80 GERMANY
Attn: R. Buck

Schlaich, Bergermann und Partner
Hohenzollernstr. 1
D-7000 Stuttgart 1 GERMANY
Attn: W. Schiel
J. Kern

ZSW Solarthermie
Hessbruhlstraee 61
D-7000 Stuttgart 80 GERMANY
Attn: J. Rheinlander
J. Kleih

MS0841	1500	D. J. McCloskey
MS0836	1501	C. W. Peterson, route to 1512, 1551, 1552
MS0827	1502	P. J. Hommert, route to 1511, 1553, 1554
MS0835	1513	R. D. Skocypec
MS0835	1513	R. E. Hogan
MS0835	1513	V. J. Romero (10)
MS0835	1513	Day File
MS0443	1561	H. S. Morgan, route to 1562
MS0724	6000	D. L. Hartley
MS0735	6200	D. E. Arvizu route to 6213, 6218, 6219
MS1127	6215	C. P. Cameron
MS1127	6215	P. G. Cordeiro
MS1127	6215	C. M. Ghanbari
MS1127	6215	K. S. Rawlinson
MS1127	6215	J. W. Strachan
MS0703	6216	C. E. Tyner
MS0703	6216	C. E. Andraka
MS0703	6216	R. B. Diver (5)
MS0703	6216	D. R. Gallup
MS0703	6216	J. W. Grossman
MS0703	6216	P. C. Klimas
MS0703	6216	T. R. Mancini (5)
MS0703	6216	D. F. Menicucci
MS0703	6216	T. A. Moss
MS0703	6216	J. B. Moreno
MS0703	6216	Library (10)
MS0899	7141	Technical Library (5)
MS0619	7151	Technical Publications
MS0100	7613-2	Document Processing for DOE/OSTI (10)
MS9018	8523-2	Central Technical Files

☆ U.S. Government Printing Office 1994-573-110-02060

DATE
FILMED
5/16/94
END